POLITECNICO
MILANO 1863

SCUOLA DI INGEGNERIA INDUSTRIALE
E DELL'INFORMAZIONE

Inclusion of reference wind turbine controller in wind tunnel experiments on the aerodynamic response of floating wind turbines

Tesi di Laurea Magistrale in
Mechanical Engineering - Ingegneria Meccanica

Author: **Elio Daka**

Student ID: 966581
Advisor: Prof. Marco Belloli
Co-advisors: Ing. Alessandro Fontanella
Academic Year: 2021-22

Abstract

The outstanding growth of wind energy sector has pushed the research world to look for ever more efficient solutions, to lower the cost of energy making it economically competitive compared to other energy sources. Moreover, floating offshore wind turbines established themselves as a possible candidate to become an energy solution, with efficiency comparable to more traditional resources.

In this context, wind turbine control is of utter importance to maximize power production and to guarantee safe operation of the system during its life-cycle. Also numerical tools and wind tunnel testing are now more than ever, of fundamental importance to validate new design solutions and reduce development time of new projects.

This thesis deals with the implementation of an OpenFAST numerical model of the Polimi 15 MW, that is 1:100 scaled model of the IEA 15 MW Reference Wind Turbine. The control problem is introduced for the reference turbine, considering the functionalities made available by the ROSCO controller. This controller is than implemented for the Polimi 15 MW, and the response of the system is analyzed through numerical simulations, considering the response of the IEA 15 MW as a reference.

The physical scaled model is then tested in wind tunnel, both in onshore and offshore configuration. The offshore configurations is made possible through an hexapod, that reproduces the motions of a floating platform due to wind loads and wave motion, in a Hardware in the Loop implementation.

The wind tunnel tests results are compared to the numerical ones. Results for bottom fixed configuration shows quite good matching. Steady state operating points obtained during tests are in good agreement with the ones of the numerical model, and also with the ones of the IEA 15 MW, especially in above rated condition. Tests in offshore configuration, with imposed platform motion show contrasting results. The matching between experimental and numerical results is not always ensured, and further investigation are needed, in particular on the experimental setup.

Keywords: Wind energy, Wind tunnel testing, Wind turbine control, Off-shore wind turbines, Floating wind turbines

Abstract in italiano

L'eccezionale crescita del settore dell'energia eolica ha spinto la ricerca verso soluzioni sempre più efficienti, per abbassare il costo dell'energia rendendola economicamente competitiva rispetto ad altre fonti energetiche. Inoltre, le turbine eoliche galleggianti si sono affermate come un possibile candidato per diventare una fonte energetica con un' efficienza paragonabile a risorse più tradizionali.

In questo contesto, il controllo delle turbine eoliche è di fondamentale importanza per massimizzare la produzione di energia e garantire il funzionamento del sistema in condiziondi di sicurezza. Anche i software di simulazione e le prove in galleria del vento sono oggi più che mai di fondamentale importanza, per validare nuove soluzioni progettuali e ridurre i tempi di sviluppo.

Questa tesi si occupa dell'implementazione di un modello numerico in OpenFAST della "Polimi 15 MW", un modello in scala 1:100 della turbina di riferimento "IEA 15 MW". Il problema del controllo di una turbina eolica viene introdotto per la turbina di riferimento, considerando le funzionalità messe a disposizione dal controllore ROSCO. Questo controllore è implementato per la Polimi 15 MW, e la risposta del sistema viene analizzata con simulazioni numeriche, considerando la IEA 15 MW come riferimento.

Il modello fisico è testato in galleria del vento, sia in configurazione onshore che offshore. La configurazione offshore è resa possibile attraverso un esapode, che riproduce i movimenti di una piattaforma galleggiante dovuti alle forze aerodinamiche e al moto ondoso, in un'implementazione di tipo "Hardware in the Loop".

I risultati dei test in galleria del vento sono confrontati con quelli numerici. I risultati per la configurazione onshore sono promettenti. I punti di funzionamento ottenuti durante i test sono in accordo con quelli del modello numerico, e anche con quelli della IEA 15 MW, specialmente per velocità del vento sopra la nominale. I test in configurazione offshore, con moto della piattaforma imposto, mostrano invece risultati contrastanti. La corrispondenza tra risultati sperimentali e numerici non è sempre garantita e sono necessari ulteriori studi e verifiche, in particolare sul setup sperimentale.

Parole chiave: Energia eolica, Test in galleria del vento, Controllo delle turbine eoliche, Turbine eoliche galleggianti

Contents

List of Figures

List of Tables

Introduction

In the last years wind energy has seen an extraordinary growth in terms of installed capacity and wind turbines size. Moreover, the commitments made globally during the cop26 to reach the net-zero scenario, will further drive wind energy growth.

As shown by figure 1 [1], in the last 10 years the installed capacity has seen a remarkable increase. In order to respect the commitment a more disruptive growth in installed capacity is expected between nowdays and the 2030. This is leading towards bigger wind turbines, with larger swept area and consequently higher rated power. The journey towards decarbonization sets ambitious goals even in terms of generated power. The trend in turbine size combined for the need to maximize the annual energy production drives the development of floating offshore wind turbines. The first development of offshore wind turbine was constrained by the depth of the seabed. Indeed, with the bottom-fixed configuration offshore wind turbines could be installed only in relatively shallow waters. With the development of floaters, the water depth is no more a constraint, and locations away from the coast with higher wind speed quality can be exploited, leading to higher and more predictable energy generation.

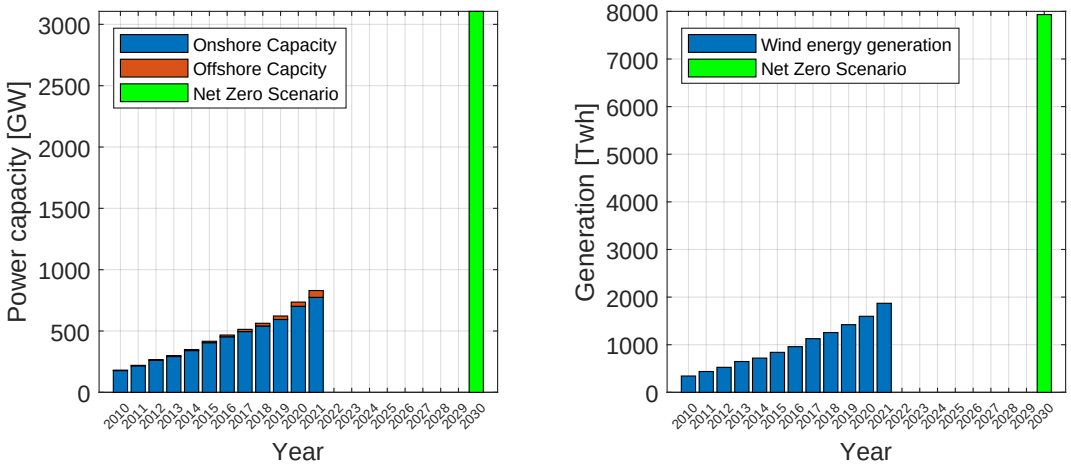

Figure 1: Global wind power capacity evolution from 2010, data taken from [1].

In this framework the role of the wind turbine controller takes on an even more important role, because of the new challenges that arise with the floating configuration.

Moreover, the level of development of wind energy is very heterogeneous in the world, with some countries installing floating wind turbines with rated power of several mega-watts, and others still focusing on smaller systems of few mega-watts. This leads to the need of a versatile controller, that should easily adapt to a large number of different wind turbines models.

The fast growth in the wind energy field, was possible also thanks to the evolution of dedicated computational tools [2]. Numerical simulations help to understand in advance possible critical issues that may occur in some particular operating condition of the wind turbine, without the need of a full-scale prototype. These software allow the implementation and testing of different control logics, reducing the development time of new projects.

Despite their incredible usefulness and accuracy, numerical software cannot predict all the possible behaviors of a wind turbine in real condition. Moreover, the results coming from numerical simulations need to be validated by experiments done on full-scale or scaled prototypes. Experiments on scaled or full-scale prototypes in real conditions are time-consuming and not cost-effectively. Wind tunnel tests on scaled prototypes help to overcome the limits of tests in real environment condition. The controlled wind-flow possible in wind tunnel facilities allows to test a wide range of operating condition in short times. Results from these experiments can be used to investigate particular aspects not predicted by numerical tools and to validate the results coming from simulations. These tests help also the continuous development and improvement of these software.

Wind tunnel tests allows the investigation of the aspects related to the aerodynamics of the model. For floating wind turbines, also the loads coming from the interaction with waves are of utter importance. To experimentally address this aspect, test in wave basins are possible [3]. These tests are focused on the floater motion in water and on the wave-induced loads. Combining aerodynamic aspects and hydrodynamic ones in a unique experimental set-up is not easy from the facility point of view. To overcome this limit, specific hardware in the loop tests have been developed. In this test the wind turbine is tested inside a wind tunnel and the motion of the floater is made possible by a robot, that uses a numerical model to correctly impose the motion and compute the loads.

0.1. About this work

The goal of this work is to develop an OpenFAST numerical model for the Polimi 15 MW wind turbine model, tune the ROSCO controller for this model and properly test it with numerical simulations. Finally, the numerical model is compared to the experimental results obtained through wind tunnel tests, both for bottom-fixed and floating conditions.

In Chapter 1 the control problem for wind turbines is presented, focusing on variable-speed variable-pitch controller, and explaining the different working regions.

In Chapter 2 the ROSCO controller is discussed, focusing on the reasons which led to its creation. The principal functionalities of the controller are presented making reference to numerical results obtained for the IEA 15 MW RWT.

In Chapter 3 the IEA 15 MW RWT is introduced. The simulation results for its numerical model are presented and discussed.

Chapter 4 focuses on the Polimi 15 MW WTM. The aerodynamic design is first presented, then the numerical model is build and the controller is tuned. OpenFAST simulations are performed to verify the controller behavior, comparing the system with the IEA 15 MW RWT results.

Chapter 5 describes the experimental setup used for wind tunnel tests. Wind tunnel tests are performed for bottom-fixed condition to assess the consistency of steady state points between the physical model and the numerical one. Tests in offshore configuration have been performed thanks to an hexapod miming the floating condition, to compare the behavior of the turbine and the control in floating configuration with respect to the numerical simulations.

In Chapter 6 the experimental results compared to the numerical ones are presented. The possible reasons for the discrepancies between numerical and experimental results are discussed, focusing on the main difference between the physical model and the numerical one and on the uncertainties on parameter estimation.

1 | Wind Turbine Control

In this chapter the control problem for wind turbines is presented. Theoretical informations about the control problem are taken from [4]. The need for a controller is intrinsic in the turbine itself. The first natural aim of the controller was to limit the power extraction at high wind speed, to prevent the turbine to work in not safe conditions.

More in detail, the three principal goals of the controller are:

- Energy capture: maximize energy capture respecting all constraints such as rated power, cut-in and cut-out speed etc.
- Mechanical loads: avoid excessive dynamic loads on the turbine for fatigue purposes.
- Power quality: provide to the grid electrical power compliant with interconnection standards.

Usually the goals are conflicting and cannot be pursued separately, so the control objective is to obtain a balanced compromise between them.

To better understand the control goal, it is good to refer to figure 1.1, where the ideal power curve is presented.

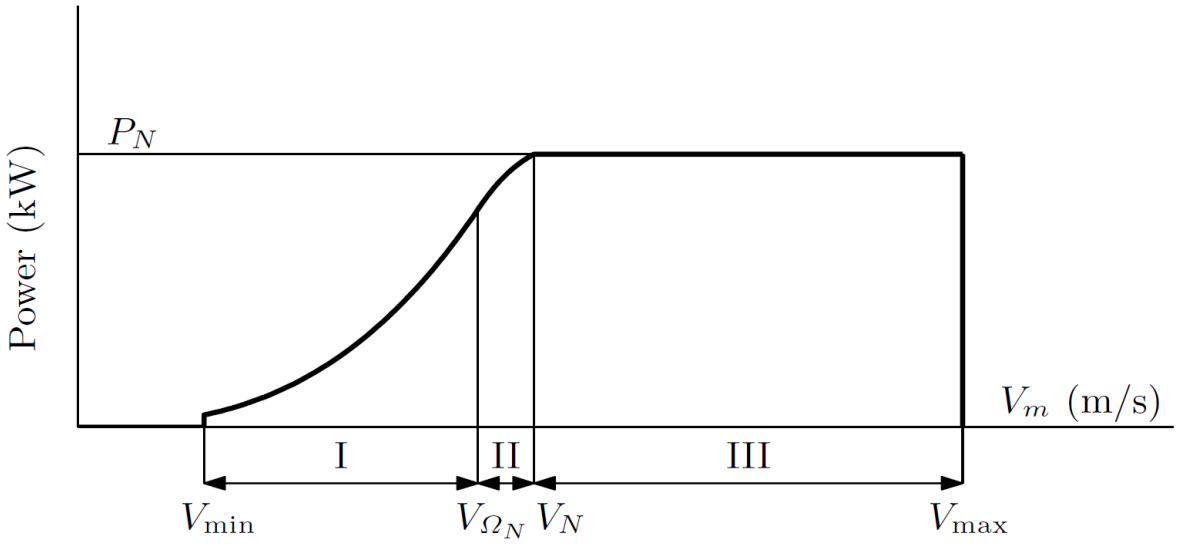

Figure 1.1: Ideal power curve [4].

Power curve is divided in three regions. At wind speeds below the rated one (V_N), the

power is below the rated one (P_N), so the control goal is to extract the maximum power possible (region I). In region III, the goal of the controller is to limit power extraction, keeping power to a constant value equal to the rated one. Region II is the transition region, where rotor speed is limited to avoid excessive noise emission. If this limit on rotor speed is not present, region II may not exists, and the optimum power curve would continue until the rated power.

1.1. Variable-Speed Variable-Pitch

As already mentioned, the main goal of the controller is to regulate rotor speed, generator power and torque. To achieve this, different modes of operation are possible. To explain the modes of operation, is better to refer to the aerodynamic coefficients and not forces, as usually done in wind energy field. We can define three non-dimensional quantities, that are thrust, power and torque coefficients

$$\begin{aligned} C_t &= \frac{F_t}{1/2\rho A_r U^2} \\ C_p &= \frac{P}{1/2\rho A_r U^2} \\ C_Q &= \frac{Q}{1/2\rho A_r R U^2} \end{aligned} \tag{1.1}$$

where A_r is the rotor area ρ is the air density, R is the rotor radius and U is the wind speed. Thrust, power and torque, and so the respective coefficients, are parameterized on the tip-speed-ratio (TSR) λ and on the collective-blade-pitch-angle β. This two parameters, λ and β, are enough do define the operational point of the wind turbine. Acting on them, is possible to control the operating point of the turbine. The modes of operation available are classified based on which parameter is controlled. In particular, being the TSR defined as

$$\lambda = \frac{\omega_{rot} R}{U}, \tag{1.2}$$

the controller acts on λ through the rotor speed ω_{rot}. Rotor speed and β can be fixed or variable, so we end up with four possible operation modes:

- Fixed-Speed Fixed-Pitch (FS-FP)
- Fixed-Speed variable-Pitch (FS-VP)
- Variable-Speed Fixed-Pitch (VS-FP)
- Variable-Speed variable-Pitch (VS-VP).

The most versatile operation mode, and the most used in modern wind turbines, is the

Variable-Speed Variable-Pitch, that allows a robust control in each working region.

Starting from the surfaces $C_P(\lambda, \beta), C_t(\lambda, \beta), C_Q(\lambda, \beta)$, the control strategy can be developed to satisfy the control goals. However, is simpler and preferred to study the control laws, on 2D plots $C_P(\omega, \bar{\beta}), C_Q(\omega, \bar{\beta})$, with fixed blade pitch angle, parameterized by the wind speed U.

1.2. Regions of operation

To address all possible wind conditions, the region of operation presented for the ideal power curve can be further specified as follows:

- Region 1: region before the cut-in speed, this region is not interesting for control purposes, since the rotor is stationary.
- Region 1.5: region above cut-in speed where the turbine cannot operate at its optimum TSR. Rotor speed increases from its minimum value to the optimal one.
- Region 2: the turbine can operate at its optimum TSR, but the power is lower than the rated one. The turbine operates to extract the maximum power possible, aiming at maximum C_P.
- Region 2.5: the wind speed is larger than the one corresponding to rated rotor speed, but less than the one corresponding to rated power. This region is used as transition between region 2 and 3.
- Region 3: wind speed is above the rated speed. The controller limits the power extraction to the rated value acting on the blade pitch angle.
- Region 4: region after the cut-out speed, a shutdown maneuver has to be properly triggered, but it is not interesting for control purposes.

The presence and the extension of some specific region, depends on the wind turbine design. Figure 1.2 shows the different regions of operation on the torque-ω_{rot} plane.

As mentioned before, in region 2 the turbine operates to extract the maximum power possible, so the generator torque overlaps to the torque that guarantees maximum C_P. Once that the turbines reaches the rated power, the generator torque is kept constant, and the blade pitch angle is adjusted such that the intersection between aerodynamic and generator torque occurs at the rated rotor speed. To better clarify the different regions, is useful to refer to the steady state operating points of a reference wind turbine model. Considering the International Energy Agency 15 MW Reference Wind Turbine (IEA 15 MW RWT), figure 1.3 shows the different operating regions in the steady state values of rotor speed, blade pitch and generator torque. Region 1 and 4 are omitted, since they are not interesting from the control point of view. The shaded grey are between region

2 and 3 is the transition region (region 2.5). It can be noticed that this region is nearly negligible because, for this wind turbine model, the wind speed corresponding to rated rotor speed is very close to the one corresponding to rated power.

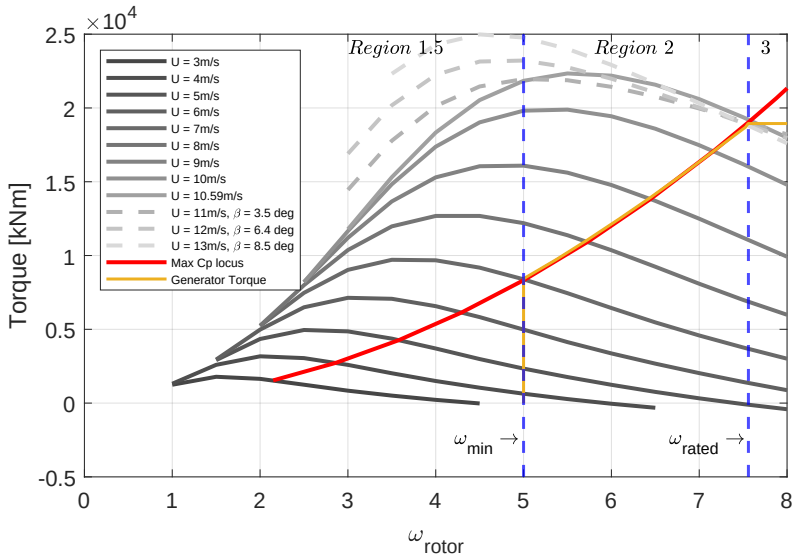

Figure 1.2: Control strategy in different regions for the IEA 15 MW RWT.

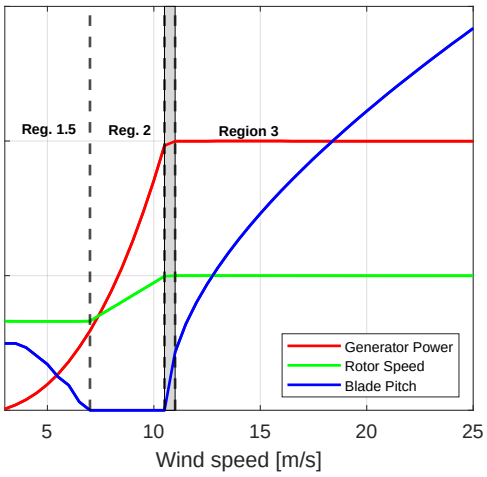

Figure 1.3: Steady state operating points in the different working region for the IEA 15 MW RWT; the shaded grey area represents the region 2.5.

2 | ROSCO

In wind energy research field a reference controller is required for two reasons. First, to serve as a baseline for the development and comparison of modern control logic. Second, to enable dynamic simulations in the investigation of other aspects of wind turbines.

Moreover, the reference controller should be easy adaptable to a large variety of models and should address the issues of the new generation of onshore and offshore wind turbines, which are larger and more flexible.

In this framework, the Reference Open-Source COntroller (ROSCO) [5] provides a baseline controller, that addresses the issues of modern wind turbines, and can be easily adapted to a large variety of different models. The controller was firstly developed at Delft University of Technology and was designed to perform comparably to existing controllers already present in literature, and to be representative of the controllers used in industry. Furthermore, it was developed to have a simple tuning process, with the ambition that a control engineer is not needed to tune it for the specific wind turbine considered.

In this chapter the control functionalities are presented, while the tuning process will be described in detail in chapter 4, referring to the specific example of the wind turbine model considered in this work.

2.1. Control Modules

ROSCO was developed with a modular architecture, such that different modules of the controller can be turned on and off according to the different needs. The baseline of the controller is a Variable-Speed Variable-Pitch control, with the addition of particular modules that address specific issues of onshore and offshore wind turbines. The general controller logic is depicted in figure 2.1.

2.1.1. Torque Controller

In ROSCO, the generator torque controller is a Variable-Speed control logic, where the generator torque is regulated according to the rotor speed. The control logic is different in below and above-rated regions.

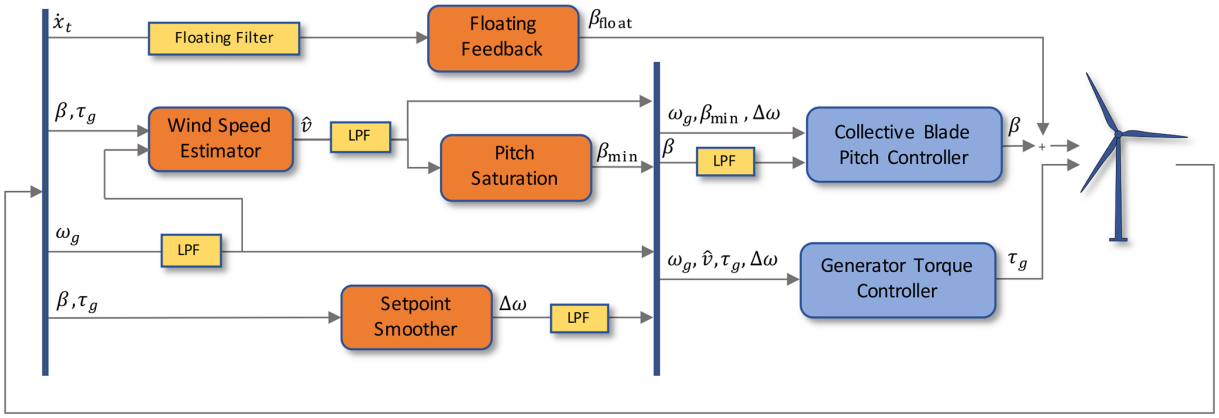

Figure 2.1: ROSCO controller logic [5].

In below-rated region, ROSCO provides two choices, with the aim of maximizing power output: k-ω^2, and TSR tracking.

With k-ω^2 logic, the generator torque is regulated following a quadratic law of the rotor speed. This is done in order to track the locus of maximum power coefficient Cp. This results in

$$\tau_g = k\omega^2, \quad \text{where} \quad k = \frac{\pi \rho R^5 C_{p,max}}{2\lambda_{opt} N_{gb}^3 \eta_{gb}}, \tag{2.1}$$

where, λ_{opt} is the optimal TSR that guarantees maximum C_P, R is the rotor radius, $C_{P,max}$ is the maximum power coefficient, N_{gb} is the gearbox ratio and η_{gb} is the efficiency of the gearbox. Although simple, this control logic is sensitive to modelling errors and wrong parameter estimation, leading the turbine to operate at operating points where C_p is not maximized.

With TSR tracking, starting form the definition of the TSR:

$$\lambda = \frac{\omega R}{U}, \tag{2.2}$$

if the wind speed U can be properly estimated, a reference rotor speed ω can be computed, that guarantees optimal TSR tracking at all wind speeds:

$$\omega_{opt} = \frac{\lambda_{opt} U}{R}. \tag{2.3}$$

Then a PI regulator is used to track this optimal rotor speed, ensuring that the the turbine operates at its maximum C_p. This is valid as long as the blade pitch angle is fixed at the value that provides maximum power coefficient.

In above-rated region, the goal of the controller is to limit the power extraction, maintaining the power in the neighborhood of the rated value. Two options are available in

ROSCO: constant torque and constant power. If constant torque logic is used, generator torque is saturated to a value computed as:

$$\tau_{g,ar} = \frac{P_{rated}}{\omega_{g,rated}} \tag{2.4}$$

In this way, torque is fixed and some oscillations of the power output are tolerated, according to the variation of the generator speed. With constant power logic instead, the generator power is kept fixed to the rated value, while the generator torque is computed as the ratio between the rated power and the instantaneous value of the generator speed:

$$\tau_{g,ar} = \frac{P_{rated}}{\omega_{g}} \tag{2.5}$$

With this logic, power output has a more constant trend, while generator torque oscillates according to the variation of generator speed.

Combining the different options available for below and above-rated operation, provides a total of four different control methods for the generator torque controller. The different control methods can differ in terms of steady state operating points of the wind turbine or in terms of dynamic performance of the controller. TSR tracking and k-ω^2 influence predominantly the below-rated region, while constant torque or power affect the above-rated region.

For what regards steady state operating points, figure 2.2 shows the differences between TSR tracking and k-ω^2, since constant torque or power does not influence this aspect.

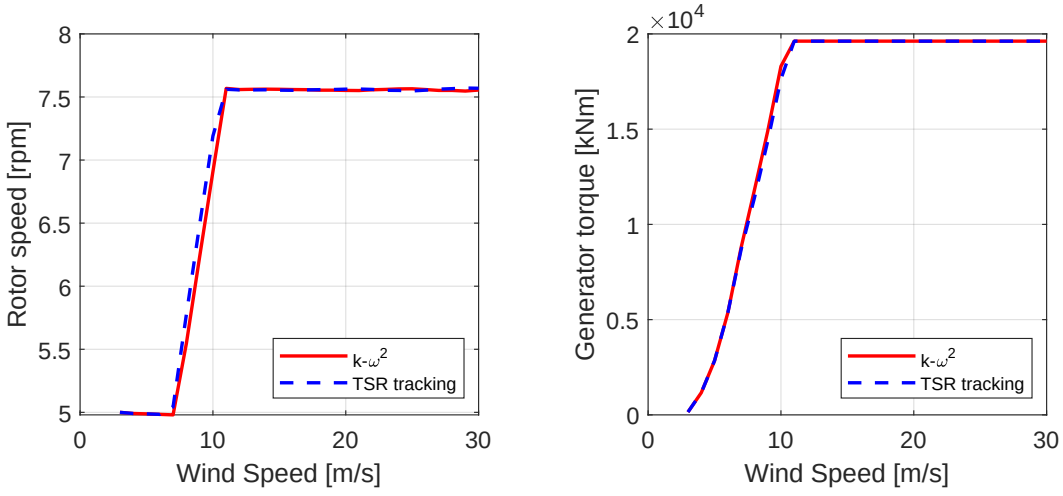

Figure 2.2: Steady state rotor speed (left) and generator torque (right) with TSR tracking and k-ω^2 for the IEA 15 MW RWT

Slight differences stand out in the below-rated region, where the logics differ, so they

could be addressed as equivalent. This is due to the fact that the model is ideal, and so each quantity present in equation 2.1 is supposed to be known without errors. Of course this is not the case for a real prototype, where the uncertainties on parameters like the gearbox efficiency can be not negligible, producing very different operating points when using k-ω^2 logic, that can be far from the optimum.

The two below-rated control logics produce even a different dynamic response to a wind step. Figure 2.3 shows generator torque and power for a step of wind velocity from 6 m/s to 7 m/s.

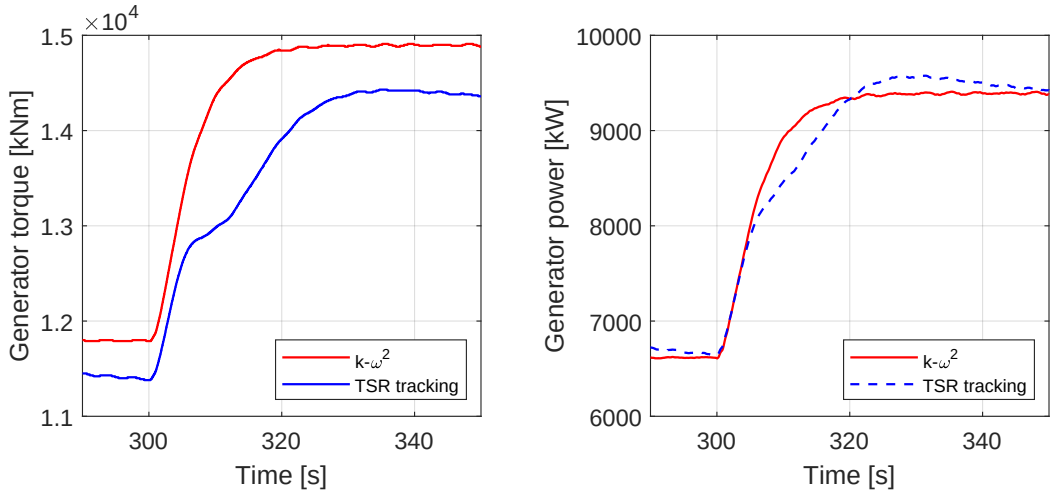

Figure 2.3: Generator torque and power during a wind step from 6 to 7 m/s for the IEA 15 MW RWT.

With k-ω^2 the response is smoother, but the turbine works at a rotor speed that does not guarantee optimal TSR; indeed, with TSR-tracking the generator power is a bit higher.

Differences between constant torque or constant power logics are relevant in above-rated region. Figure 2.4 shows a detail of the response of the controller in terms of generator torque and power, for a step of wind velocity from 17 m/s to 18 m/s.

It is evident the difference between constant torque operation, where the generator torque is kept constant and power increases as the rotor speed increases, while with constant power the overshoot of the generator power is less pronounced and the torque drops in order to keep the power constant as the rotor speed increases.

The four combinations of control logics for the torque controller produce differences in how the transition from below to above-rated region is handled in terms of rotor speed, as shown in figure 2.5.

It can be observed that constant torque or power influences the overshoot of rotor speed, and in particular the overshoot with constant power logic is higher. It can also

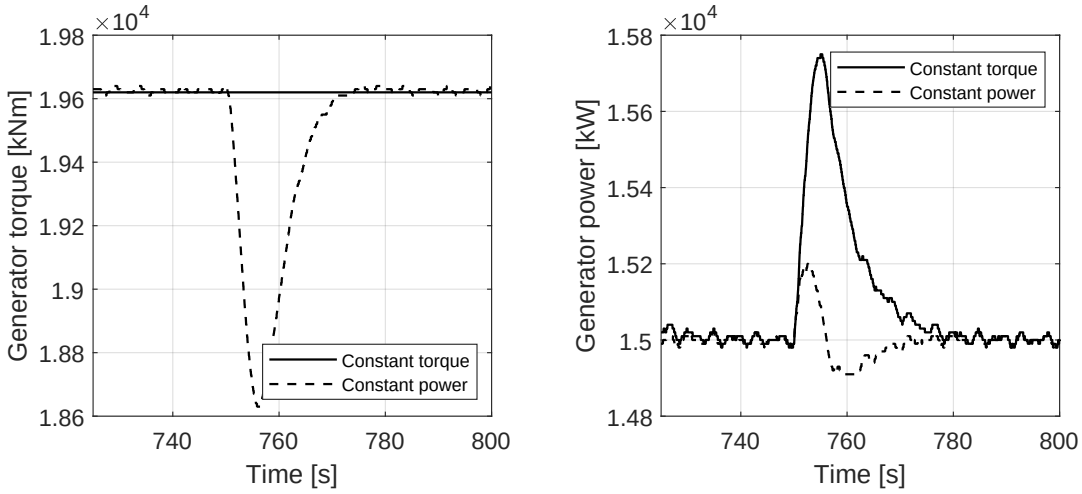

Figure 2.4: Generator torque and power during wind step from 17 to 18 m/s for the IEA 15 MW RWT.

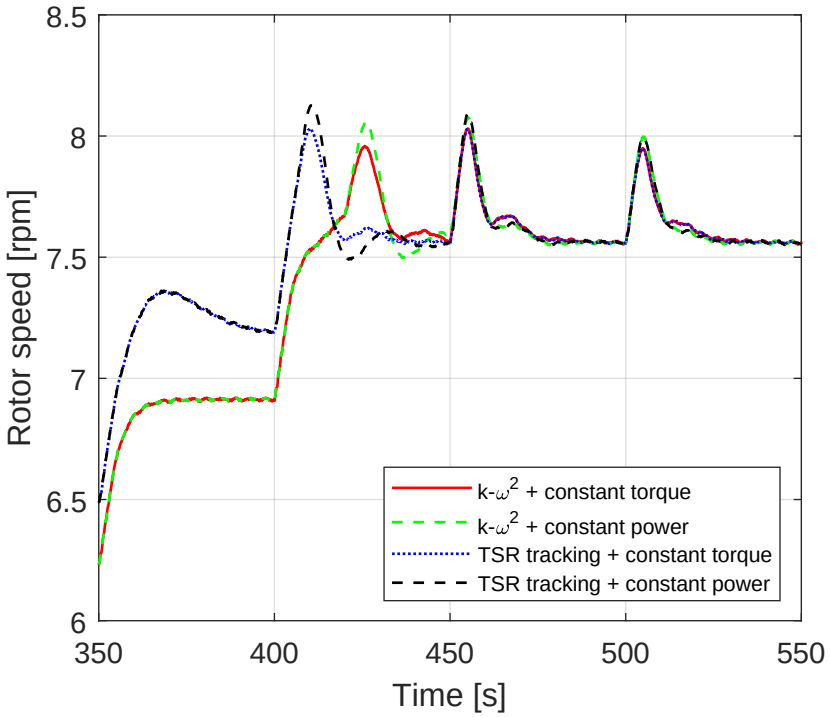

Figure 2.5: Rotor speed transition from below- to above-rated region (wind step from 10 to 11 m/s) for the IEA 15 MW RWT.

be observed that with k-ω^2 the transition is in delay with respect to TSR tracking. This is due to how the two below-rated control logic handle the transition region. With k-ω^2 transition is regulated with a PI controller and the turbine is considered in above-rated condition if the blade pitch angle is above a certain treshold. While, in TSR tracking, transition is handled by the set-point smoother only, which will be later discussed in this section.

2.1.2. Pitch Controller

In below-rated region, the blade pitch controller saturates the blade pitch to its minimum value, unless a minimum pitch saturation routine is scheduled. In above-rated condition, the blade pitch controller adjusts the blade pitch angle in order to track the rated rotor speed, limiting the power extraction to the rated value of the wind turbine. This is done by a PI controller acting on the rotor speed error. Figure 2.6 shows the steady state blade pitch for the IEA 15 MW RWT.

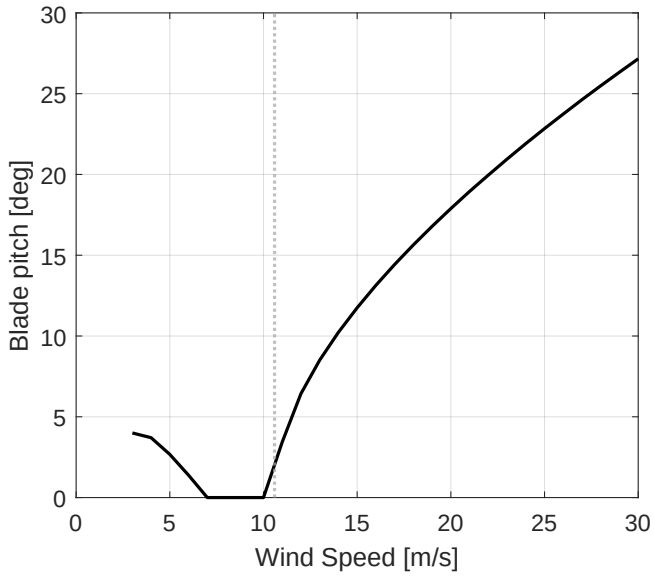

Figure 2.6: Steady state blade pitch for the IEA 15 MW RWT

The dotted vertical grey line is the rated wind speed and separates the below and the above-rated region. In below-rated region the pitch is not fixed to a defined value, but varies according to the minimum pitch saturation routine that will be discussed in a dedicated subsection.

The controller impacts more on the dynamic of blade pitch, than on its steady state value. In doing this, it interacts with the generator torque controller and is affected by the control logic used to define the generator torque, as shown in figure 2.7.

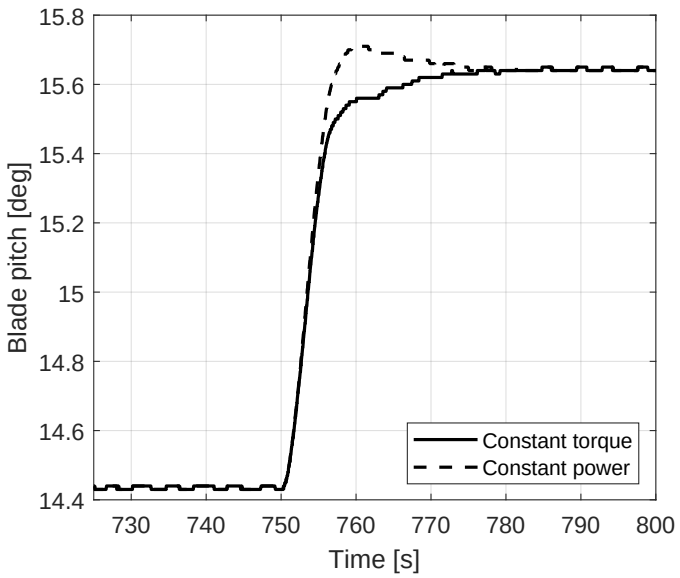

Figure 2.7: Blade pitch during wind step from 17 to 18 m/s for the IEA 15 MW RWT

With constant power the overshoot is higher because the rotor speed oscillates more and the pitch controller effort to keep it at the rated value is higher. Conversely, with constant torque, the generator torque is kept steady, avoiding too large overshoot of the rotor speed and so the pitch controller effort is reduced.

Also the transition of blade pitch from below to above-rated region is affected by the interaction between the two controllers as depicted in figure 2.8.

As pointed out before, with constant power the blade pitch overshoot is higher. Moreover, as already discussed for the torque controller, the different way of handling the transition region between k-ω^2 and TSR tracking, produces a delay in the pitch controller action.

2.1.3. Set-Point Smoother

In the near rated region, both the torque controller and the blade pitch controller will follow the same rotor speed reference: the rated one. This would lead the controllers to conflict in this region, producing undesired oscillations and vibrations in the system. To avoid this conflict the set-point smoother shifts the reference speed signals of the two controllers, in order to keep only one of them active. This is done by defining an offset $\Delta\omega$ as:

$$\Delta\omega = \left[\left(\frac{\beta - \beta_{min}}{\beta_{max}}\right) k_{vs} - \left(\frac{\tau_{g,max} - \tau_g}{\tau_{g,max}}\right) k_{pc}\right] \omega_{g,rated} \tag{2.6}$$

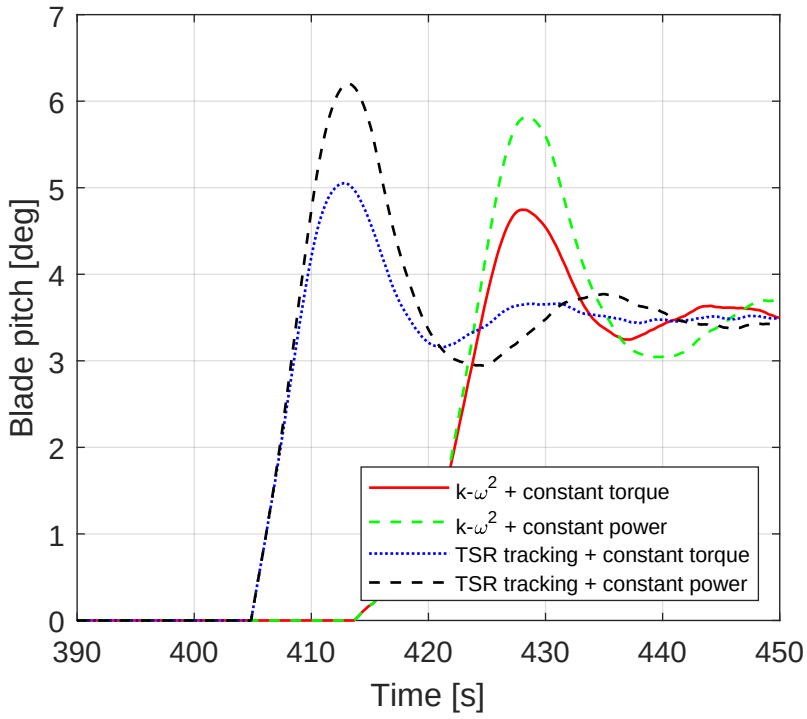

Figure 2.8: Blade pitch transition (wind step from 10 to 11 m/s) for the IEA 15 MW RWT

where β and τ_g are the instantaneous values of blade pitch angle and generator torque, β_{min} is the minimum blade pitch coming from the minimum pitch saturation routine, β_{max} is the blade pitch at the cut out speed and $\tau_{g,max}$ is the saturation generator torque in above-rated region. The constants k_{vs} and k_{pc} are unitless positive gain factors, that has to be tuned according to the wind turbine model.

Defined $\Delta\omega$, the reference speed for the torque controller $\omega_{ref,\tau}$ and the one for the blade pitch controller $\omega_{ref,\beta}$ are shifted according to:

$$\omega_{ref,\tau} = \begin{cases} \omega_{ref,\tau} - \Delta\omega & \Delta\omega \geq 0 \\ \omega_{ref,\tau} & \Delta\omega < 0 \end{cases} \quad , \quad \omega_{ref,\beta} = \begin{cases} \omega_{ref,\beta} & \Delta\omega \geq 0 \\ \omega_{ref,\beta} - \Delta\omega & \Delta\omega < 0 \end{cases} \tag{2.7}$$

With this definition the set-point smoother shifts the speed reference of the saturated controller while the unsaturated one is kept active. For instance, in above-rated region, where the generator torque is saturated to its maximum and the blade pitch angle is grater than its minimum value, $\Delta\omega$ is greater than zero. Being $\Delta\omega \geq 0$ the speed reference for the torque controller is shifted to a smaller value, so the generator will keep the torque saturated in the attempt to slow down the rotor, while the blade pitch controller will

keep the rotor speed at the rated value. Focusing on the transition region, the effect of the set-point smoother is shown in figure 2.9 and figure 2.10, where the response of the system during a linear increase of the wind speed across the transition region is plotted.

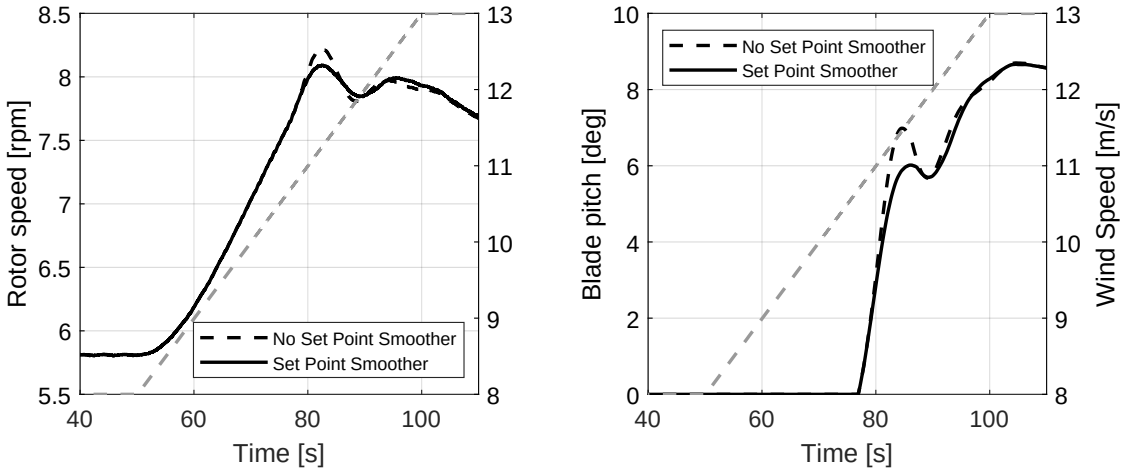

Figure 2.9: Set-point smoother effect on rotor speed and blade pitch for the IEA 15 MW RWT, grey dotted line represents the wind speed.

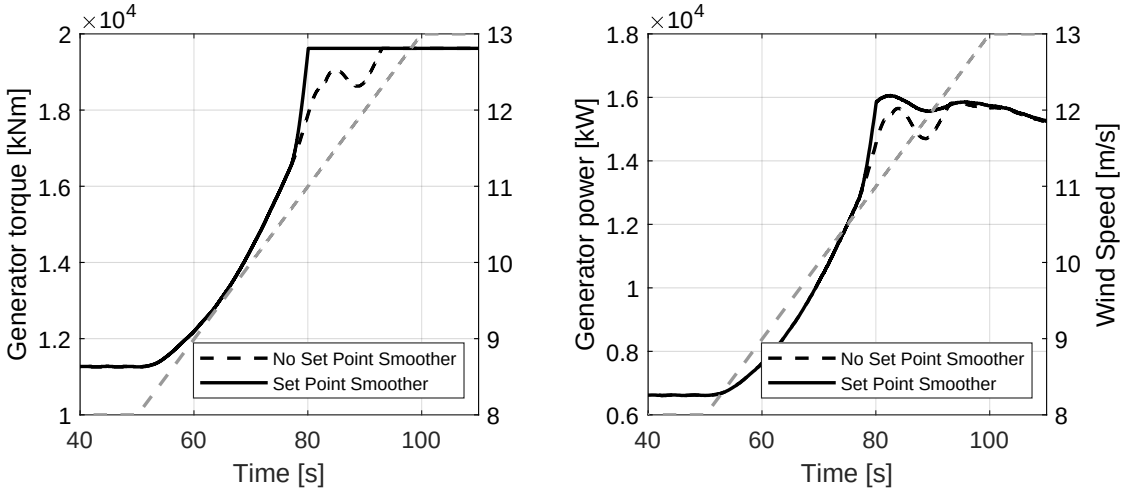

Figure 2.10: Set-point smoother effect on generator torque and generator power for the IEA 15 MW RWT, grey dotted line represents the wind speed.

With the set point smoother we have a better response. In particular, rotor speed overshoot and the blade pitch controller effort are reduced. Moreover, the generator torque transition from below to above-rated condition occurs without oscillations. Generator power is higher during the transition, ensuring a higher overall power extraction for a wind speed that oscillates around the rated value.

2.1.4. Minimum Pitch Saturation

The minimum pitch saturation routine allows to saturate the blade pitch angle to a predefined value, according to the wind speed estimation. This allows to maximize the power extraction at low wind speed. For instance, for certain wind turbine designs like the IEA 15 MW RWT, the minimum rotor speed can be limited to avoid the excitation of tower natural frequencies. For this reason the turbine is forced to work at a higher TSR with respect to the optimum one at low wind speeds. To extract the maximum power in this condition, a certain blade pitch angle greater than zero must be imposed, according to the $C_p(\lambda, \beta)$ curve. This blade pitch angle is scheduled according to the TSR. Being the rotor speed saturated at the minimum accepted value, it means that the pitch is scheduled on the wind speed, so a quite accurate wind speed estimator is needed to perform the routine.

The estimated wind speed U_{est} is used to compute the TSR as

$$\bar{\lambda} = \frac{\omega_{min} R}{U_{est}}, \tag{2.8}$$

than $\beta_{scheduled}$ is the blade pitch angle that maximizes $Cp(\bar{\lambda})$. In figure 2.11 the blade pitch schedule is plotted on the Cp surface.

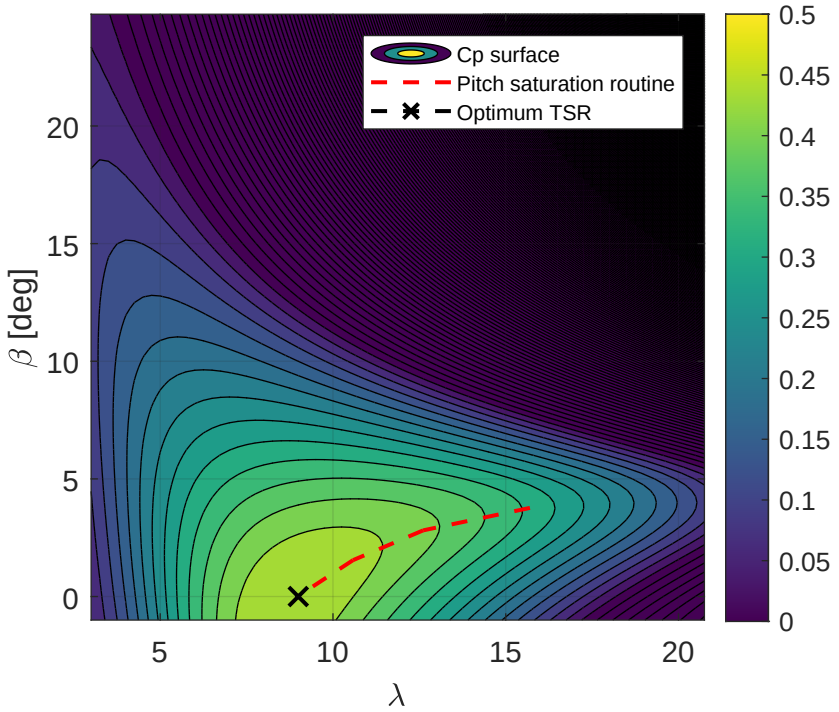

Figure 2.11: Pitch schedule in below-rated operation for the IEA 15 MW RWT

As mentioned before the pitch is scheduled to maximimize power extraction. Indeed, at a given tip-speed-ratio $\bar{\lambda}$ higher than the optimal one, the steady state point is on the maximum of the curve $Cp(\bar{\lambda})$.

A part from this, minimum pitch saturation routine, can also be used to reduce the maximum rotor thrust and consequently tower base loads, with the so called peak-shaving. Rotor thrust can be defined by

$$T_r(U) = \frac{1}{2}\rho A_r U^2 C_t(\lambda, \beta), \tag{2.9}$$

where ρ is the air density, A_r is the rotor swept area, U is the wind speed and $C_t(\lambda, \beta)$ is the rotor thrust coefficient. Given the fraction of the maximum thrust that we are willing to accept, with respect to the maximum thrust without peak-shaving, the maximum C_t can be obtained, for each wind speed:

$$C_{t,max}(U) = \frac{2aT_{r,max}}{\rho A_r U^2} \tag{2.10}$$

where a$\leq$1. For all wind speeds, and so for all operational TSR, the minimum blade pitch angle β_{min} that guarantees the proper $C_{t,max}(U)$ can be scheduled. Once again, it is necessary to have a proper wind speed estimator to correctly schedule the minimum pitch. Figure 2.12 shows the comparison of the steady state pitch and yaw bearing longitudinal load with and without peak shaving.

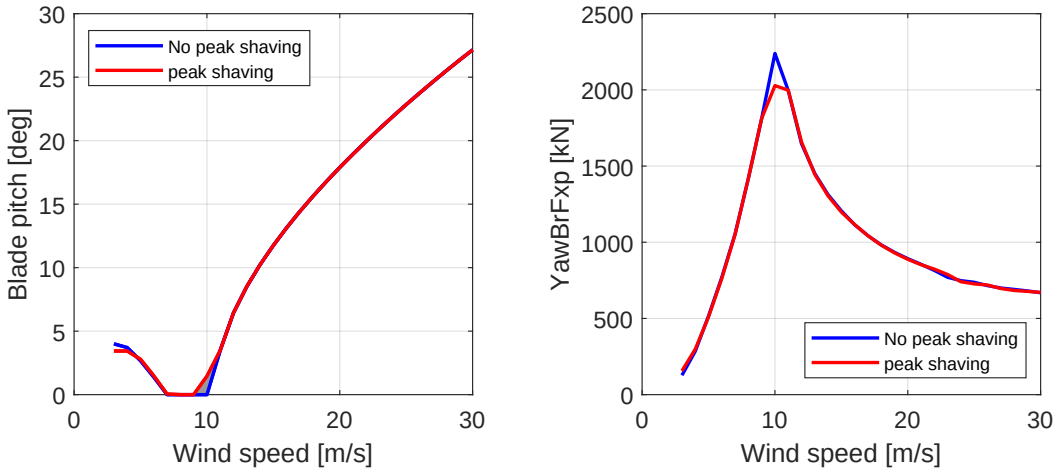

Figure 2.12: Peak shaving effect on blade pitch and yaw bearing axial load at steady state for the IEA 15 MW RWT.

It is evident the shaving effect of the pitch schedule. In this case the coefficient a was set to 0.9, and indeed, the maximum thrust with peal shaving is 90% of the maximum thrust without peak shaving. The shaded area in grey, in the blade pitch comparison,

represent all the pitch angles that, without peak shaving, would lead to thrust values higher than the acceptable.

2.1.5. Floating Feedback

The floating feedback module is added to account for floating offshore wind turbines (FOWTs). When the turbine is free to oscillate due to wind and hydrodynamic forces, a specific problem arises. If the platform oscillates in pitch direction, the motion of the nacelle increases or decreases the apparent rotor wind speed. The torque and pitch controller reacts to this apparent wind speed properly controlling the rotor speed through generator torque and blade pitch. In above-rated condition, where the rotor speed should be kept constant, when the nacelle moves towards wind, the apparent wind speed increases and the pitch controller increases the blade pitch angle in the attempt to slow down the rotor. Being the derivative of thrust force with respect to the pitch angle usually negative for the wind turbine rotor, the thrust force is reduced causing the nacelle to move further forward. The converse is true when the nacelle is moving backwards. This behavior can cause instability in the pitch motion of the platform, known as 'negative damping problem' [6].

This issue can be addressed with different methods. An idea is to reduce the bandwidth the pitch controller, such that variation in rotor speed at frequencies higher than the pitch natural frequency of the platform are not followed. Of course, this affects the performance of the controller and the power extraction and quality. Another method consists in rescale the gains of the pitch controller based on Ziegler–Nichols method as described in [7] stabilizing the system and affecting the least possible the performances of the controller.

The method implemented in ROSCO, does not influence the bandwidth of the pitch controller, and is known as parallel compensation [8]. It consists in adding a new term to the blade pitch angle reference coming from the blade pitch controller, defined as:

$$\beta_{ff} = k_{\beta_{float}} \dot{x}_{nac} \tag{2.11}$$

where $\dot{x}_{nac}$ is the nacelle fore-aft velocity and $k_{\beta_{float}}$ is the floating feedback gain. If the nacelle fore-aft velocity is properly filtered and the floating feedback gain is properly tuned, the additional term β_{ff} can stabilize the system, reducing the effect of the platform pitch motion. Figure 2.13 show a comparison between floating feedback and detuning performances in terms of rotor speed and blade pitch, for the IEA 15 MW RWT coupled with the Volturnus US floater [9].

It is evident the effect of the detuning. The reduced bandwidth of the pitch controller reduce its promptness, so the rotor speed overshoot increases notably. Also the platform

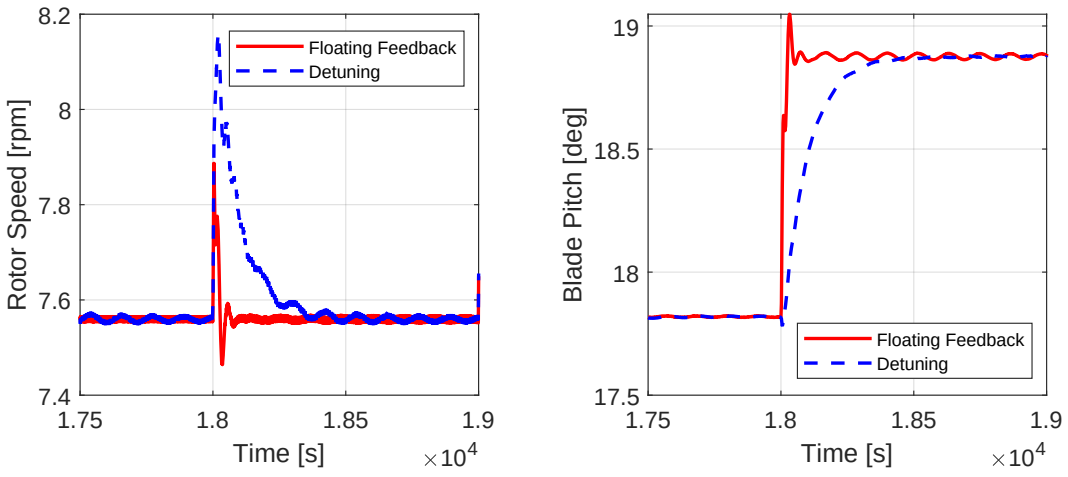

Figure 2.13: Rotor speed and blade pitch for offshore turbine, for a wind step from 20 m/s to 21 m/s. Comparison between floating feedback and detuning.

pitch and the yaw bearing load are affected, as shown in Figure 2.14.

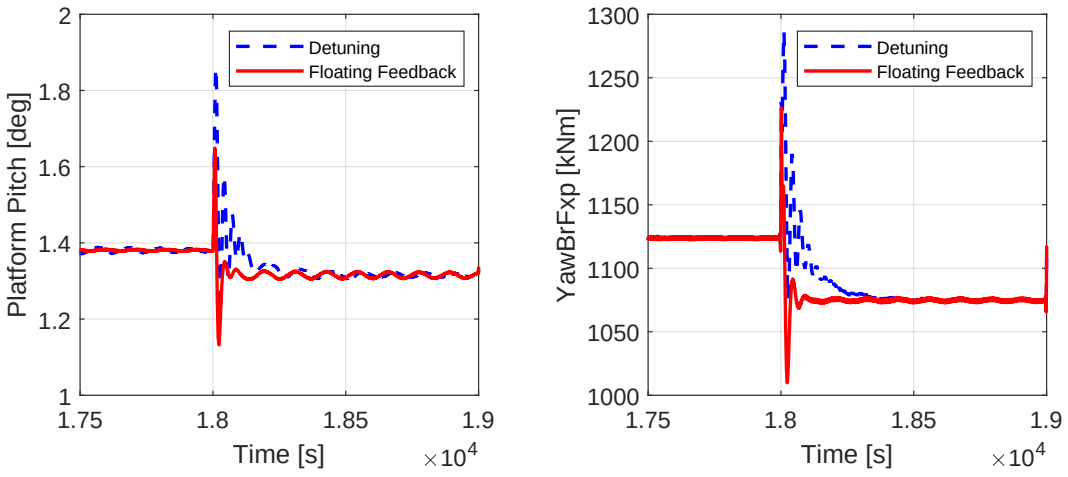

Figure 2.14: Platform pitch and yaw bearing load for offshore turbine, for a wind step from 20 m/s to 21 m/s. Comparison between floating feedback and detuning.

With the floating feedback the action on the blade pitch is prompter, this reduces the rotor thrust and its oscillations, reducing platform pitch and the load on the yaw bearing.

2.1.6. Filters

To avoid undesired oscillations in turbine operations, signals should be properly filtered. Making reference to figure 2.1, it can be observed that different signals are filtered in different parts of the block diagram, where the filters are indicated by the blocks labelled

as LPF (Low-Pass-Filter). Signals are properly filtered to avoid undesired and unpredicted oscillations that the controller is not designed to reject, and that would be amplified. Moreover, this ensures a smooth control action. In ROSCO first- and second-order low-pass filters, a first-order high-pass filter, and a notch filter are available. The first- and second-order low pass filters are formulated as:

$$LPF_{1^{st}}(s) = \frac{\omega_f}{s + \omega_f} \qquad LPF_{2^{nd}}(s) = \frac{\omega_f^2}{s^2 + 2\xi_f\omega_f + \omega_f^2} \tag{2.12}$$

The cut-off frequency ω_f and the damping ratio ξ_f of the filter, have to be tuned according to different variables to which the filter is applied. For instance, the frequency of the filter for the rotor speed is set to the first torsional frequency of the drivetrain, and the same filter is used for the blade pitch.

The first order-high pass filter is formulated as

$$HPF_{1^{st}}(s) = \frac{s}{s + \omega_f} \tag{2.13}$$

while the notch filter is formulated as

$$F_{Notch}(s) = \frac{s^2 + 2\omega_f\xi_{f1} + \omega_f^2}{s^2 + +2\omega_f\xi_{f2} + \omega_f^2} \tag{2.14}$$

The notch-filter is used to remove a specific frequency from a signal. Tuning the variables ξ_{f1} and ξ_{f2}, defines how much the filter attenuates the selected frequency and how much the nearby frequencies are altered.

Combining the high pass filter with a low pass filter and the notch filter the floating filter is built. For this filter the cut-in frequency of the high pass filter is placed usually at 0.01 rad/s, the cut-off frequency of the low pass filter at the platform's first fore–aft natural frequency, and the notch filter is placed at tower fore–aft frequency. All the filters are then discretized for the implementation, using the simulation time step as sample time and the bi-linear transformation. Figure 2.15 shows an example of a floating filter, highlighting the platform and the tower fore-aft frequencies.

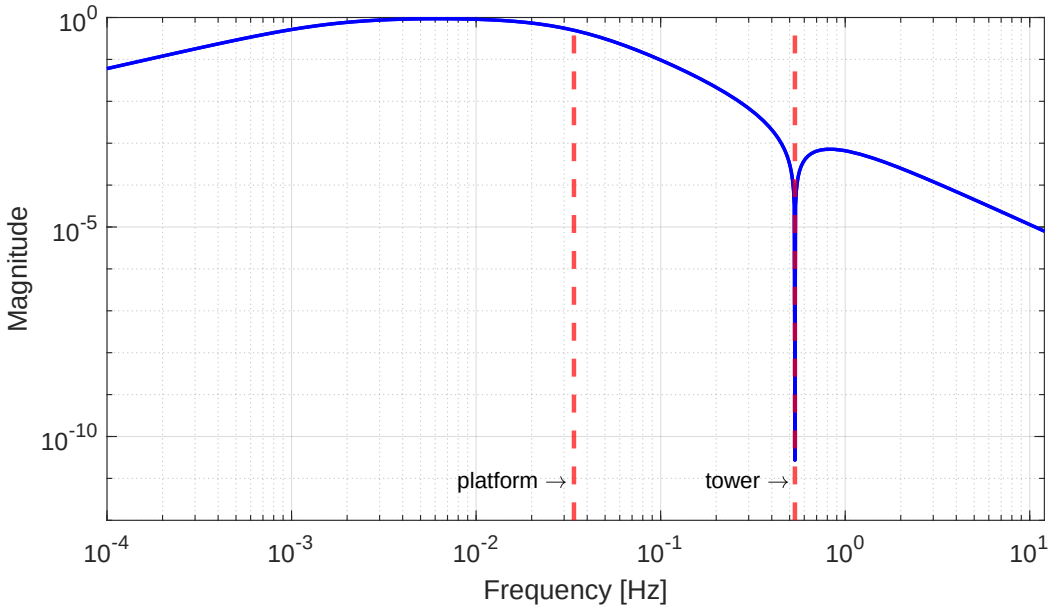

Figure 2.15: Magnitude of the floating feedback filter

3 | IEA 15 MW Reference Wind Turbine

The International Energy Agency 15 MW Reference Wind Turbine [10] has been developed by NREL and DTU, to serve as a reference for the new generation of floating wind turbines. Reference wind turbines have grown in importance in the last years, serving principally two roles. First, they serve as an open design benchmark that can be used to explore new solutions. Second, being publicly available, they allow the collaboration between industry and external researchers. The choice for the size of the reference wind turbine has been made by looking at the average size of the installed offshore wind turbine, and by analyzing the trend of growth in power of these turbines. In 2020 the average rated power of the new installed wind turbines in Europe was 8.2 MW [11], with some full scale prototypes already at test reaching 14 to 15 MW, such as the Siemens Gamesa SG 14-222 DD [12]. Therefore, the reference wind turbine should be above 10 MW but below 20 MW, to avoid the need for aggressive technology innovations. These motivations lead to the effort in the design of the IEA 15 MW RWT. The turbine is of Class IB with a rotor diameter of 240 m, and a hub height of 150 m. The turbine was developed for offshore applications with a monpile configuration. Table 3.1 shows the key parameters of the model.

The controller provided for the IEA 15 MW RWT is ROSCO, already presented in chapter 2. A numerical OpenFAST model of the reference wind turbine is publicly available on https://github.com/IEAWindTask37/IEA-15-240-RWT, allowing to simulate the system. Details about OpenFAST software will be given in section 4.2.1.

Figure 3.1, shows the steady state operating points for the IEA 15 MW RWT, obtained through OpenFAST simulations, with TSR-tracking and constant torque generator control logic.

Figure 3.2, shows the the trajectory imposed by the controller on the $C_p(\lambda, \beta)$ surface. It is evident the effect of the minimum pitch saturation, as already mentioned in section 2.1.4. In region 3, the trajectory does not follow the maximum C_P locus, since the rotor speed is fixed and the goal is to limit the power extraction to the rated value.

To verify the controller behavior, the system has been simulated subjected to wind

Parameter	Value	Units
Power rating	15	MW
Rotor orientation	Upwind	-
Number of blades	3	-
Cut-in speed	3	m/s
Cut-off speed	25	m/s
Rated wind speed	10.59	m/s
Rotor diameter	240	m
Airfoil series	DTU FFA-W3	-
Hub height	150	m
Drivetrain	Direct drive	-
Design tip-speed ratio	9	-
Maximum rotor speed	7.56	rpm
Minimum rotor speed	5	rpm

Table 3.1: Key parameters for the IEA 15 MW RWT.

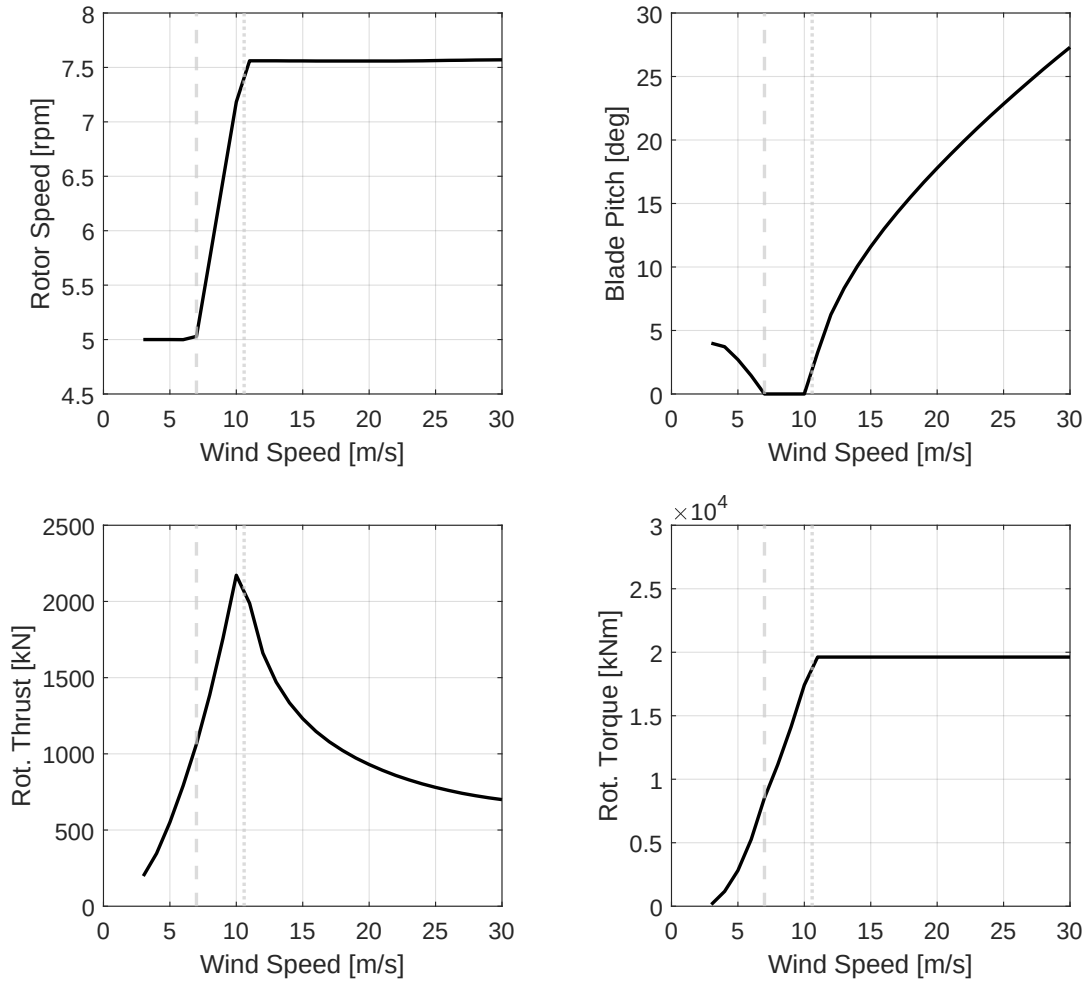

Figure 3.1: Steady state operating points for the IEA 15 MW RWT.

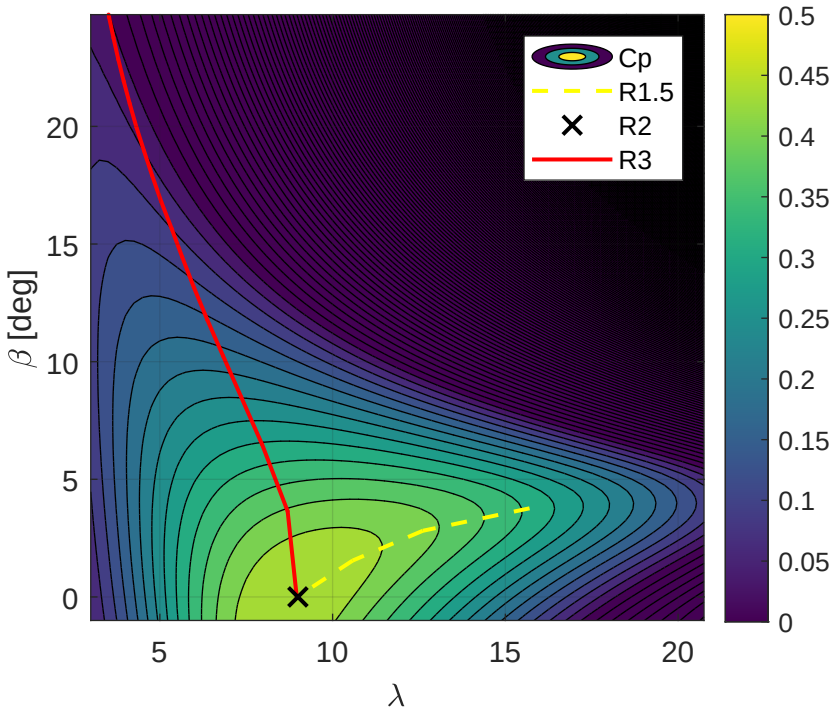

Figure 3.2: Control trajectory on the $C_p(\lambda, \beta)$ surface for the IEA 15 MW RWT.

speed steps, from 3 m/s to 30 m/s. At each step the wind speed increases of 1 m/s in 0.1 s, and the step duration has been set equal to 50 s, enough for the system to reach a steady state condition. Table 3.2 summarizes the principal ROSCO modules used for the simulations.

Controller Module	Flag	Meaning
Torque controller	2	TSR-tracking + constant torque
Pitch controller	1	Pitch controller active
Pitch saturation	1	Maximum power extraction at low wind speeds
Set-point smoother	1	Set-point smoother active

Table 3.2: Controller modules used in the step wind simulations for the IEA 15 MW RWT.

Figure 3.3 shows the result of the simulations. It can be observed that the rotor speed presents a not negligible overshoot in correspondence of the wind step. This is due to low inertia of the rotor causing high rotor over-speed when the wind speed increases. Despite this, the overshoot is still acceptable.

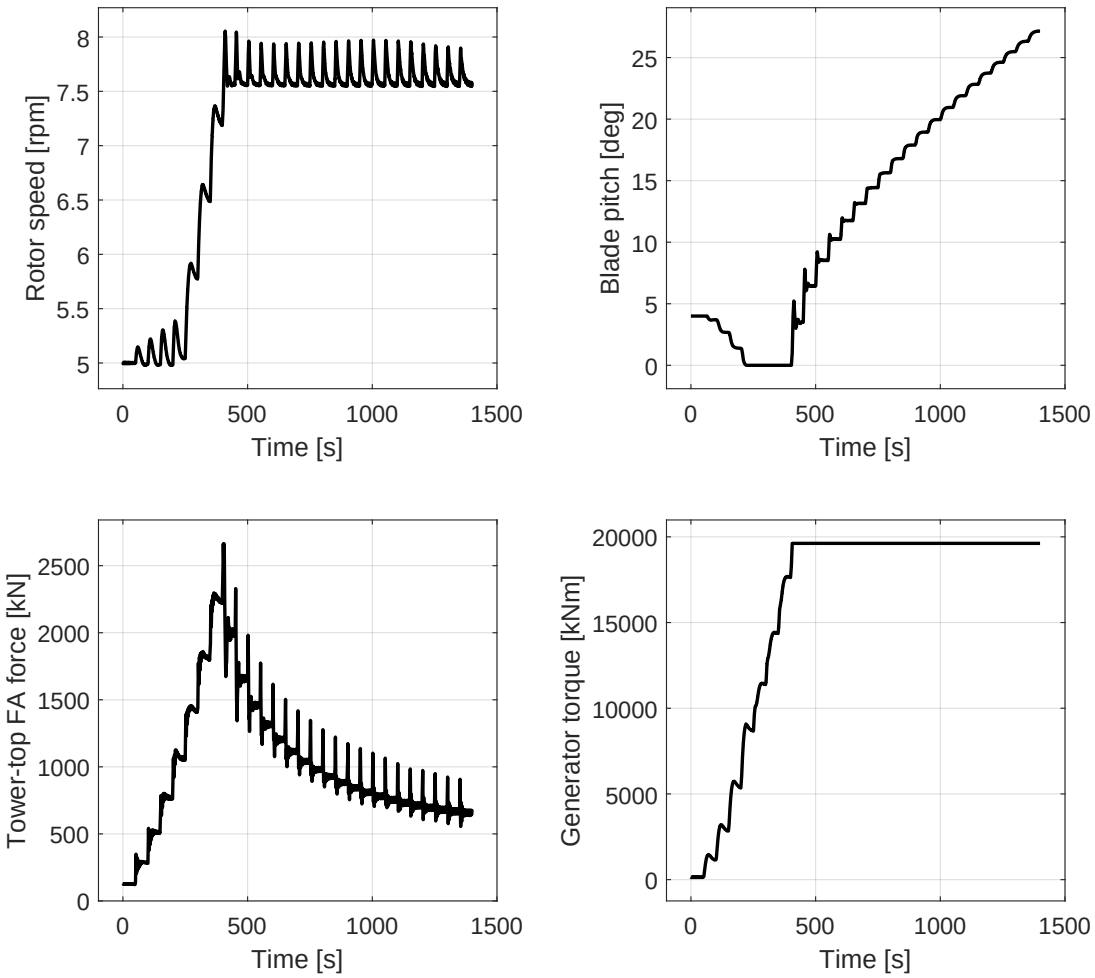

Figure 3.3: IEA 15 MW RWT response to wind speed steps.

4 | Polimi 15 MW WTM

In this chapter the Polimi 15 MW Wind Turbine Model (WTM) is described. The model is a 1:100 scaled prototype of the IEA 15 MW RWT. First the aerodynamic design of the model is described, then the numerical model implementation is presented.

4.1. Rotor Aerodynamic Design

Usually, in wind tunnel tests, the Froude similitude is guaranted, which means that the model has the same Froude number as the full-scale prototype. Froude number is a non dimensional quantity defined as:

$$F_r = \frac{U}{\sqrt{gL}} \tag{4.1}$$

Froude number represent the ratio between inertia and gravitational forces and is of particular importance in structures where the weight affects the characteristic of the structure itself, for example its overall stiffness. Defining the length scale as:

$$n_l = \frac{L_{full-scale}}{L_{model-scale}} \tag{4.2}$$

the other scales are obtained accordingly thanks to dimensional analysis:

$$n_v = \sqrt{n_l} \qquad n_M = n_l^3 \qquad n_t = \sqrt{n_l}. \tag{4.3}$$

Using the scale factors defined above would be good if only the effect of the platform of the offshore wind turbine was under investigation, where a consistent part of the overall stiffness comes from weight. However, in wind tunnel tests, the aerodynamic forces are of utter importance. It is well proven that the Reynolds number plays an important role in the aerodynamic of a body immersed in an airflow. Reynolds similitude implies that the Reynolds number of the model should match the one the full-scale prototype. In order to achieve this we need to impose that:

$$n_v = 1/n_l. \tag{4.4}$$

This is in contrast with Froude similitude, so a choice has to be taken.
During the design of the model used in the experimental tests, neither the Froude or Reynolds similitude has been respected. The choice was driven by the necessity to exploit at maximum the 'Politecnico di Milano Wind Tunnel', and focusing on the model aerodynamics, so trying to respect as much as possible the Reynolds similitude.

The length scale factor was chosen to have the largest possible model, ensuring an acceptable blockage ratio, while the velocity scale factor was chosen to have the largest possible flow speed, according to the performance of the wind tunnel.

The resulting scale factors are reported in Table 4.1.

Scale factor	Definition	Value
Lenght	n_l	100
Velocity	n_v	3
Time	$n_\mathrm{t} = n_\mathrm{l}/n_\mathrm{v}$	100/3
Frequency	$n_\omega = n_\mathrm{v}/n_\mathrm{l}$	3/100
Mass	$n_\mathrm{m} = n_\mathrm{l}^3$	100^3
Force	$n_\mathrm{F} = n_\mathrm{l} n_\mathrm{m}/n_\mathrm{t}^2$	100^3

Table 4.1: Scale factors for the PoliMi 15 MW turbine model

To overcome the limitations on Reynolds similitude the blades were specifically designed to match the performance of the IEA 15 MW RWT, in terms of thrust and force coefficients. In particular, since the model is used for investigating a floating system, the thrust matching is of utter importance, because it influences the floating dynamics more than torque. In order to achieve this the procedure described in [13] was used.

Since in wind tunnel testing the Reynolds number is much lower than in the full scale prototype, using the same airfoils as the IEA 15 MW RWT, would lead to poor aerodynamic efficiency at model scale. For this reason low Reynolds airfoil profile SD7032 was used. Than the model is designed in order to ensure the same lift distribution along the entire blade span between the model and the full scale reference. In particular, the chord length and the blade twist were optimized with the aim of matching lift distribution and its variation with the angle of attack along the the entire blade span. Differently from [13] the matching of the first flap-wise natural frequency was not ensured, so no particular optimization of the blade cross-section relative thickness distribution was carried on. Figure 4.1 shows the lift and drag coefficients and the aerodynamic efficiency versus the angle of attack at different Reynolds number for the generic profile used for the Polimi 15 MW WTM.

It can be observed that lift coefficient dependency on Reynolds number is low, while

for drag coefficient the dependency is higher. This leads to a reduction in aerodynamic efficiency C_L/C_D at low Re numbers, that can affect the aerodynamic performances of the model at low wind speeds.

Looking at figure 4.2 it can be observed that the efficiency is maximum for C_L near 1, for all Re number higher than 30000.

It is important to notice that, following the aerodynamic design presented in [13], only lift force is directly controlled, while the drag force is the one that comes from the blade at the end of the design process. Being the rotor torque influenced both by lift and drag, the aerodynamic torque that the rotor generates is not fully controlled.

Defined the aerodynamic properties of the blades, power and thrust coefficients of the rotor can be experimentally measured and numerically computed. Power coefficient C_p and thrust coefficient C_t were measured in wind tunnel at fixed wind speed, varying rotor speed and blade pitch angle. These coefficients were also numerically computed, simulating the same conditions in OpenFAST. Both in simulation and experimental test, the turbine controller was not operating, and rotor speed an blade pitch were fixed to the desired value. The system was tested for blade pitch angles from -6° to 24° with step of 3°, and with TSR from 2 to 10 approximately, with step of 0.3. Results are shown in figure 4.3.

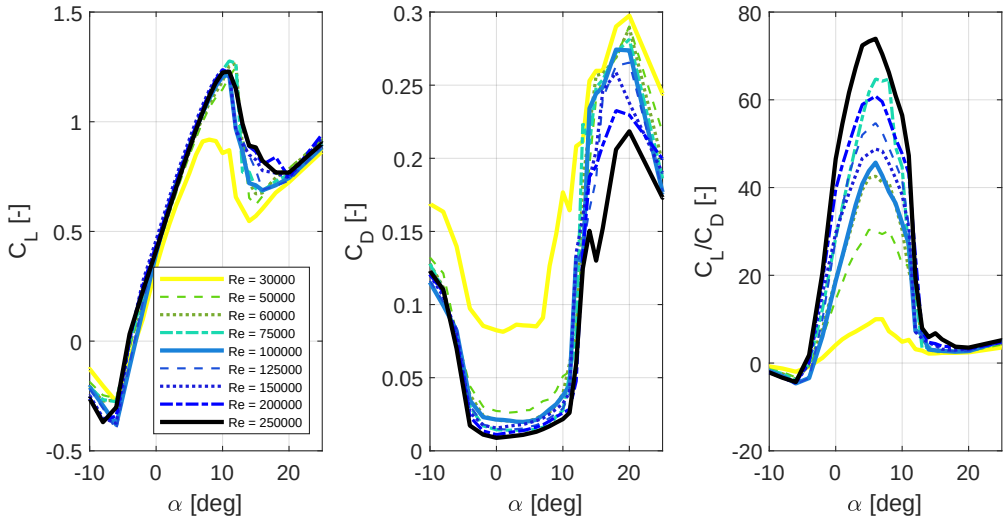

Figure 4.1: Aerodynamic coefficients of the airfoil at different Reynolds number

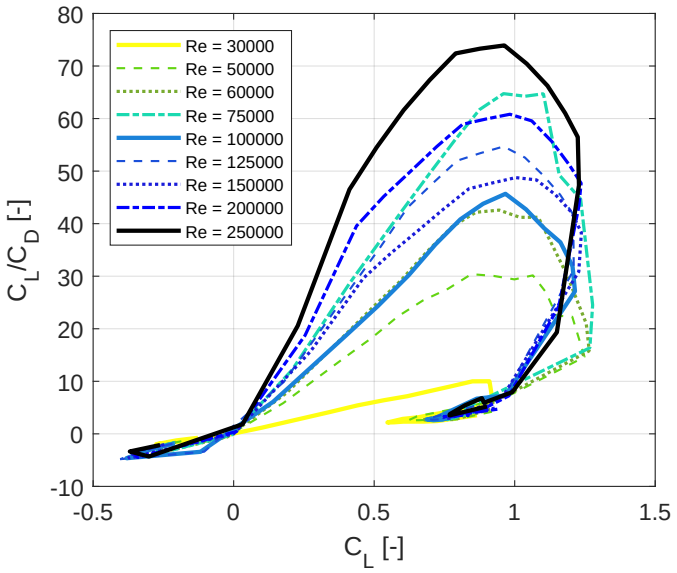

Figure 4.2: Aerodynamic efficiency versus lift coefficient

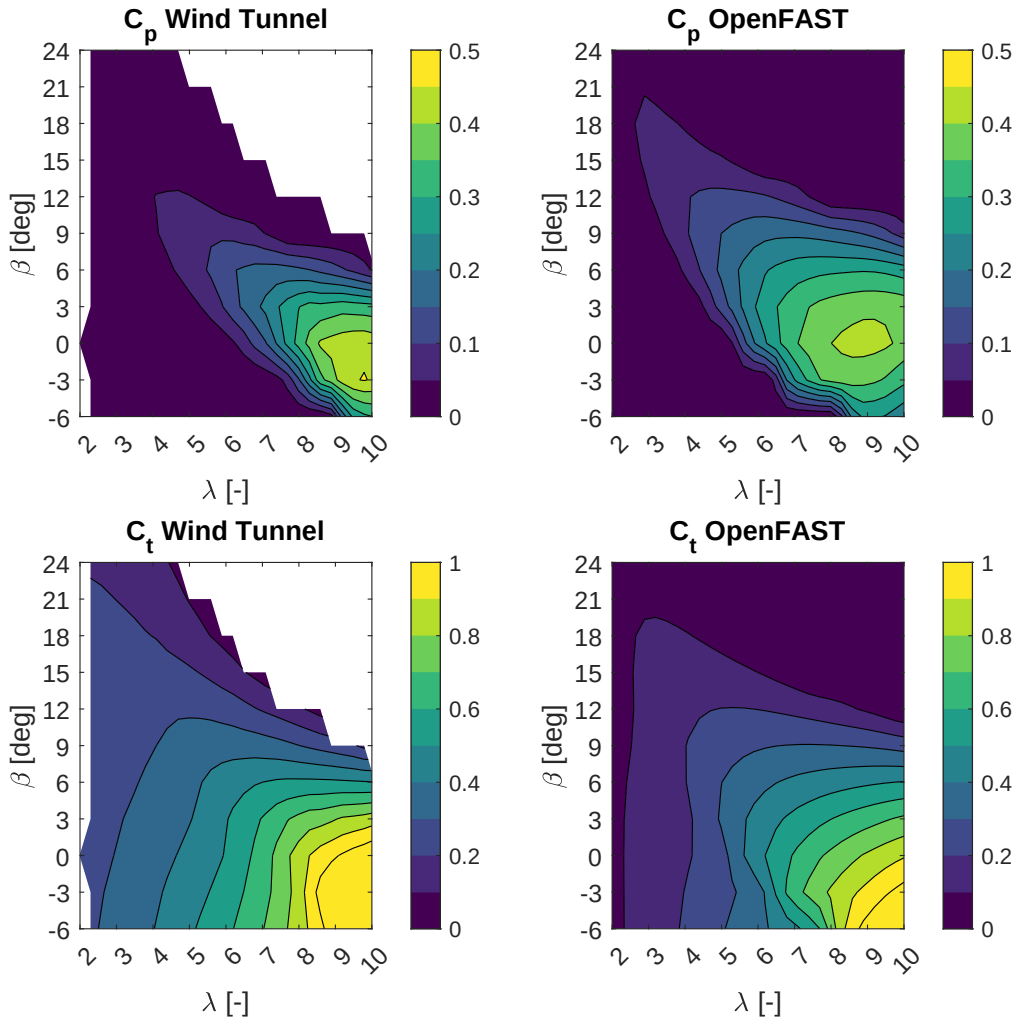

Figure 4.3: Power and thrust coefficient: Wind tunnel vs OpenFAST

It can be noticed that the C_t and to a lesser extent the maximum C_p, is higher in the experiment than in the numerical simulation. This can be partially due to blockage or to the effective blade pitch angle. This aspect will be discussed thoroughly in chapter 6, where the results of the experimental campaign will be presented.

4.2. Numerical Model

In order to simulate the response of the Polimi 15 MW WTM, a numerical model for OpenFAST v3.1.0 was developed. ROSCO was tuned for the numerical model and simulation was performed to verify the behavior of the system and to check the goodness of the controller.

4.2.1. OpenFAST

OpenFAST is an aero-hydro-servo-elastic open-source software used to simulate onshore and offshore wind turbine, already established in wind energy field and chosen as a simulation tool for project like LIFES50+ [14] and CoreWind [7]. The software, available at https://github.com/OpenFAST, has a modular framework. This means that computation relative to different physical domains, are performed in dedicated modules, that interacts with each other through some inputs and outputs. It is relevant to mention some of this domains in relation to the built model:

- ElastoDyn [15] [16]: is the module dedicated to structural computations. In this module the physical characteristics of the turbine and the degrees of freedom of the system that will be active during the simulation are defined. A multi-body approach is used to compute the rigid motion of the system, while the response due to flexible modes is based on polynomial mode-shapes defined in advance. The Polimi 15 MW numerical model is a rigid model and only the degree of freedom of the generator (or rotor) is active for onshore simulations, while for offshore simulation also the platform pitch is active.
- AeroDyn [17]: in this module the aerodynamic loads are computed using the blade element momentum theory. Here are defined the properties of the airfoils of the blade and the model for its aerodynamics, that was a steady model, that accounts also for the wake effect.
- ServoDyn [15] [16]: this module is responsible for the turbine control. Acting mainly on generator torque, blade pitch angle and nacelle yaw angle. Some simple control logics can be implemented directly in the ServoDyn input file, or can be defined separately and interfaced with OpenFAST by means of dedicated DLLs. This is the case of ROSCO, which parameters are defined in a separated input file, and through a specific DLL it interacts with OpenFAST at each time step.
- InflowWind [18]: here are defined the characteristics of the wind acting on the turbine. The wind can be laminar or turbulent, constant or varying with time and a specific wind shear profile can be defined. In this work, laminar uniform wind was mainly considered. In the case of step wind, each step is of 1 m/s and has a duration of 0.1 s.

4.2.2. Aerodynamic Up-scaling

In building the numerical model to simulate the system two choices have been taken into consideration:

1. Perform the simulations at the model scale.
2. Up-scale the numerical model to the full-scale size.

In order to have a direct comparison between the results obtained for the Polimi 15 MW WTM and the one from the IEA 15 MW RWT, the choice fell on the second option. The numerical model was built up-scaling the model, according to the scale factors reported in table 4.1. In doing this some precautions need to be taken into account. The data of the airfoils used to design the blade are available at model scale, so all the aerodynamic coefficients are tabulated for different Reynolds number computed at model scale. Up-scaling geometry and wind speed will make the Reynolds number higher according to

$$Re_{full-scale} = Re_{model-scale} \cdot n_l \cdot n_v \tag{4.5}$$

The blade sections will be operating at higher Reynolds number, so the aerodynamic performance of the airfoils will be very different from model to full scale. To avoid this inconsistency, the Reynolds number in the airfoils table has been up-scaled according to the scale factor, in order to have the same aerodynamic coefficients between model and full scale at corresponding wind speeds. If the up-scaling process is consistent, the model-scale and full-scale numerical models, should have the same power and thrust coefficient. This was checked computing C_p and C_t coefficients in the two cases and comparing them. Figure 4.4 shows a comparison between model and full scale for power and thrust coefficients versus TSR, at different pitch angles.

The curves overlaps, so it can be stated that the up-scaling process was carried out correctly from the aerodynamic point of view.

Choosing to simulate the up-scaled model, also brings advantages from the computational point of view. Indeed, if for the up-scale simulations the time step for the numerical integration is fixed to 0.01 s, for the model-scale this time step should be divided by the time scale, leading to long simulations and higher computational burden. Moreover, at model-scale the aerodynamic forces would be very low, such that the round-off errors of the software cannot be considered negligible.

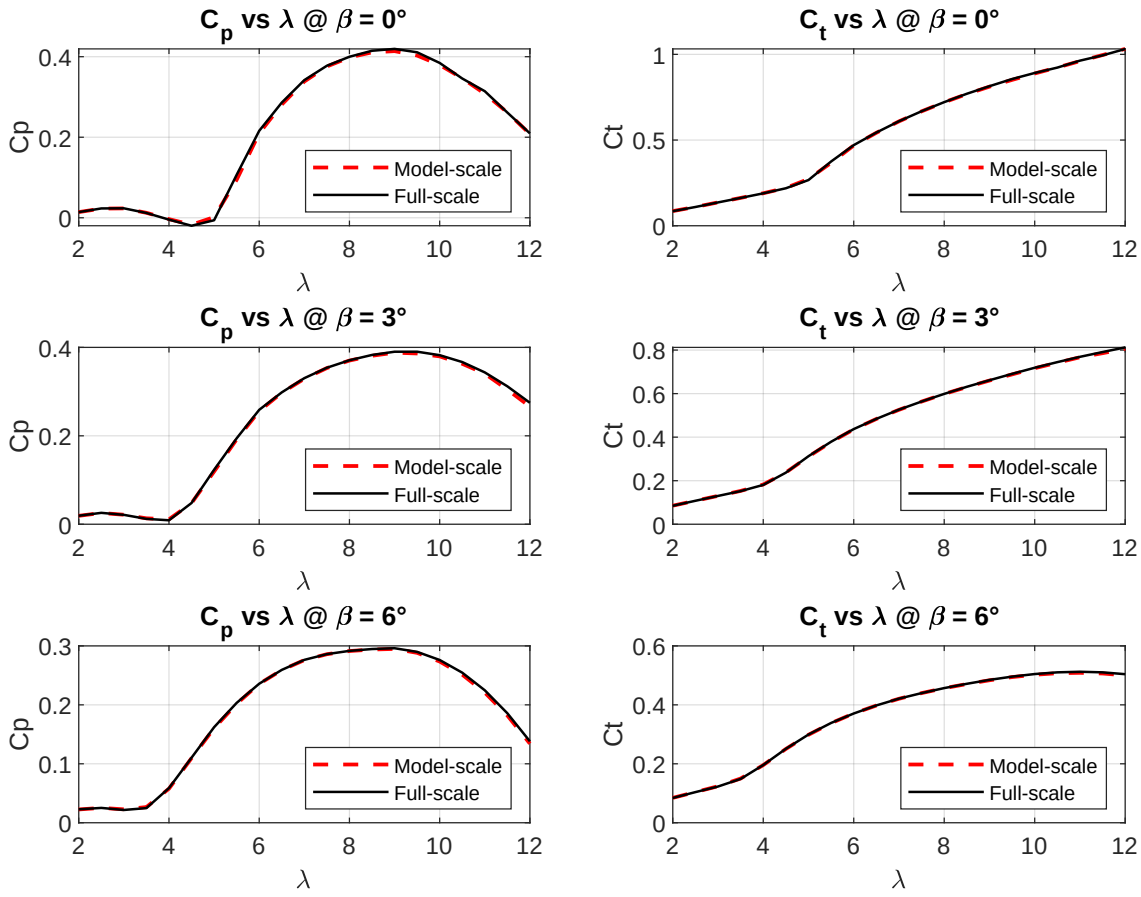

Figure 4.4: Power and thrust coefficient comparison between model and full scale.

4.2.3. Control Tuning

In order to tune ROSCO for the numerical model of the Polimi 15 MW, the tuning procedure described in [5] was followed. The procedure is model-based, and the system is approximated as a single degree of freedom system described by

$$J^* \dot{\omega}_g = N_{gb}(\tau_a - N_{gb}\tau_g \eta_{gb}) \tag{4.6}$$

where J^* is the equivalent inertia at rotor side, N_{gb} is the gearbox reduction ratio, η_{gb} is the gearbox efficiency, τ_g is the generator torque, and τ_a is the rotor aerodynamic torque defined by

$$\tau_a = \frac{1}{2}\rho A_r \frac{C_P(\lambda, \beta)}{\omega_r} U^3 \quad . \tag{4.7}$$

The rotor torque is a non-linear function of wind speed, rotor speed and blade pitch angle. Linearizing this torque around a steady state value defined by $U_0, \beta_0, \omega_{r,0}$ results

in

$$\tau_a = \tau_{a,0} + \Delta\tau_a = \tau_{a,0} + \left.\frac{\partial \tau_a}{\partial \omega_r}\right|_0 (\omega_r - \omega_{r,0}) + \left.\frac{\partial \tau_a}{\partial \beta}\right|_0 (\beta - \beta_0) + \left.\frac{\partial \tau_a}{\partial U}\right|_0 (U - U_0) \tag{4.8}$$

that in a more compact form becomes

$$\tau_a = \tau_a(U_0, \omega_{r,0}, \beta_0) + K_{\omega Q}\Delta\omega_r + K_{\beta Q}\Delta\beta + K_{UQ}\Delta U \tag{4.9}$$

where

- $\tau_a(U_0, \omega_{r,0}, \beta_0)$ is the rotor torque at the steady state condition
- $\Delta\omega, \Delta\beta, \Delta U$ are the perturbations around the steady state values of rotor speed, blade pitch and wind speed respectively
- $K_{\omega Q}, K_{\beta Q}, K_{UQ}$ are the aerodynamic torque sensitivities with respect to rotor speed, blade pitch angle and wind speed respectively.

Substituting equation 4.9 the linearized system model is obtained

$$J^*\Delta\dot{\omega}_g = N_{gb}(K_{\omega Q}\Delta\omega_r + K_{\beta Q}\Delta\beta + K_{UQ}\Delta U - N_{gb}\eta_{gb}\Delta\tau_g) \tag{4.10}$$

that can be rewritten as

$$\Delta\dot{\omega}_g = \frac{1}{J^*}K_{\omega Q}\Delta\omega_g + \frac{N_{gb}}{J^*}K_{\beta Q}\Delta\beta + \frac{N_{gb}}{J^*}K_{UQ}\Delta U - \frac{N_{gb}^2}{J^*}\eta_{gb}\Delta\tau_g. \tag{4.11}$$

Defining:

$$\begin{aligned} A(U_{op}) &= \frac{1}{J^*}K_{\omega Q}, \quad B_\beta(U_{op}) = \frac{N_{gb}}{J^*}K_{\beta Q}, \\ B_U(U_{op}) &= \frac{N_{gb}}{J^*}K_{UQ}, \quad B_{\tau_g}(U_{op}) = -\frac{N_{gb}^2}{J^*}\eta_{gb} \end{aligned} \tag{4.12}$$

where U_{op} is the operating wind speed at the steady state condition considered. The plant equation becomes:

$$\Delta\dot{\omega}_g = A(U_{op})\Delta\omega_g + B_\beta(U_{op})\Delta\beta + B_U(U_{op})\Delta U + B_{\tau_g}(U_{op})\Delta\tau_g \tag{4.13}$$

The plant linearized model depends on the steady state point and on the aerodynamic sensitivities, that can be computed starting from the C_P curve and the steady state operating points of the model. The steady state points have to be obtained by proper linearization tools or by simulating the system in OpenFAST with the controller active. Since the steady state points are an input to the controller tuing process the second option is not directly viable. As a first guess the steady state points of the IEA 15 MW was

used in order to obtain a first set of controller gains. Then with this gains the system was simulated to obtain more reliable steady state points, that were used to better tune the controller.

Aerodynamic sensitivities are shown in figure 4.5.

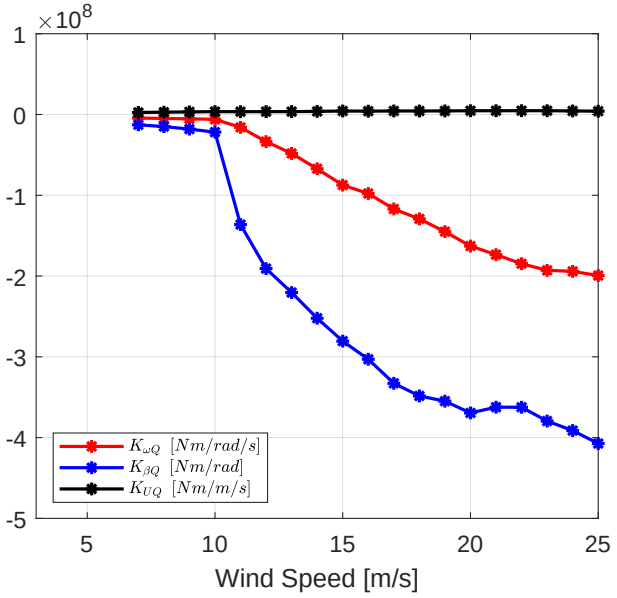

Figure 4.5: Torque aerodynamic sensitivities for the Polimi 15 MW RWT

With this premise the controller can be introduced in the plant model starting from equation 4.13. As anticipated in sections 2.1.1 and 2.1.2, torque and pitch controller are PI controllers acting on generator speed error. For the general PI controller we have

$$y = k_p u + k_i \int_0^t u \, dt \tag{4.14}$$

where the control input is $u = \Delta\omega_{g,ref} - \Delta\omega_g$, while the control output y is $\Delta\tau_g$ for the torque controller and $\Delta\beta$ for the pitch controller. Of course, since we want to follow a certain reference speed, that can be either the one defined by TSR tracking or the rated rotor speed, $\Delta\omega_{g,ref}$ is null, while $\Delta\omega_g = \omega_g(t) - \omega_{g,ref}$. Passing in Laplace domain we obtain:

$$\begin{cases} \Delta\omega_g(s)s = A(U_{op})\delta\omega_g(s) + B_{\tau_g}(U_{op})\Delta\tau_g(s) + B_\beta(U_{op})\Delta\beta(s) & \\ \Delta\beta(s) = \left(k_p + \frac{k_i}{s}\right)\left(\Delta\omega_{g.ref}(s) - \Delta\omega_g(s)\right) & pitch \\ \Delta\tau_g(s) = \left(k_p + \frac{k_i}{s}\right)\left(\Delta\omega_{g.ref}(s) - \Delta\omega_g(s)\right) & torque \end{cases} \tag{4.15}$$

Being the two controllers independent, only one of them is active at time, so substituting the control action inside the plant equation we can obtain the following transfer

function

$$\frac{\Delta\omega_g(s)}{\Delta\omega_{g,ref}(s)} = \frac{B(U_{op})\left[k_p s + k_i\right]}{s^2 + \left[B(U_{op})k_p - A(U_{op})\right]s + B(U_{op})k_i} \tag{4.16}$$

where B is either B_{τ_g} for below-rated operation or B_β for above-rated. The denominator is the one of a simple second order system that is usually written in the form $s^2 + 2\xi_{des}\omega_{des}s + \omega_{des}^2$, where ω_{des} and ξ_{des} are the desired bandwidth and damping ratio of the controlled system. Choosen these parameters, the values of the control gains k_p and k_i can be obtained and results in:

$$\begin{aligned} k_p(U_{op}) &= \frac{1}{B(U_{op})}\left[2\xi_{des}\omega_{des} + A(U_{op})\right] \\ k_i(U_{op}) &= \frac{\omega_{des}^2}{B(U_{op})} \end{aligned} \tag{4.17}$$

Being $B(U_{op})$ and $A(U_{op})$, function of the operating point of the turbine, also the control gains depend on the operating wind speed U_{op}. At the end the whole control tuning for torque and pitch controller, relies on the choice of 4 hyperparameters, that are ω_{des} and ξ_{des} for each controller.

Below-rated - Torque controller

In below-rated operation $B = B_{\tau_g}$, that is constant. Referring to figure 4.5, it can be observed that for wind speeds below the rated one, the aerodynamic torque sensitivities are more or less constant. This suggests that the dynamic of the system is not changing much with wind speed, so a gain scheduling is not necessary. It was found that fixing the gains to those found for the rated wind speed, simplify the controller implementation without affecting the performance of the system. For the variable speed torque controller the gains are computed as:

$$\begin{aligned} k_{p,vs} &= \frac{1}{B_{\tau_g}(U_{rated})}\left[2\xi_{des}\omega_{des} + A(U_{rated})\right] \\ k_{i,vs} &= \frac{\omega_{des}^2}{B_{\tau_g}(U_{rated})} \end{aligned} \tag{4.18}$$

Setting $\omega_{des} = 0.12\ rad/s$ and $\xi_{des} = 0.85$, gives good results for big flexible wind turbines, such as the IEA 15 MW RWT.

Parameter	Polimi 15 MW	IEA 15 MW RWT	Units
$k_{p,vs}$	-2905630.5	-38676765.2	$\frac{Nm}{rad/s}$
$k_{i,vs}$	-237025.8	-4588245.2	$\frac{Nm}{rad}$

Table 4.2: Gains of the torque controller for the Polimi 15 MW and the IEA 15 MW RWT

The difference in gains between the two models is significant and is mainly due to the higher rotor inertia of the Polimi 15 MW and, to a lesser extent, differences in the aerodynamic torque sensitivity with respect to rotor speed. As shown in figure 4.6, the sensitivities are very similar in below-rated region.

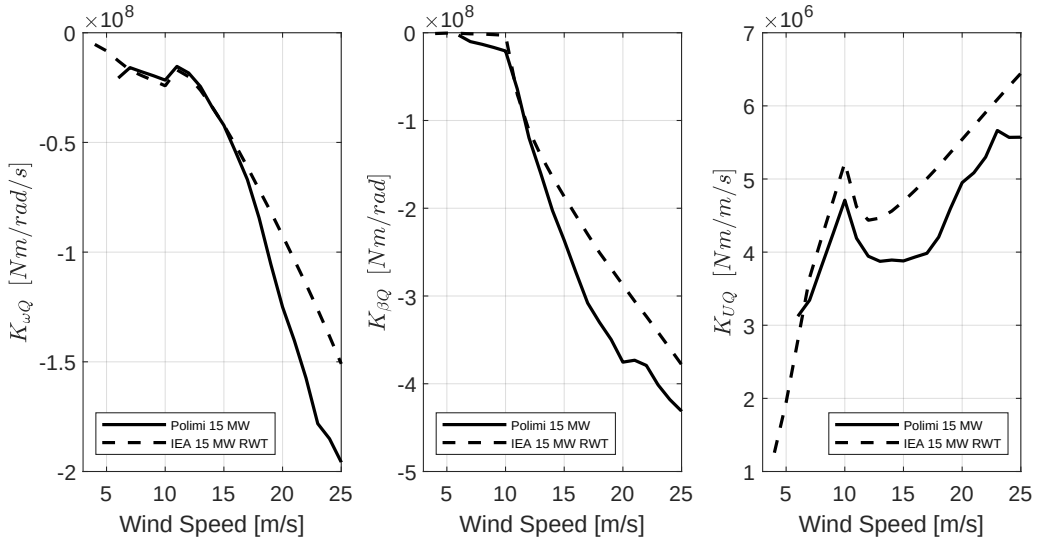

Figure 4.6: Aerodynamic torque sensitivities, comparison between Polimi 15 MW and IEA 15 MW RWT

Above-rated - Pitch controller

In above-rated condition $B = B_\beta$ and, assuming constant generator torque, $\Delta\tau_g = 0$. For wind speed greater than the rated one, the torque sensitivities with respect to rotor speed and blade pitch are both dependent on wind speed. Therefore, in order to keep constant the performance of the close loop controlled system, the control gains have to vary according to the wind speed. This results in a gain scheduling for the pitch controller, where the scheduling variable should be wind speed. However, since at each wind speed corresponds a steady state collective blade pitch angle, this latter variable can be used as scheduling variable, bypassing the problems related to the wind speed estimator.

For the variable pitch controller the gains are computed as:

$$k_{p,pc}(U) = \frac{1}{B_\beta(U)} \left[2\xi_{des}\omega_{des} + A(U)\right]$$
$$k_{i,pc}(U) = \frac{\omega_{des}^2}{B_\beta(U)} \tag{4.19}$$

As made explicit by equations 4.19, the control gains for the pitch controller depend on the wind speed, and so on the operating condition of the wind turbine. Defined ω_{des} and ξ_{des} it is possible to compute the control gains. Reasonable values of the two hyperparameters are 0.6 rad/s and 0.7 [19].

Figure 4.7 shows the control gains scheduled on the collective blade pitch angle, for the Polimi 15 MW and the IEA 15 MW RWT.

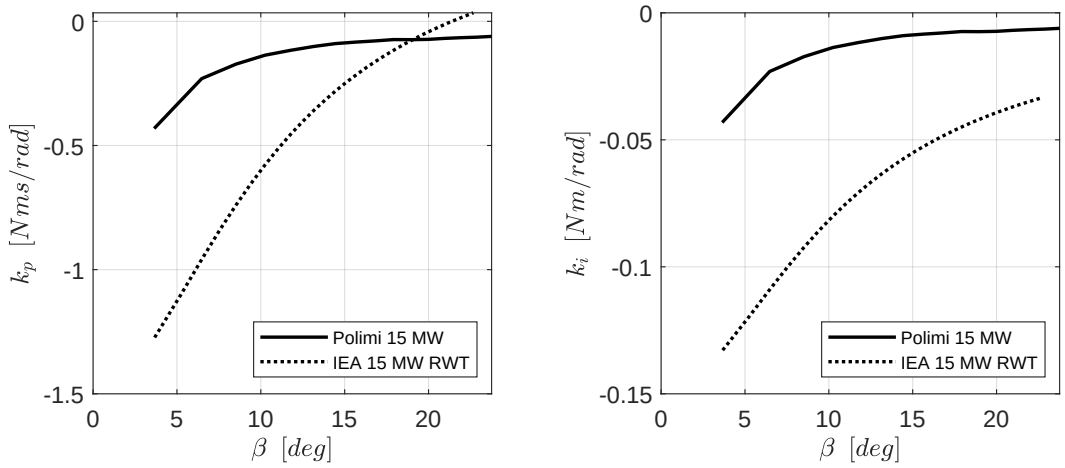

Figure 4.7: Control gains of the blade pitch controller, comparison between Polimi 15 MW and IEA 15 MW RWT.

Also for the pitch controller, the gains for the two models are significantly different. In this case differences are caused by the different rotor inertia, but also by the differences in the aerodynamic torque sensitivity with respect to pitch, that are not negligible in above-rated condition, as already seen in figure 4.6.

4.3. Simulations Results

The numerical model has been tested in OpenFAST, to validate it in comparison to the IEA 15 MW RWT, and to the verify if the tuned controller works properly.

The first check has been done in terms of steady state operating points. Figure 4.8 shows the steady state points obtained through the numerical model compared to the one

of the reference wind turbine.

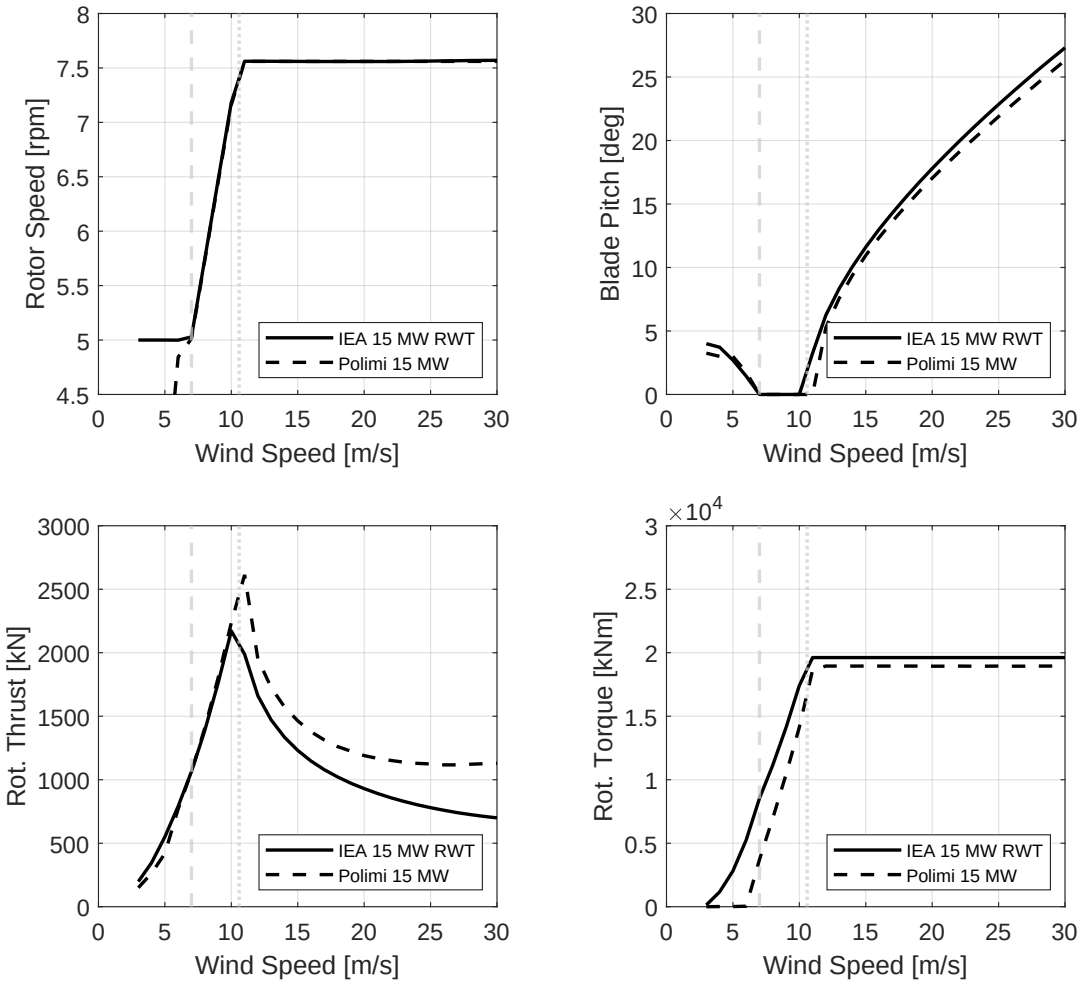

Figure 4.8: Steady state operating points of the Polimi 15 MW compared to the ones of the IEA 15 MW RWT. The grey dashed and dotted line represents the transition regions.

Steady state points have been obtained by simulation at constant laminar wind speed, with a simulation time long enough such that variations on the considered variables could be addressed as negligible.

For the rotor speed the two curves overlaps, exception made for the low wind speeds, where the Polimi 15 MW cannot reach minimum rotor speed before 7 m/s, due to the low aerodynamic efficiency at low Reynolds number. Differences in rotor torque in below-rated region can be related to the lower aerodynamic efficiency of the blade profiles. Instead, in above-rated region, the different saturation value of the torque is related to the generator efficiency. Indeed, the IEA 15 MW RTW, is designed to produce 15 MW of electrical power, accounting for a generator efficiency equal to 96.55%. Conversely, the Polimi 15 MW is designed to produce 15 MW of aerodynamic power, without accounting for a

specific generator with its own efficiency. The lower rotor torque explains even the lower blade pitch angle in above-rated region and consequently, the higher rotor thrust.

To verify the controller behavior, the system has been simulated subjected to wind speed steps, from 3 m/s to 30 m/s. At each step the wind speed increases of 1 m/s in 0.1 s, and the step duration has been set equal to 300 s, enough for the system to reach a steady state condition. The controller has the same active modules and flags as the one used for the IEA 15 MW RWT, reported in table 3.2. Figure 4.9 shows the results of the simulation.

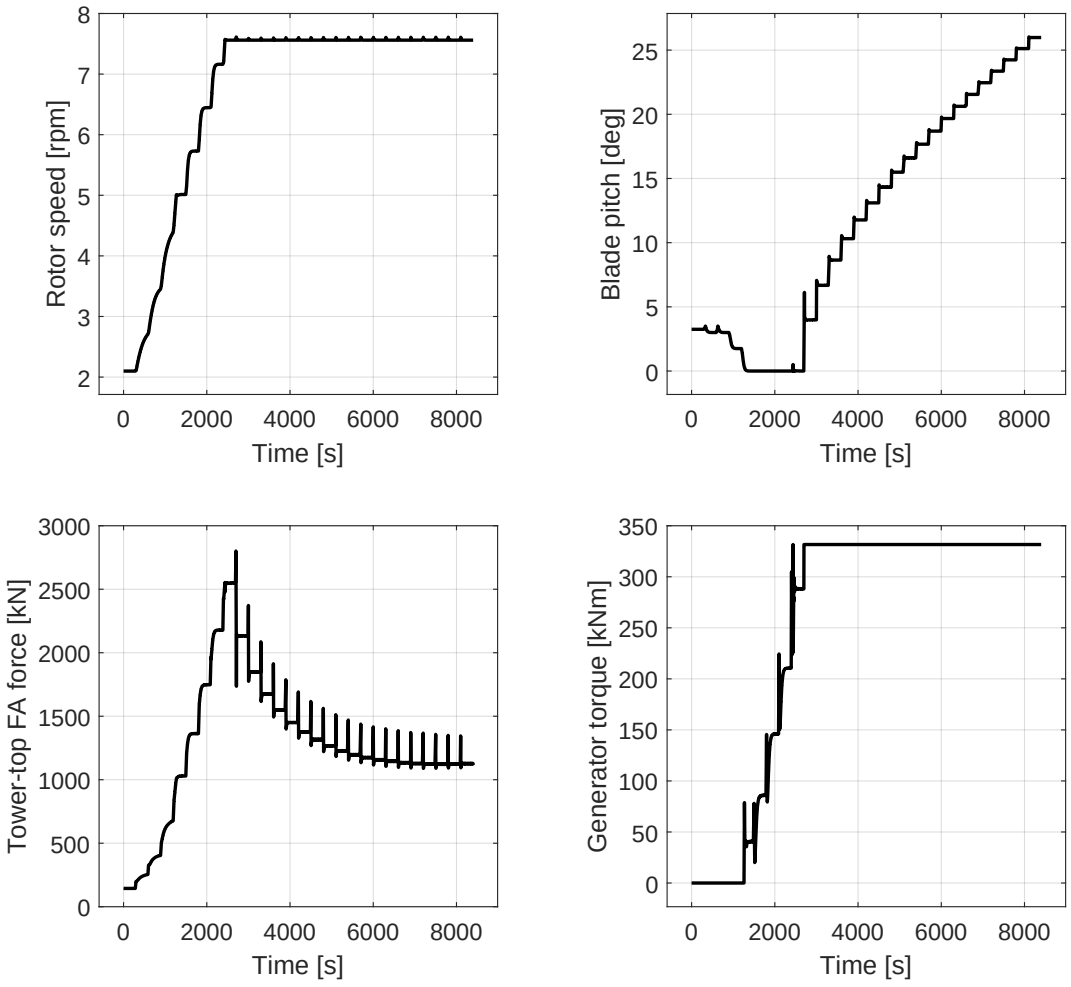

Figure 4.9: System response to wind speed steps.

It can be observed that the rotor speed appears always increasing until it reaches the 5 rpm. This is because of the minimum rotor speed imposed by the controller. Since the rotor cannot reach the minimum rotor speed of 5 rpm before a certain wind speed, due to low aerodynamic efficiency, the rotor speed seems to not reach a steady state value before that wind speed. This behavior is reflected even by the generator torque, that is

saturated to zero in the attempt to speed up the rotor. Focusing again on rotor speed, it can be observed that in correspondence of the wind step, the overshoot is very limited. This is because of the high inertia of the rotor that implies low rotor angular acceleration, that are compensated by the controller action keeping the rotor speed nearly constant. It is evident the difference with the IEA 15 MW RWT results presented in figure 3.3 , where the overshoot of rotor speed is clear at each wind step, due to the lower rotor inertia.

The peculiar behavior of generator torque in below-rated region, showed in the bottom-right sub-figure in figure 4.9, has to be discussed. As a matter of fact, the sudden oscillations of generator torque at the wind step, have repercussions on the generator power, leading to poor power quality. To better explain the causes of this trend of generator torque, is better to refer to a single wind step.
Figure 4.10 shows the results for a single wind step from 8 to 9 m/s, together with the wind speed seen by the controller.

In ROSCO the wind speed seen by the controller is the estimated wind speed, coming from the wind speed estimator, filtered by a first order low pass filter. In the presented simulation the estimated wind speed was simply the real wind speed filtered by the same first order low pass filter. The double filtering causes the trend of the filtered wind speed presented in figure 4.10. The delay introduced by this filter causes the overshoot of generator torque and the subsequent undershoot. This is because the rotor speed increases in correspondence of the wind step, but the reference rotor speed computed by the TSR tracking is in delay due to the action of the wind speed filter. Although this behavior is not optimal, reducing the filtering action will cause the reference speed to be in advance with respect to the rotor speed increase, due to the high rotor inertia. This will lead to a large undershoot of the generator torque, since the controller will try to increase rotor speed following the reference, reducing the generator power. With these settings of filter and control gains, this is the best achievable result that does not imply a loss of power. Since the goal of this work is not to optimize the ROSCO controller for the numerical model of the Polimi 15 MW, the result is accepted. Figure 4.11 shows the trajectory imposed by the controller on the $C_p(\lambda, \beta)$ surface.

Once again it can be observed that for low wind speed in region 1.5, the controller does not follow the optimal C_p curve, since the rotor cannot reach the minimum rotor speed. In region 3, that corresponds to above-rated region, the rotor speed is fixed so it is not possible to follow the maximum C_p curve. Indeed, the goal of the controller in this region is to limit the power extraction to the rated the one.

To further verify the controller behavior, the system has been simulated in more realistic conditions, under turbulent wind speed. The turbulent wind speed has been generated in TurbSim [20], with a turbolence intensity of 13%, modeling the wind profile with a

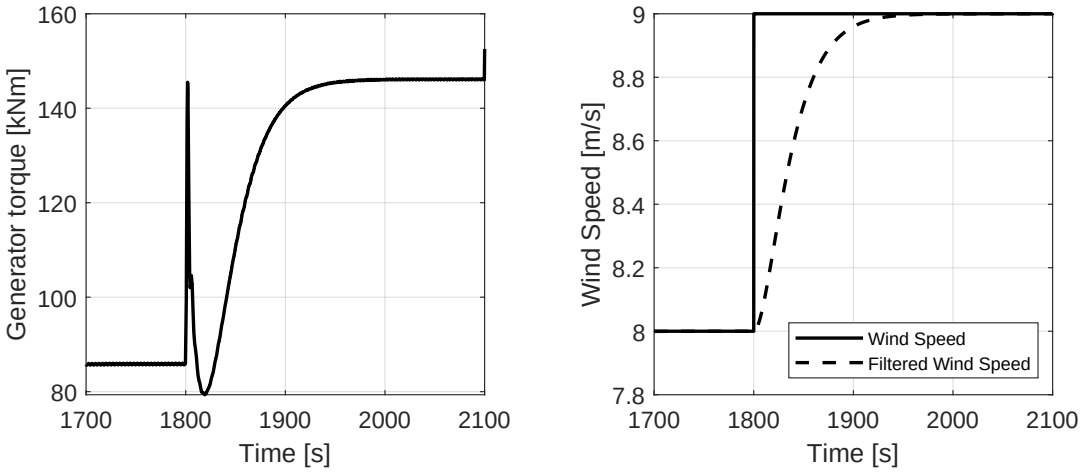

Figure 4.10: Generator torque response to a wind step from 8 m/s to 9 m/s (left), wind speed and filtered wind speed seen by the controller (right).

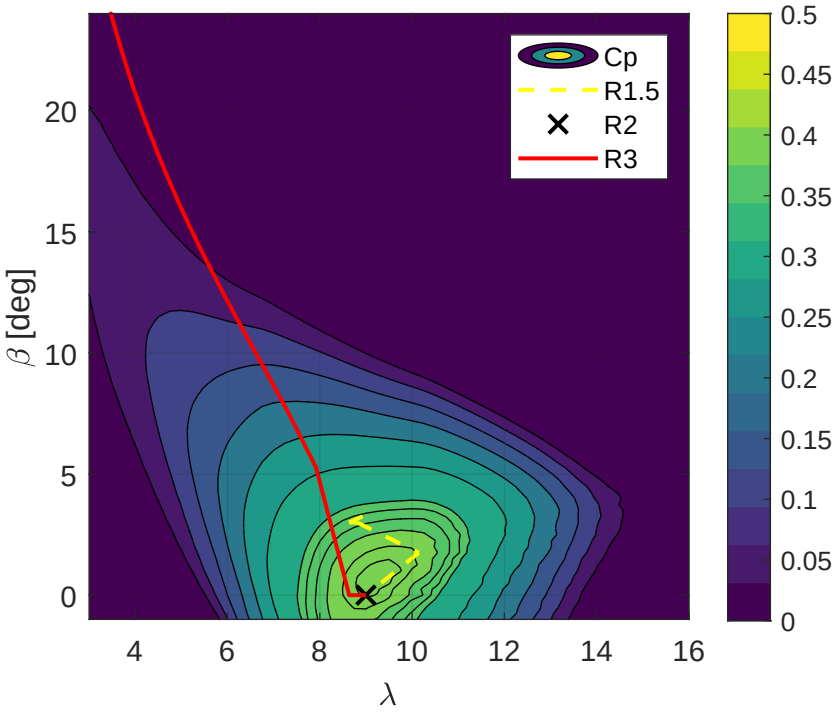

Figure 4.11: Control trajectory on the $C_p(\lambda, \beta)$ surface for the Polimi 15 MW.

power law with an exponent equal to 0.14. The mean wind speed at the hub height has been set equal to 17 m/s. Figure 4.12 shows the wind speed together with the estimated wind speed by the Extended Kalman Filter (EKF).

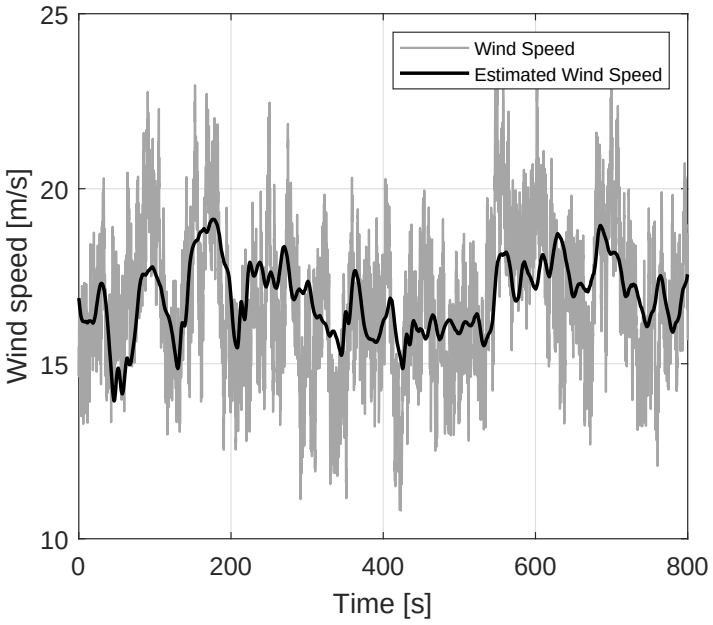

Figure 4.12: Turbulent wind speed and estimated wind speed with the EKF.

The EKF correclty estimates the wind speed in terms of mean value, filtering out the high frequency fluctuations, that can affect the controller performance.

Figure 4.13 shows the simulation results. The controller correctly keeps the rotor speed around the rated value, with very limited variations. In doing so, the oscillations in torque are very marked, leading to high oscillations in the generator power. This happens because of the large oscillations in wind speed due to the high turbulence intensity. The wind speed arrives at values close to the rated wind speed, in a region where the set-point smoother affects the transition from below- to above-rated. If the generator torque is not saturated the torque controller is active and reacts to the variations of rotor speed according to the control logic.

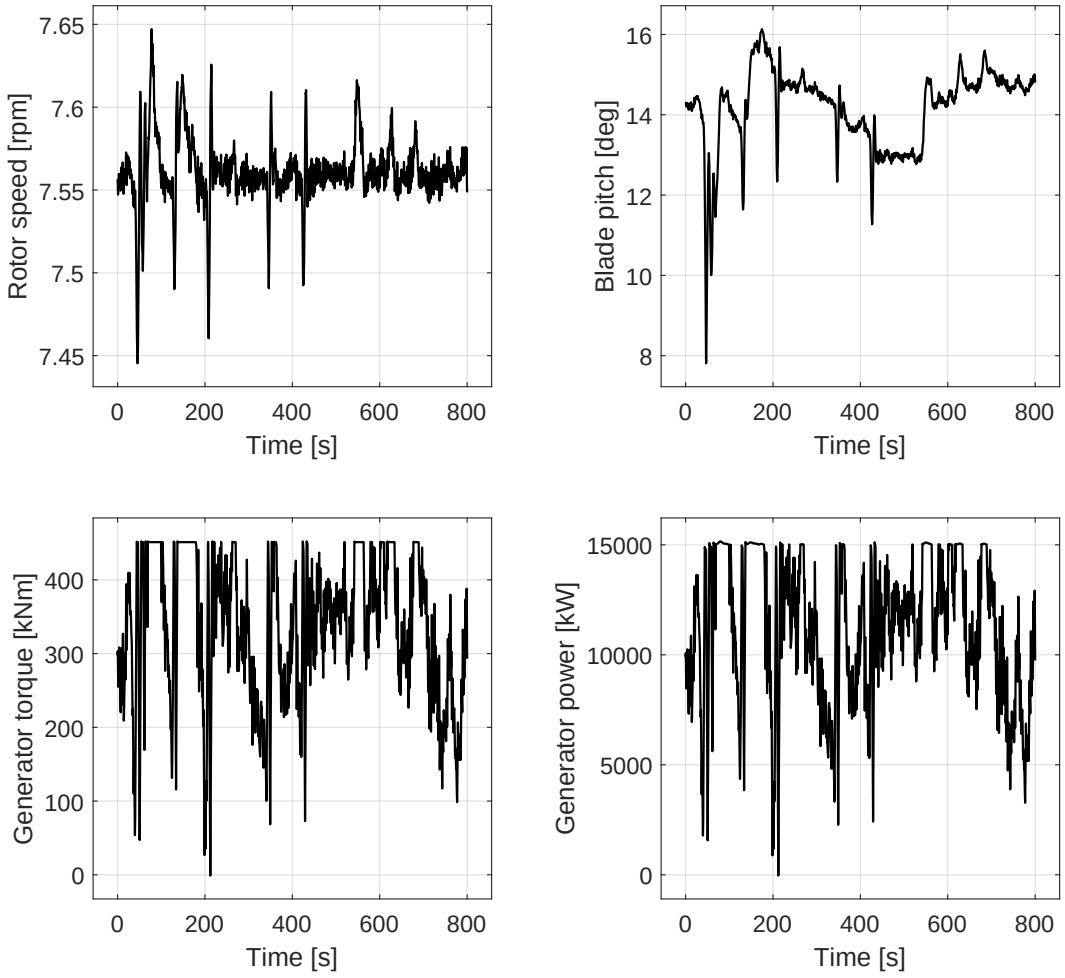

Figure 4.13: System response under turbulent wind speed.

5 | Experimental setup

In this section the experimental setup used in the wind tunnel testing is described. An overview of the system is depicted in Figure 5.1. The system consists of the wind turbine

Figure 5.1: Experimental setup overview

model mounted on an hexapod that simulates the motion of the system in water in offshore configuration. A pitot tube is placed 7.15 meters ahead the turbine and at the same height as the hub, measuring the dynamic pressure of the incoming wind. A more in depth description of the different parts of the system, and of the wind tunnel facility, is given in the following subsections.

5.1. Wind Tunnel Facility

The wind tunnel is a specific tool designed to solve aerodynamic problems involving fluid-structure interaction, using scaled models and not full-scale prototypes. Wind tunnels can be categorized according to the flow speed and the tunnel geometry:

- Flow-Speed: the flow-speed is compared to the speed of sound defining the Mach number:
$$M_a = \frac{V_{flow}}{V_{sound}} \tag{5.1}$$
According to the Mach number wind tunnels are classified as: subsonic (Mach $<$ 0.4), transonic (Mach up to 1.3), supersonic (Mach up to 4-5) and hypersonic (Mach $>$ 5).
- Geometry: the wind tunnel can be open-circuit and closed-circuit. In open-circuit configuration the air flow is continuously taken directly from the outside at atmospheric pressure. In closed-circuit configuration the same air circulates in the wind tunnel, allowing a better control on the flow pressure.

The wind tunnel facility of "Politecnico di Milano", in italian "Galleria del Vento Politecnico di Milano " (GVPM), is a closed-circuit subsonic wind tunnel, which layout is depicted in figure 5.2.

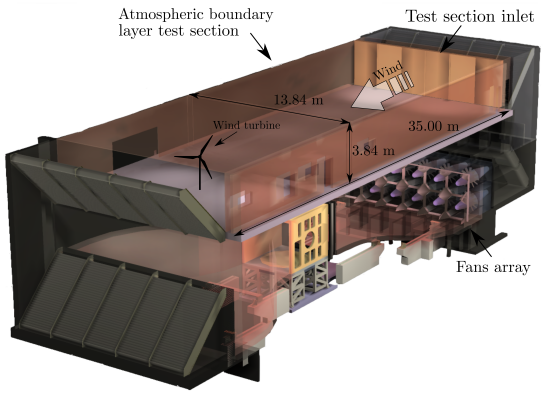

Figure 5.2: GVPM layout.

Two tests section are present, the high speed one located in the bottom of the closed-circuit, and the boundary layer section located in the upper part. All the wind tunnel tests presented in this work have been carried out in the atmospheric boundary layer section, given the dimension of the used model. The cross-section of the boundary layer section has a width of 13.84 meters and a height of 3.84 meters. The dimensions of the section are important in comparison to the model dimensions. In particular, is important the ratio between the model area and the wind tunnel sectional area, called blockage ratio

and computed as in the following equation:

$$b = \frac{S_{model}}{S_{section}} \tag{5.2}$$

If the blockage ratio is above 1%, the flow distortion introduced by the reduced area caused by the presence of the model is not negligible and a correction in the flow speed is required.

5.2. Wind turbine model

The wind turbine model is a 1:100 scaled version of the IEA 15 MW RWT. Figure 5.3 shows a more detailed picture of the wind turbine model. The tower is made of steel, while the blades are made of carbon fiber.

Figure 5.3: Wind Turbine Model.

The gross properties of the model are reported in table 5.1.

Parameter	Value	Units
Rotor radius	1200	mm
Tower height	1500	mm
Hub height	2190	mm
Hub diameter	180	mm
Rotor inertia	0.279	kgm^2
Generator inertia	$6.44 \cdot 10^{-6}$	kgm^2
Optimum TSR	9	-
Rated rotor speed	254	rpm
Rated wind speed	3.53	m/s

Table 5.1: WTM properties.

Between the tower and the nacelle a 6-component load cell is mounted, allowing to measure forces in the direction x,y,z, and the correspondents moments. The sensor is an ATI mini 45, with a SI-580-20 calibration. Its performance are reported in table 5.2. In particular, it measures the thrust force F_x and the rotor torque M_x, The other force components are used by the "Hardware in the loop (HIL)" numerical model to correctly move the hexapod (more details in Section 5.3).

	Range (N or Nm)	Resolution (N or Nm)
F_x,F_y	580	1/4
F_z	20	1/4
M_x,M_y	20	1/188
M_z	20	1/376

Table 5.2: ATI sensing performance

5.2.1. Mechatronics

For what reguards the power electronics needed to actuate and control the wind turbine model, a similar implementation developed in [21] has been used. In this work the component relevant from the control point of view are briefly described. For a more complete description of the mechatronic implementation of the turbine model, please refer to the reference.

Rotor Actuator: The variable speed control is ensured by an electric motor, wich is a brushless *Maxon EC-4pole 30*, connected to a small pulley by means of a *Maxon Planetary*

Gearhead GP 32 HP. The main characteristics of the motor and the transmission are reported in Table 5.3. The motor is connected to the rotor by a belt drive, ensuring a reduction ratio of 2, so the total transmission ratio from motor to rotor is 42:1. The rotor angular speed is measured through a *Maxon Encoder MR Type ML* encoder, directly coupled with the motor itself.

Parameter	Value	Units
Nominal voltage	24	V
Nominal speed	16100	rpm
Nominal torque	94.6	mNm
Nominal current	7.58	A
Max efficiency	89.4	%
Nominal reduction	21:1	-

Table 5.3: EC motor technical data

The EC motor is driven by a *Maxon ESCON 50/10* PWM servo controller. Two versions of this device have been used, which differs from the embedded closed loop control. One features a speed control (closed loop) and a subordinated current (torque) control; vice versa, the other features a current control (closed loop) and a subordinated speed control. The first takes as analogue input an external speed reference and is used in test with imposed rotor speed, while the latter takes a torque reference as an external analogue input that is used to actively control the rotor. The first, is used for imposed rotor speed tests, such as the characterization of the rotor in terms o C_p and C_t coefficients. The second, is used to actively control the rotor speed by acting on the generator torque, according to the implemented control logic.

Blade-pitch Actuators: The pitch angle of each blade is individually controlled. Each blade is connected on the pitch axis to a *Harmonic Drive RSF-5B-30-E050-C* servo-actuator. Each pitch actuator is driven by a *Maxon EPOS 24/2* motion controller that features an embedded closed loop controller. This controller can be tuned using "EPOS Studio" and, in particular, the maximum rotational speed of the pitch actuator motor can be set. This allows to avoid undesired vibration of the blades around the pitch axis, but it also changes the transfer function between the desired pitch and the actual pitch of the blades, affecting the controller performances.

Since the pitch control is a collective pitch control, only the pitch of one of the three blades is measured and used as a control variable by the controller.

5.2.2. Controller Implementation

The ROSCO based controller for the turbine model was implemented in Simulink®. Not all modules available in ROSCO were implemented. In particular, only torque control, blade pitch control, set-point smoother and pitch saturation modules was considered. Figure 5.4 shows an overview of the implemented controller.

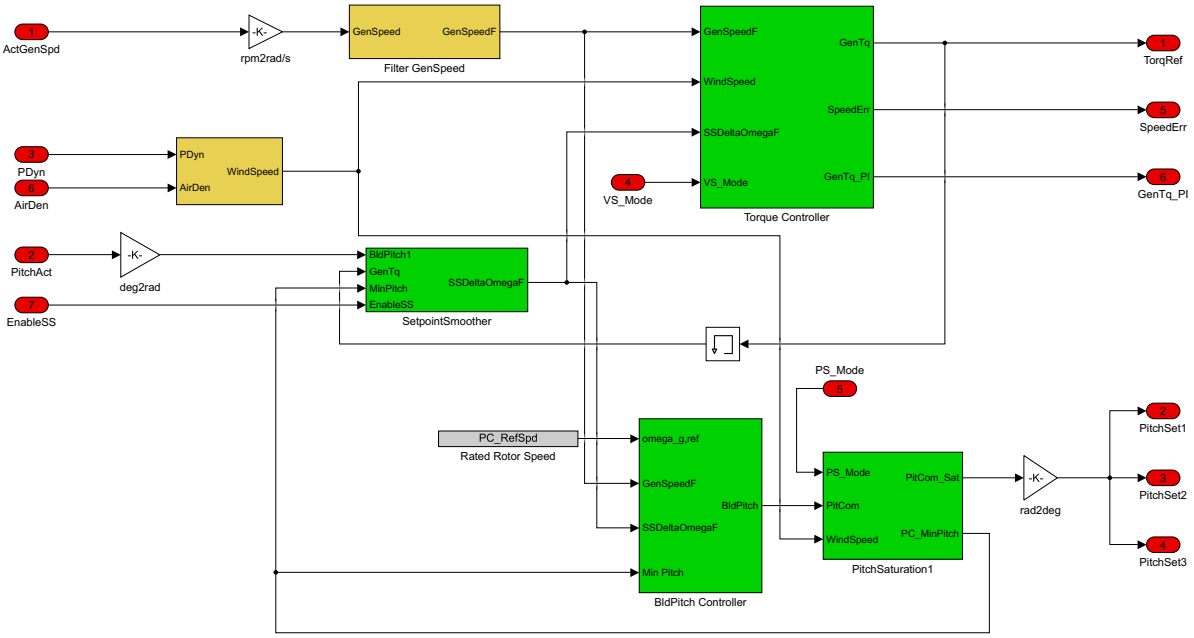

Figure 5.4: Overview of ROSCO based controller implemented on the WTM.

In the Simulink model, in-ports represent either an acquired signal, a manual switch or a variable. In particular "ActGenSpd" and "PitchAct" are the acquired rotor speed and collective blade pitch respectively. "PDyn" and "AirDen" are the dynamic pressure and the air density measured from the wind tunnel sensors, that are manually inserted to compute the wind speed. "Enable SS", "VS_Mode" and "PS_Mode, are used to activate the set-point smoother module, change between constant torque or constant power operation, and activate pitch saturation module respectively. The out-ports represent either a reference signal computed by the controller for the actuator, or a signal that can be digitally acquired for debug purposes. In particular, "TorqRef" is the torque reference signal for the generator, "PitchSet1-2-3" is the reference blade pitch angle. In the torque controller module, only TSR tracking was implemented and only constant torque operation mode was used.

The simulink model is than compiled trough NI VeriStand®, in order to make it compatible with the used hardware. To allow the wind turbine model to work continuously and

autonomously during wind tunnel testa, an Embedded Control and Monitoring (ECM) system is required, which base is guaranted by a PXI (PCI eXtensions for Instrumentation).

5.3. HexaFloat

The floater displacements and the hydrodynamic loads are numerically integrated by the the HIL numerical model, and fed to the floating system by the actuator of the HexaFloat. The HexaFloat is a 6 degrees of freedom (surge, sway, heave, roll, pitch and yaw) parallel kinematic robot. The hybrid/HIL test methodology is described in [22]. In this work the HexaFloat was used to perform imposed platform motion tests, to investigate how the controller reacts to imposed motion in a floating configuration. Figure 5.5 shows the configuration of the HexaFloat.

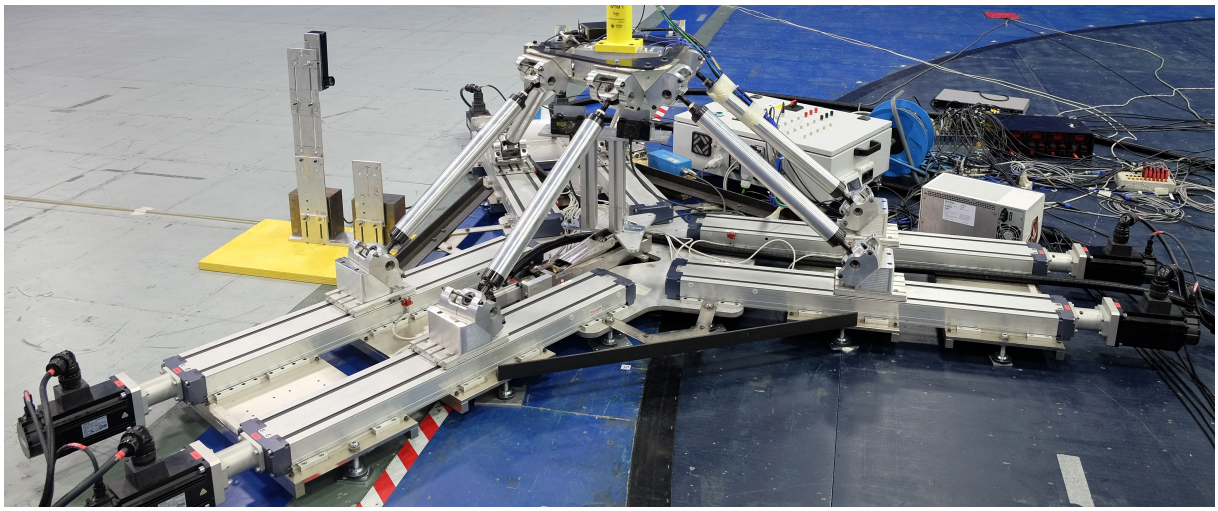

Figure 5.5: HexaFloat configuration

The reference displacement signals coming from the numerical model of the robot are acquired. To check if the robot is actually reproducing the reference signals, 3 lasers are used to measure the physical displacement of the robot. The laser placed in the front of the robot (left side of the figure above) measures the displacement in surge direction, while two lasers placed under the robot connection to the WTM, measure the vertical displacement of the plate and then derive the pitch angle of the platform.

6 | Experimental results

In this chapter the experimental results obtained during the wind tunnel tests on the Polimi 15 MW WTM are presented and discussed. All experimental tests was conducted in smooth flow condition at constant wind speed. The dynamic pressure acquired by the pitot tube placed upfront the turbine is not directly fed in the controller loop, but the measured pressure is manually inserted in the controller to have a constant estimated wind speed, avoiding undesired noises introduced by the sensor. Experimental results are compared to the numerical simulations performed on the numerical model presented in section 4.2, where simulations have been carried out in order to be as representative as possible of the experimental tests. Results are also compared to the numerical simulations of the IEA 15 MW RWT. Since the numerical simulations are performed on full-scale model, the comparison is carried on either at model-scale, down-scaling the numerical results, or at full-scale up-scaling the experimental results.

The experimental campaign was divided in two categories: static test and imposed motion tests, that will be presented separately.

6.1. Static Tests

During static tests, the goal was to characterize the wind turbine model from the static point of view, so to obtain the experimental power and thrust coefficients, and the steady state values at different wind speeds. Steady state values of thrust and torque at different wind speed are important to understand the static loads that the turbine undergoes during its life. Moreover, static values of blade pitch and rotor speed, are important to characterize the wake of the turbine downwind, to investigate the reciprocal position of the turbines in a wind farm.

The experimental power and thrust coefficients (C_p and C_t), have been already presented in figure 4.3. The curves are obtained at a fixed wind speed of the wind tunnel of 4 m/s, varying collective blade pitch angle and rotor speed. In this test the controller is not implemented, since we want to keep blade pitch and rotor speed constant, to characterize the rotor power and thrust coefficients against λ and β.

To check the steady state operating points the turbine model has been tested at four

different wind tunnel flow speeds, summarized in table 6.1.

#	Wind speed	Units
1)	2.48	m/s
2)	4.13	m/s
3)	5.02	m/s
4)	5.80	m/s

Table 6.1: Tested wind speeds

Of the four tested wind speeds, only one is in the below-rated region. Because of the velocity scale factor, to test wind speed in the below-rated region, the speed of the flow in the wind tunnel would be very low. At these low speeds, the limited Reynolds number causes a drop in the aerodynamic efficiency of the blades of the wind turbine model, and the rotor cannot generate torque nor power.

In each test the signals are recorded for an acquisition time of 60 seconds, than the mean value of each signal is reported as the steady state value. This mean values are than up-scaled to full-scale to be comparable with the numerical models results. Signals considered at this stage were the rotor speed, the blade pitch angle, the rotor torque and the rotor thrust.

Figure 6.1 shows the results of the static tests compared to the steady state operating points of the IEA 15 MW RWT and the ones of the numerical model of the Polimi 15 MW. The experimental points match quite good the numerical ones. Uncertainties are due to statistical dispersion between the different tests, sensors systematic errors, and wrong parameter estimation. Considering the top-left plot in figure 6.1, it can be noticed that the experimental rotor speed is always higher than the steady state point predicted by the numerical simulations. This can be related to a systematic error of the encoder used to measure the rotor speed. Focusing on blade pitch depicted in the top-right plot of figure 6.1, the experimental results are in good agreement with the numerical ones, both for the IEA 15 MW RWT and for the Polimi 15 MW, exception made for the below-rated points, in particular for the tests labelled as "TN 205-208". This discrepancy can be explained by the errors introduced in the setting of the zero pitch angle of the blades. For instance, the zero blade pitch angle was searched and set manually by imposing the zero twist section of the blade to be parallel to the direction of the incoming wind. In this way, determining the real blade pitch angle at what is considered as zero is difficult, in particular in below-rated region, where the blade pitch controller is not active.

For what regards rotor thrust and torque the agreement between experimental and numerical results is still acceptable, but differences have to be investigated. In below-rated region the matching is good, a part for the test "TN 205-208", for the same problem on

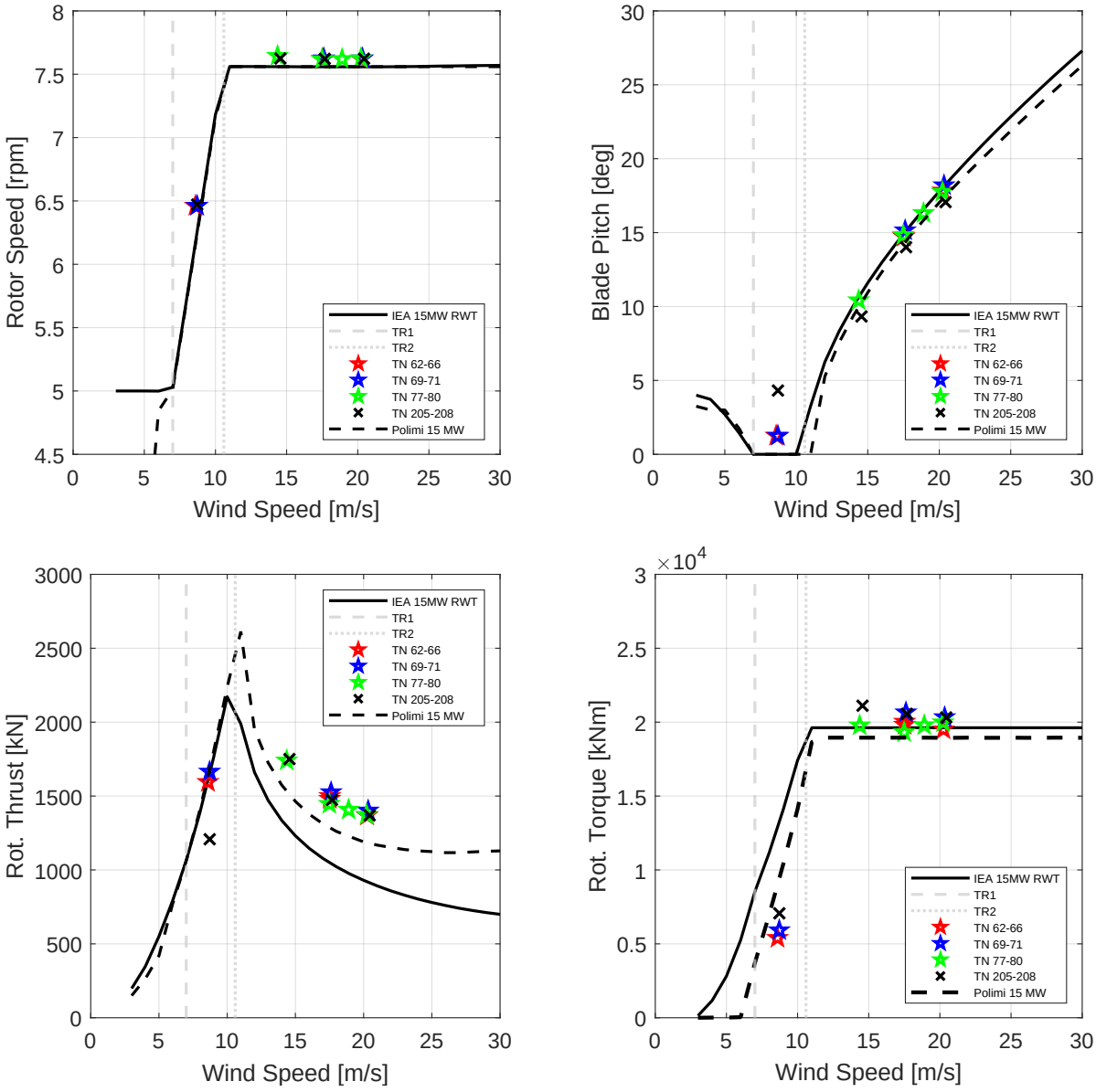

Figure 6.1: Experimental results of static tests, up-scaled and reported on the steady state curves of the IEA 15 MW RWT and of the numerical model of the Polimi 15 MW.

pitch angle already mentioned. The good matching in below-rated region also confirms the consistence of the aerodynamic up-scaling presented in section 4.2.2. In above-rated region the differences are noticeable. For these two parameters, the uncertainties on the estimation of some parameters can have a huge impact. Indeed, the efficiency of the gearbox estimated as 73.5%, is susceptible of errors. An error of 5% on this parameter can change significantly the steady state values of rotor torque and blade pitch angle, and consequently of the rotor thrust. This is shown in figure 6.2, where the steady state operating points of the numerical model of the Polimi 15 MW are reported for the case of gearbox efficiency reduced or incremented of 5%.

Increasing or decreasing the gearbox efficiency in the numerical simulation changes the rotor torque. That happens because the saturation torque imposed by the controller remains the same, but the resultant resistant torque applied to the rotor changes according to gearbox efficiency. Changing the rotor torque produces a variation in the blade pitch angle. It can be noticed that the numerical results closer to the experimental ones, are those obtained for a gearbox efficiency reduced of 5% with respect to the baseline value. Therefore, the real gearbox efficiency was probably lower than the estimated one.

Other source of uncertainty is the efficiency of the generator, that changes again the resistant torque at the rotor. No estimation was present on this quantity, therefore in the numerical model the generator efficiency is assumed unitary.

Moreover, other reason of discrepancies is the fact that rotor torque and thrust are actually measured in the reference system of the load cell mounted between the tower and the nacelle. Theoretically this aspect should be negligible, if the forces acting on the rotor were only thrust and torque. Since the rotor may not be perfectly aligned with the flow direction, some other forces may arise that the load cell measures and that contribute to the total thrust and torque.

Steady state points have been checked also in terms of power and thrust coefficients. Results are presented in figure 6.3.

Also for the non dimensional coefficients the agreement between experimental and numerical results is good, in particular in above-rated region. In below-rated the Reynolds effect is evident and leads to a reduced power coefficient.

It can be concluded that the model reproduces good enough the steady state values of the IEA 15 MW RWT in above-rated condition. In below-rated region the results are quite different in terms of torque and power coefficient, mainly due to the Reynolds effect. This is correctly reproduced by the numerical model.

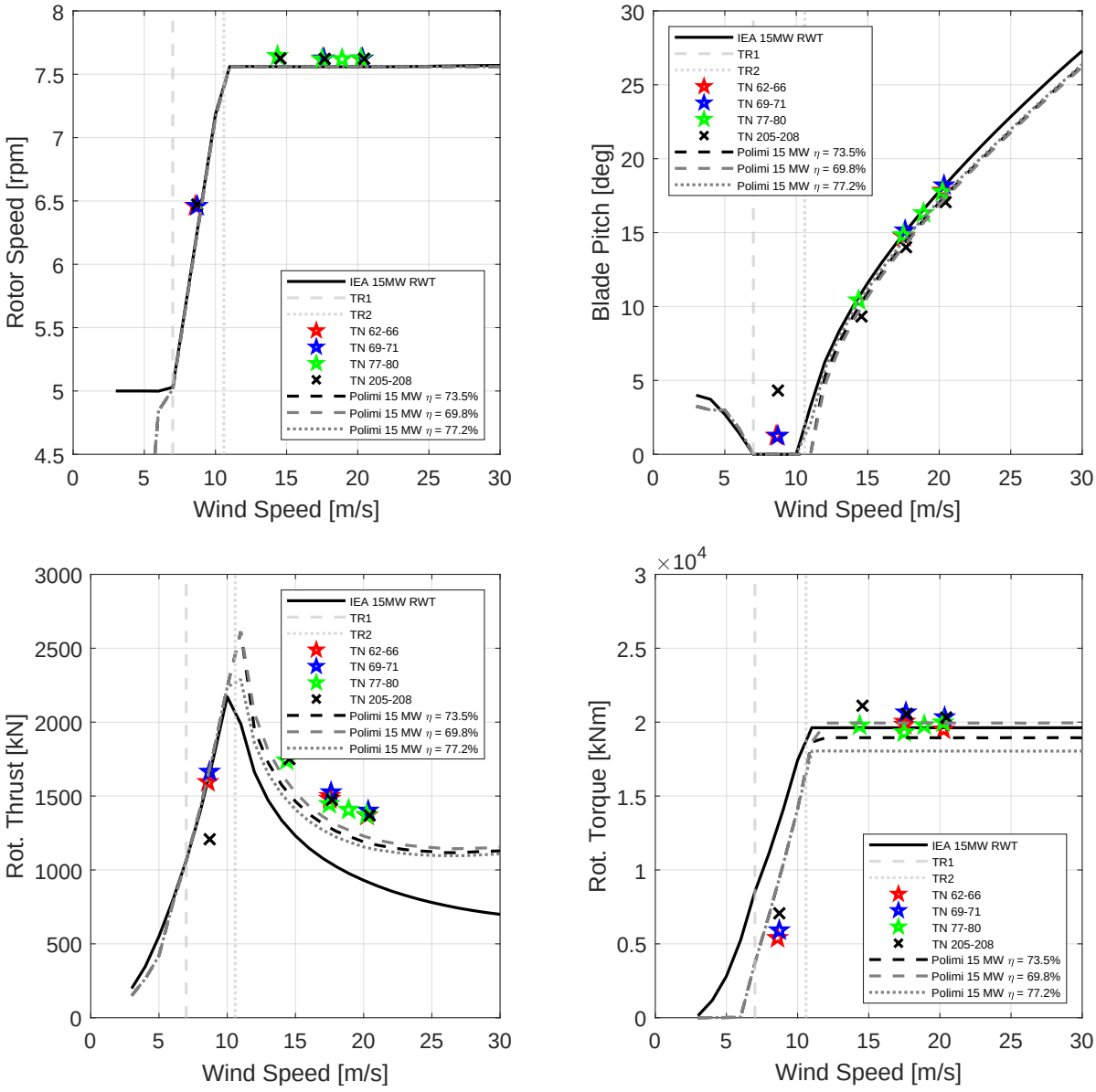

Figure 6.2: Experimental results of static tests, up-scaled and reported on the steady state curves of the IEA 15 MW RWT and of the numerical model of the Polimi 15 MW.

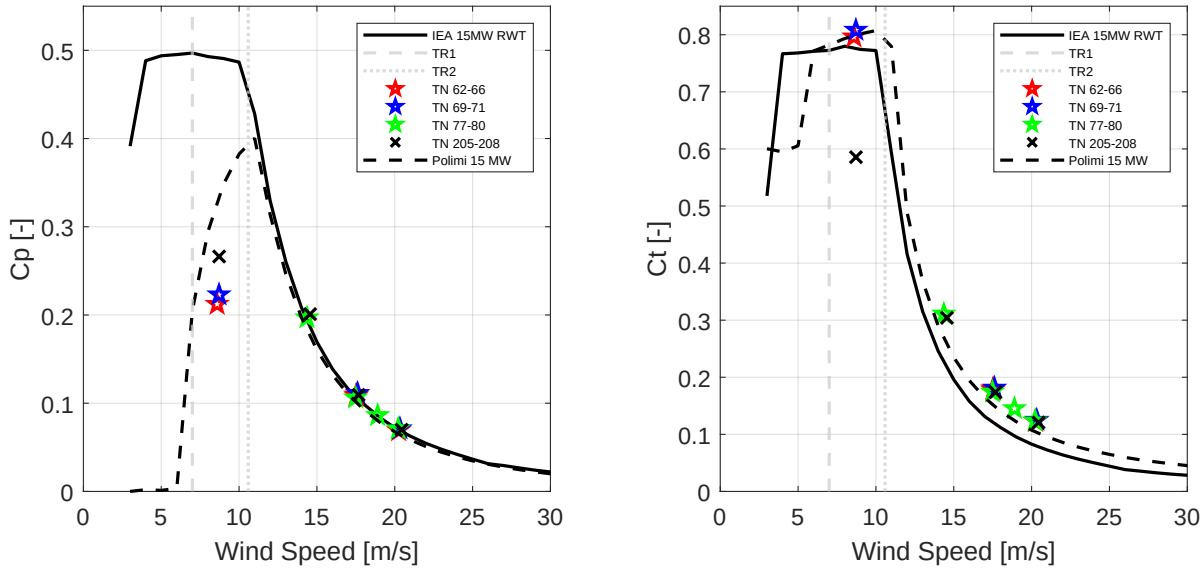

Figure 6.3: Experimental power and thrust coefficients reported on the steady state curves of the IEA 15 MW RWT and of the Polimi 15 MW

6.2. Imposed Motion Tests

During imposed motion tests, a sinusoidal motion in pitch direction have been imposed to the hexapod, in order to verify the behavior of the controller in an off-shore configuration, and to check the consistency between experimental and numerical results in that case. Figure 6.4 shows the platform reference system and degrees of freedom for a generic floating wind turbine.

Investigating the behavior of the system during imposed motion tests is important to better understand the dynamic of a floating turbine and how the controller reacts to the floater motion.

The system have been tested for different frequencies at different amplitudes of pitch oscillation, reported in table 6.2.

Frequency [Hz]	Amplitude [deg]
0.25	3.0
1.25	2.0
2.0	0.75

Table 6.2: Frequencies and amplitudes of imposed motion tests.

The same tests have been performed for below and above-rated condition. The selected wind speed was $U = 2.87\ m/s$ for below-rated and $U = 4.85\ m/s$ for above-rated.

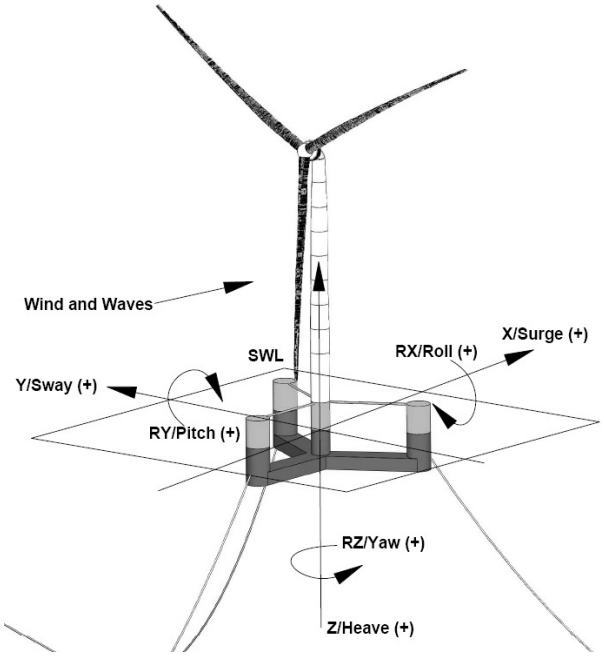

Figure 6.4: Platform reference system and degrees of freedom for a generic floating system [9].

Before analyzing experimental results and the comparison with the numerical ones, it is better to discuss analytically the response of the floating wind turbine to the sinusoidal pitch motion of the platform.

6.2.1. Linearized dynamic of the floating turbine

Recalling equation 4.13, the linearized equation describing the wind turbine in the rotor degree of freedom is

$$\Delta\dot{\omega}_g = A(U_{op})\Delta\omega_g + B_\beta(U_{op})\Delta\beta + B_U(U_{op})\Delta U + B_{\tau_g}(U_{op})\Delta\tau_g. \tag{6.1}$$

Considering above-rated operation with constant generator torque, the term $B_{\tau_g}(U_{op})$ is null, while the blade pitch is defined by the controller as:

$$\Delta\beta = -k_p\Delta\omega_g - k_i\int_0^t \Delta\omega_g\, dt \tag{6.2}$$

Introducing the variable $\dot{\tilde{\theta}} = \Delta\omega_g$, the plant model cam be written as:

$$\ddot{\tilde{\theta}} + (k_p - A(U_{op}))\dot{\tilde{\theta}} + k_i\tilde{\theta} = B_U(U_{op})\Delta U \tag{6.3}$$

The wind speed perturbation with respect to the steady state wind speed, is due to

turbolence and to the motion of the platform in pitch direction, that generates an apparent wind speed. Being in smooth flow condition, it can be assumed that the wind turbolence in longitudinal direction is negligible, so that perturbation of wind speed is only due to the apparent wind speed, and can be expressed as:

$$\Delta U = \dot{\beta}_{ptfm} h \tag{6.4}$$

where, β_{ptfm} is the platform pitch rotation, and h is the distance between the center of rotation of the platform and the rotor centre. The linearized plant model for the floating wind turbine becomes:

$$\ddot{\tilde{\theta}} + (k_p - A(U_{op}))\dot{\tilde{\theta}} + k_i \tilde{\theta} = B_U(U_{op})\dot{\beta}_{ptfm} h \tag{6.5}$$

The system is modelled as a second order system, where the platform pitch rotation acts as the forcing term. If the goal is to reproduce the same dynamics at model scale as the full scale, all parameters present in equation 6.5 have to be dimensionally scaled. In particular, the control gains k_p and k_i for the wind turbine model, should be the ones computed for the full-scale numerical model, properly scaled according to the scale factors. Also the terms $A(U_{op})$ and $B_U(U_{op})$, the rotor inertia J^*, and the aerodynamic torque sensitivities, should be properly scaled. If some errors are introduced during the scaling process, differences in the dynamic response will result. The correct scaling of the control gains have been ensured in the controller implementation. For what regards the rotor equivalent inertia, it has been correctly up-scaled in the numerical model, although there might be some errors in the estimation of this parameter. Starting from equation 4.7 the aerodynamic torque sensitivities can be formulated as

$$\begin{aligned} K_{\omega Q} &= \frac{\tau_{a,0}}{\omega_{g,0}} \left(\frac{\partial C_Q}{\partial \lambda}\bigg|_0 \frac{\lambda_0}{C_{Q,0}} \right) \\ K_{\beta Q} &= \frac{1}{2}\rho \pi R^3 U_0^2 \left(\frac{\partial C_Q}{\partial \beta}\bigg|_0 \right) \\ K_{UQ} &= \frac{\tau_{a,0}}{\omega_{g,0}} \left(2 - \frac{\partial C_Q}{\partial \lambda}\bigg|_0 \frac{\lambda_0}{C_{Q,0}} \right) \end{aligned} \tag{6.6}$$

and it can be noticed that they depend on the steady state operating point of the rotor and on the torque non-dimensional coefficient C_Q, that is characteristic of the rotor itself. To correctly scale the aerodynamic sensitivities, effort has been spent on trying to simulate the same steady state points obtained in the wind tunnel tests. The C_Q coefficient is strictly related to the C_p coefficient that is not perfectly the same between

the physical and numerical model. Unfortunately, the differences on the C_Q coefficient cannot be mitigated, thus some differences on the aerodynamic torque sensitivities are present and accepted.

6.2.2. Data Acquisition and Post-process

For each test the acquisition time have been set in order to acquire an integer number of period according to the frequency of the test. The acquired data have been post-processed in order to remove random noise and apply some corrections. The following actions have been implemented:

- Acquired data have been cut in order to have an integer number of platform pitch oscillations.
- Rotor thrust and torque signals have been processed by a zero-phase digital filter. The filter is a fourth order Butterworth filter with cut-off frequency two times the motion frequency. This operation allows to remove high frequency oscillations of these signals without introducing phase distortion.
- The blade pitch signal has been processed to account for the pitch actuator transfer function, since the acquired signal was the pitch reference signal and not the real pitch of the blade.
- The time histories have been cut into stories of length equal to the period of the motion. A time-averaging process have been performed on the different time histories, in order to remove random noises and focus on the frequency component equal to the motion frequency.
- The result should be a clean signal at the frequency of the motion.

After the post-processing signal are reported against the motion phase of the platform, focusing on a single oscillation.

6.2.3. Imposed Motion Simulations

The imposed motion numerical simulations have been performed trying to be as adherent as possible to the experimental ones. In doing so the controller in the numerical model was adapted to follow as speed reference the mean value of rotor speed acquired in the wind tunnel tests. The actual platform pitch rotation have been acquired using two lasers as described in section 5.3. The amplitude of this signal have been imposed as amplitude to the pitch motion in the simulations. The imposed platform motion have been implemented in the numerical model using the super-element theory as described in [23]. With the module ExtPtfm [24] available in OpenFAST, the platform is modelled as

a concentrated mass with fictitious inertial properties, summarized by a mass, stiffness and damping matrices. Defined the desired motion in the desired direction, a force is computed and applied to the super-element, generating the proper motion. The wind speed was set to be the same as the one acquired in the wind tunnel adjusted to account for the blockage effect, estimated at 2%, as in the following equation:

$$U_{num} = U_{exp} \cdot 1.02 \tag{6.7}$$

The simulation time has been set to be the up-scale of the acquisition time and the same post-processing has been applied to the numerical data.

At the end the numerical results have been down-scaled to model scale in order to be comparable with the experimental ones.

6.2.4. Tests Results

The results of this experimental campaign in comparison to the numerical simulations are first presented in tabular form. The data reported are the oscillation amplitude at the platform motion frequency for rotor thrust, torque, rotational speed and blade pitch angle. The phase reported is the phase delay of each signal with respect to the motion of the platform. Table 6.3, shows the results in below-rated region. In this table the blade pitch angle is reported for sake of completeness, although in below-rated region the blade pitch is fixed. The matching between experimental and numerical results is quite good for thrust force, while it is not for rotor torque and rotor speed, where amplitudes of oscillations are way higher in the experimental tests.

Table 6.4 show the results for above-rated region. Also in this case the matching between experimental and numerical results is quite good for thrust force, and less for the other parameters. Amplitudes of oscillations are comparable for some frequencies and not for others, without a specific trend. Also the matching in phase is good in some cases and not in others.

With tabular comparison only amplitude and phase can be compared, loosing the information on the mean value of the considered signal.

To better understand the reasons for the good matching and the discrepancies between experimental and numerical results, also the mean value matters. Therefore, is better to refer to the plots comparing experimental and numerical results over a complete oscillation of the platform.

The comparison will be carried on focusing on below and above-rated region separately, reporting figures for each tested frequency.

Starting from below-rated, figure 6.5 shows the results for the test at f = 0.25 Hz.

		f = 0.25 Hz		f = 1.25 Hz		f = 2.00 Hz	
		Exp	Num	Exp	Num	Exp	Num
Thrust	| | [N]	0,94	1,01	2,99	3,29	2,21	1,83
	∠ [deg]	-94,18	-95,78	-92,10	-91,37	-89,54	-90,09
Torque	| | [Nm]	0,08	0,19	0,22	0,62	0,16	0,34
	∠ [deg]	-116,11	-95,96	93,65	-91,58	81,55	-90,34
Rotor Speed	| | [rpm]	0,79	0,05	2,14	0,33	0,91	0,23
	∠ [deg]	-99,29	-35,46	-174,43	-58,31	-179,08	-56,24
Blade Pitch	| | [deg]	0,01	0,00	0,01	0,00	0,01	0,00
	∠ [deg]	-137,77	97,41	176,32	55,52	-154,90	-102,36

Table 6.3: Experimental results compared with numerical ones for imposed motion tests in below-rated region.

		f = 0.25 Hz		f = 1.25 Hz		f = 2.00 Hz	
		Exp	Num	Exp	Num	Exp	Num
Thrust	| | [N]	0,41	0,38	2,06	4,04	3,17	3,10
	∠ [deg]	-105,44	69,59	55,78	10,25	14,07	-33,20
Torque	| | [Nm]	0,08	0,02	0,16	0,80	0,13	0,70
	∠ [deg]	-119,98	52,14	147,90	-2,94	121,17	-39,42
Rotor Speed	| | [rpm]	0,19	0,42	1,60	3,32	1,43	1,78
	∠ [deg]	-86,98	-37,73	-75,26	-93,35	-90,19	-130,36
Blade Pitch	| | [deg]	0,33	0,75	2,70	3,06	2,26	1,34
	∠ [deg]	-91,02	256,25	-104,74	224,34	-136,86	-176,89

Table 6.4: Experimental results compared with numerical ones for imposed motion tests in above-rated region.

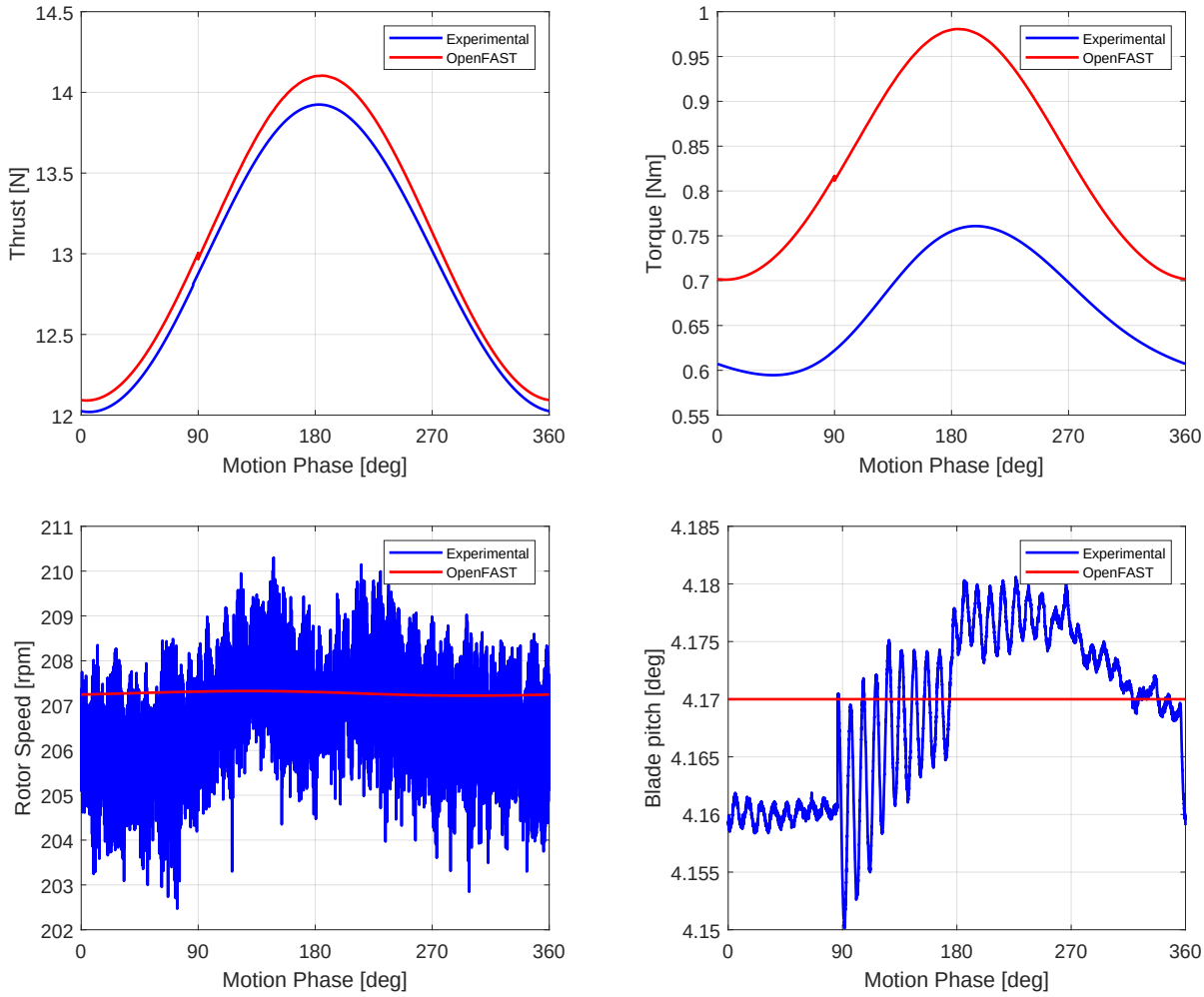

Figure 6.5: Comparison between experimental and numerical results for imposed motion test at f = 0.25 Hz, in below-rated region.

As already pointed out the matching for thrust force is good, with a slightly higher mean value in the numerical results. For what regards rotor torque, the trend is matched, but the mean value is notably higher in the numerical test. The higher rotor torque can be due to differences in the steady state value of torque, already pointed out in the bottom-right plot of figure 6.1 and discussed in section 6.1. Moreover, it can be observed that the rotor speed signal, despite the phase averaging process, is still very noisy. This means that the measure coming from this sensor is not so accurate and can bring an offset to the rotor speed signal that leads to a different generator torque. At last, the blade pitch angle comes from the manual zero setting and the post-processing correction to account for the actuator. This can lead to a different real pitch angle that can affect both thrust and torque. Since the blade pitch angle is the main factor affecting thrust force, considering the good matching for thrust, it can be said that this last aspect is not the main source of discrepancies for rotor torque.

Figure 6.6 and 6.7 show the results for the platform motion frequency f = 1.25 Hz and f = 2.0 Hz respectively.

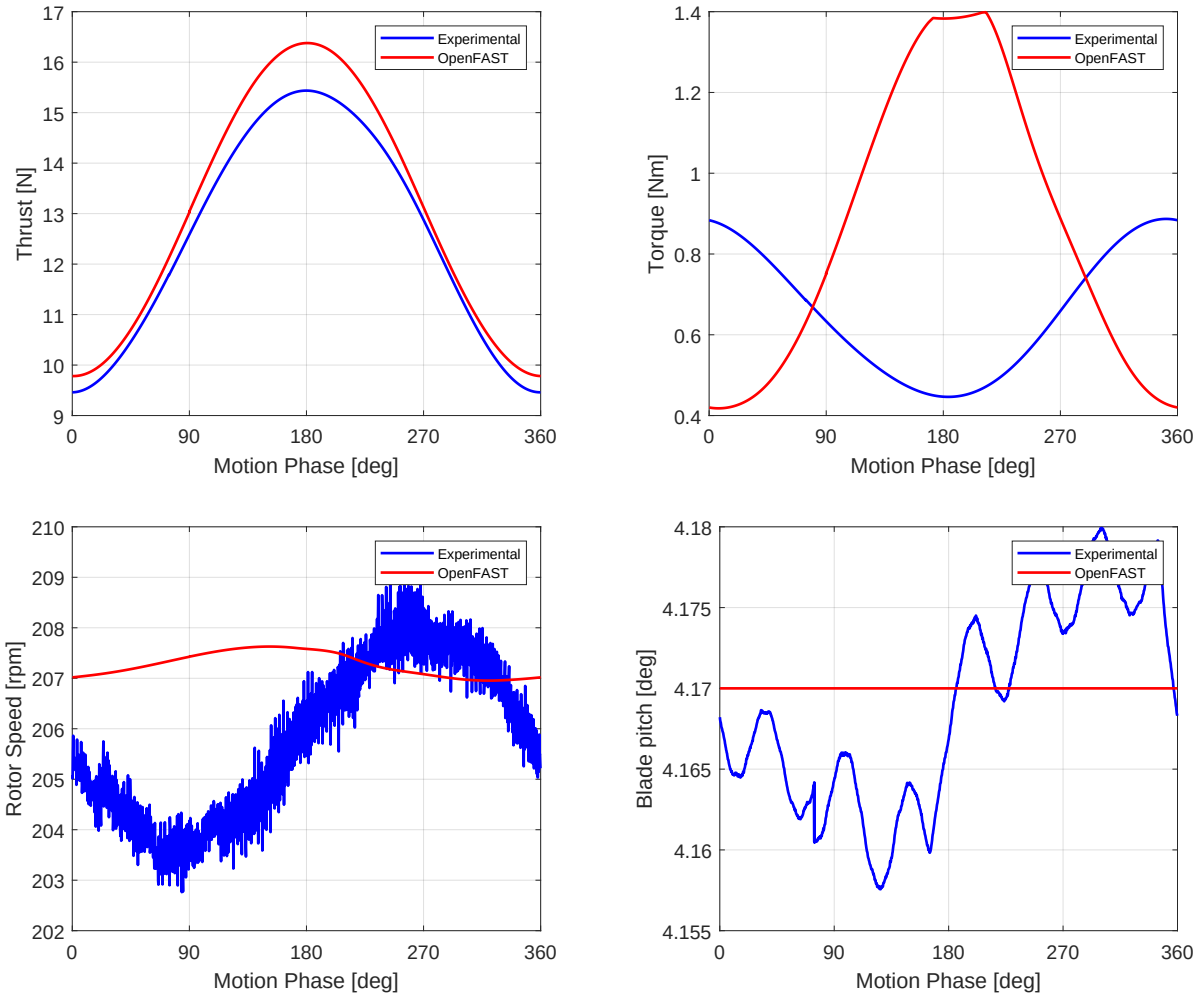

Figure 6.6: Comparison between experimental and numerical results for imposed motion test at f = 1.25 Hz, in below-rated region.

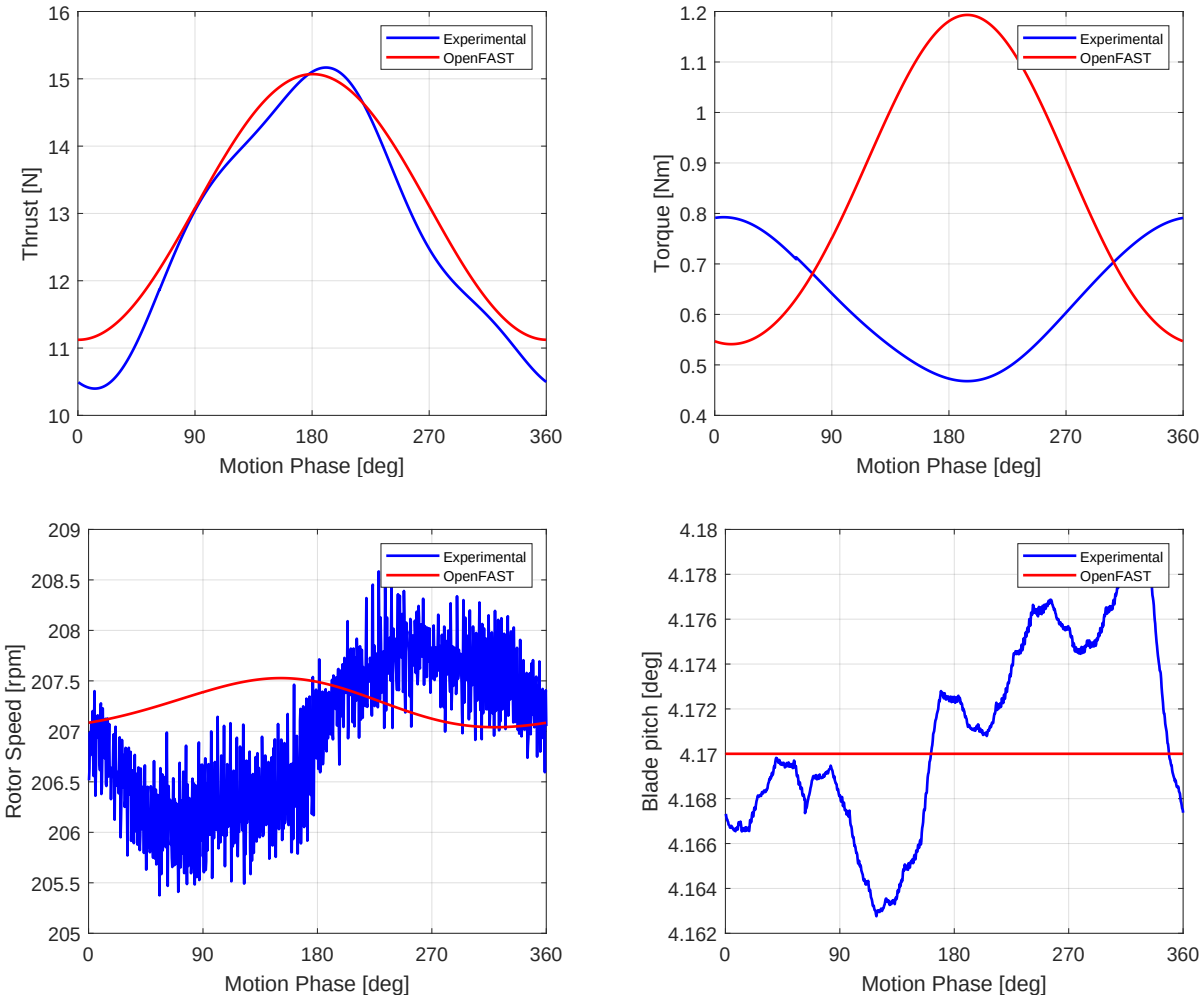

Figure 6.7: Comparison between experimental and numerical results for imposed motion test at f = 2.0 Hz, in below-rated region.

For this two cases again the matching for thrust is good, while for torque a higher amplitude and a phase shift of about 180° is noticed. This can be related to the rotor speed signal. Indeed, in both these two last cases, rotor speed oscillations are higher in the experimental tests than in the numerical ones. This justifies the higher amplitude of oscillation in the torque signal. Moreover, there is a phase shift in the rotor speed signal, between experimental and numerical results, and this can explain the phase shift in the torque signal.

Moving to the above-rated region, figure 6.8 shows the result for the test at f = 0.25 Hz.

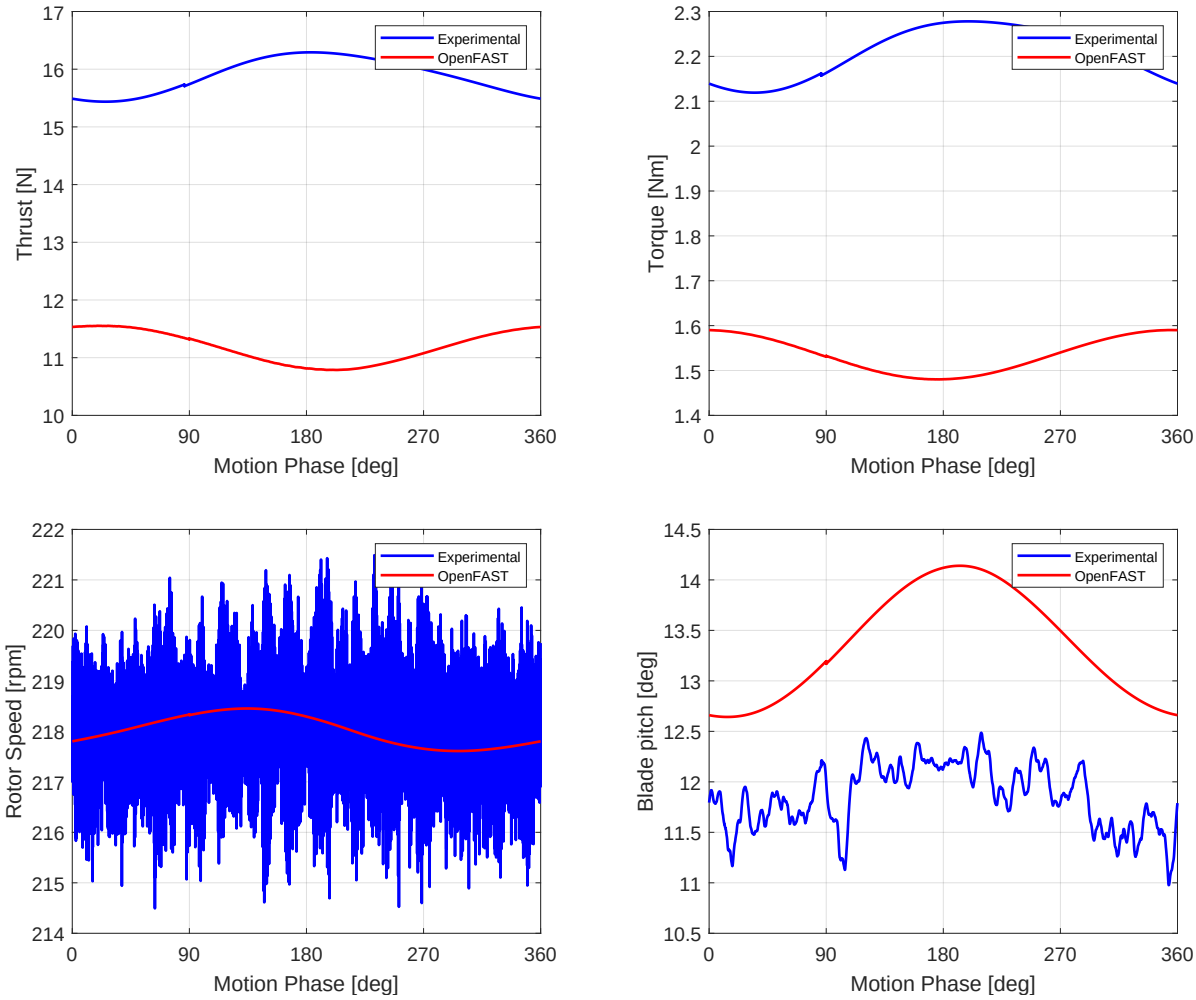

Figure 6.8: Comparison between experimental and numerical results for imposed motion test at f = 0.25 Hz, in above-rated region.

In this case, thrust and rotor signal are similar in oscillation amplitudes, but the mean value and the phase are not comparable. For torque signal the discussion is analogous to the below-rated case. In addition the difference in the blade pitch angle mean value, can further introduce errors in the torque mean value. For what regards thrust the difference in the mean value is related to the difference in the mean value observed for the blade pitch. This differences can be related to the wrong estimation of the drivetrain efficiency, leading to a lower generator torque and a higher blade pitch in the simulations. Discussing the phase shift is difficult, because both rotor speed and blade pitch signal are very noisy.

Figure 6.9 and 6.10 shows the results for the tests at f = 1.25 Hz and f = 2.0 Hz.

In these two cases the discussion for torque is the same already done. For thrust force instead, the same trend is observed in experimental and numerical tests, with a different mean value and phase shift. The difference in mean value is again explicable by the

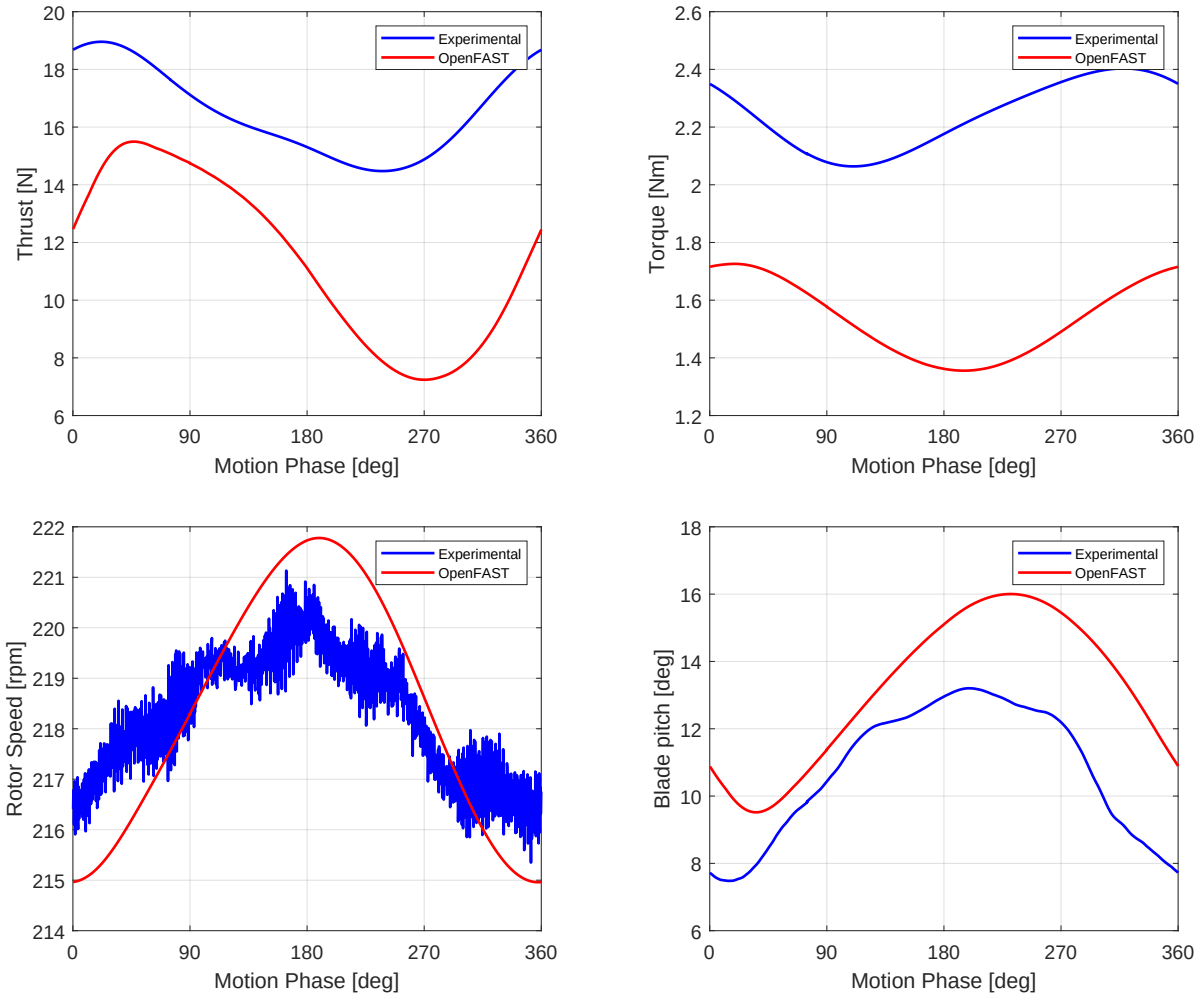

Figure 6.9: Comparison between experimental and numerical results for imposed motion test at f = 1.25 Hz, in above-rated region.

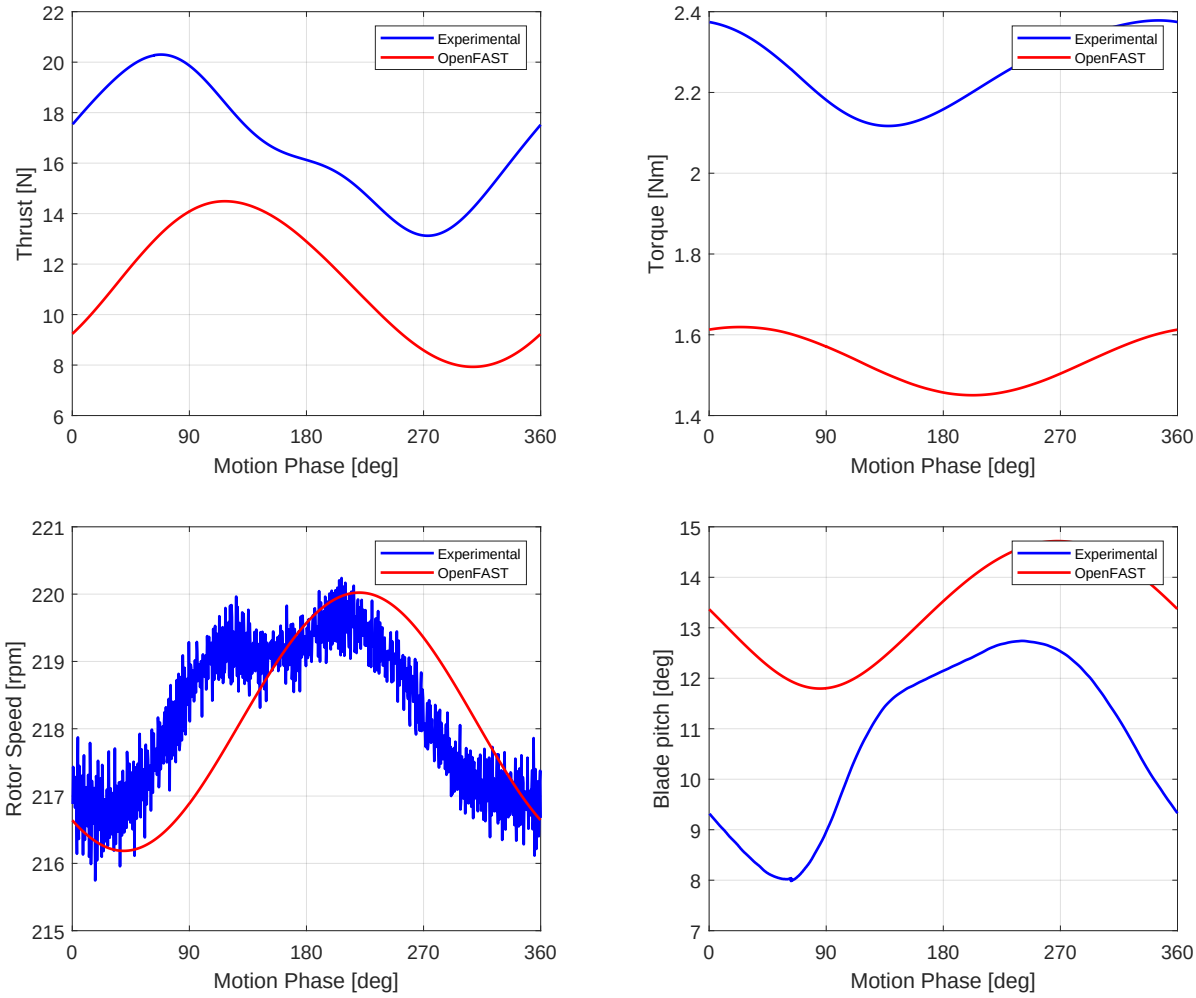

Figure 6.10: Comparison between experimental and numerical results for imposed motion test at f = 2.0 Hz, in above-rated region.

different blade pitch mean value. Differently from the case at frequency of 0.25 Hz, the pitch signal is no more noisy and also the rotor speed signal has a clear global trend. It can be observed that both rotor speed and blade pitch are in delay in the numerical tests with respect to the experimental ones. This can be a reason for the delay observed in thrust signal.

6.2.5. Comparison with the IEA 15 MW RWT

The tested wind turbine model is a scaled version of the IEA 15 MW RWT. Therefore, the experimental and numerical results obtained for the Polimi 15 MW with imposed platform motion, should also be compared to the numerical results obtained for the reference wind turbine. The results for the reference turbine are obtained simulating the system in OpenFAST, as done for the numerical model of the Polimi 15 MW, in the same wind and platform motion condition. The results are than reported at model scale to be comparable with the experimental results. The comparison is carried out reporting similar plots, as done in the previous section, avoiding the tabular comparison.
Figure 6.11 shows the results for the test at f = 0.25 Hz.

It can be observed that thrust matching is good in terms of mean value, but the amplitudes of oscillations are notably higher for the IEA 15 MW. This high oscillations are due to the high oscillations in the rotor speed, which in turn are due to the lower rotor inertia. Discussing the phase difference in rotor speed, and so in thrust, is again difficult being the experimental data very noisy. It can be noticed that thrust force and rotor speed are more or less in phase, with a phase displacemente of around $\pi/4$. For torque signal the trend is similar to what already observed for experimental data and numerical data from the Polimi 15 MW, but the mean value is higher. This can be related to the imposed minimum pitch and to the difference in the steady state rotor torque, that can generate this high discrepancy in the torque mean value.

Figures 6.12 and 6.13 show the results for the tests at f = 1.25 Hz and f = 2.0 Hz respectively, always in below-rated. For these two cases what was discussed above is still valid, but thrust force and rotor speed seems now in phase quadrature. This difference between the first test and the last two is due to the flexible fore-aft vibration mode of the tower. Indeed, in the numerical model of the IEA 15 MW RWT, the tower flexibility is accounted. For the tests at frequency of 1.25 Hz and 2.0 Hz, the system is no more in the quasi-static zone for the tower, and the vibration of the tower can cause the phase shift in the thrust signal. Moreover, the irregular behavior noted in thrust force in figure 6.12, is due to the action of the blade pitch induced by the set-point smoother. For what regards torque, again the mean value is higher for the IEA 15 MW RWT, and the signal is more

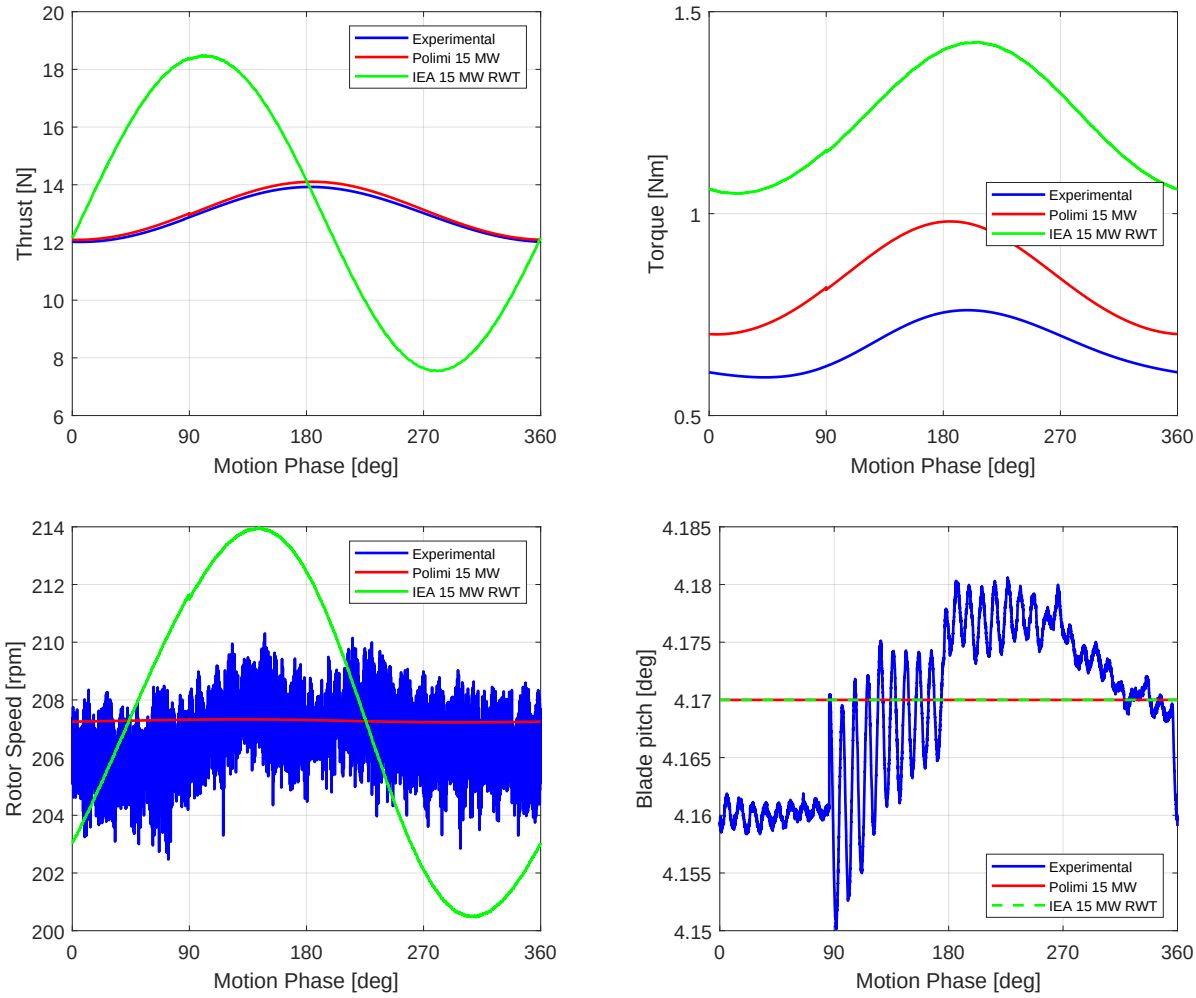

Figure 6.11: Comparison with the IEA 15 MW RWT for imposed motion test at f = 0.25 Hz, in below-rated region.

or less in phase with rotor speed.

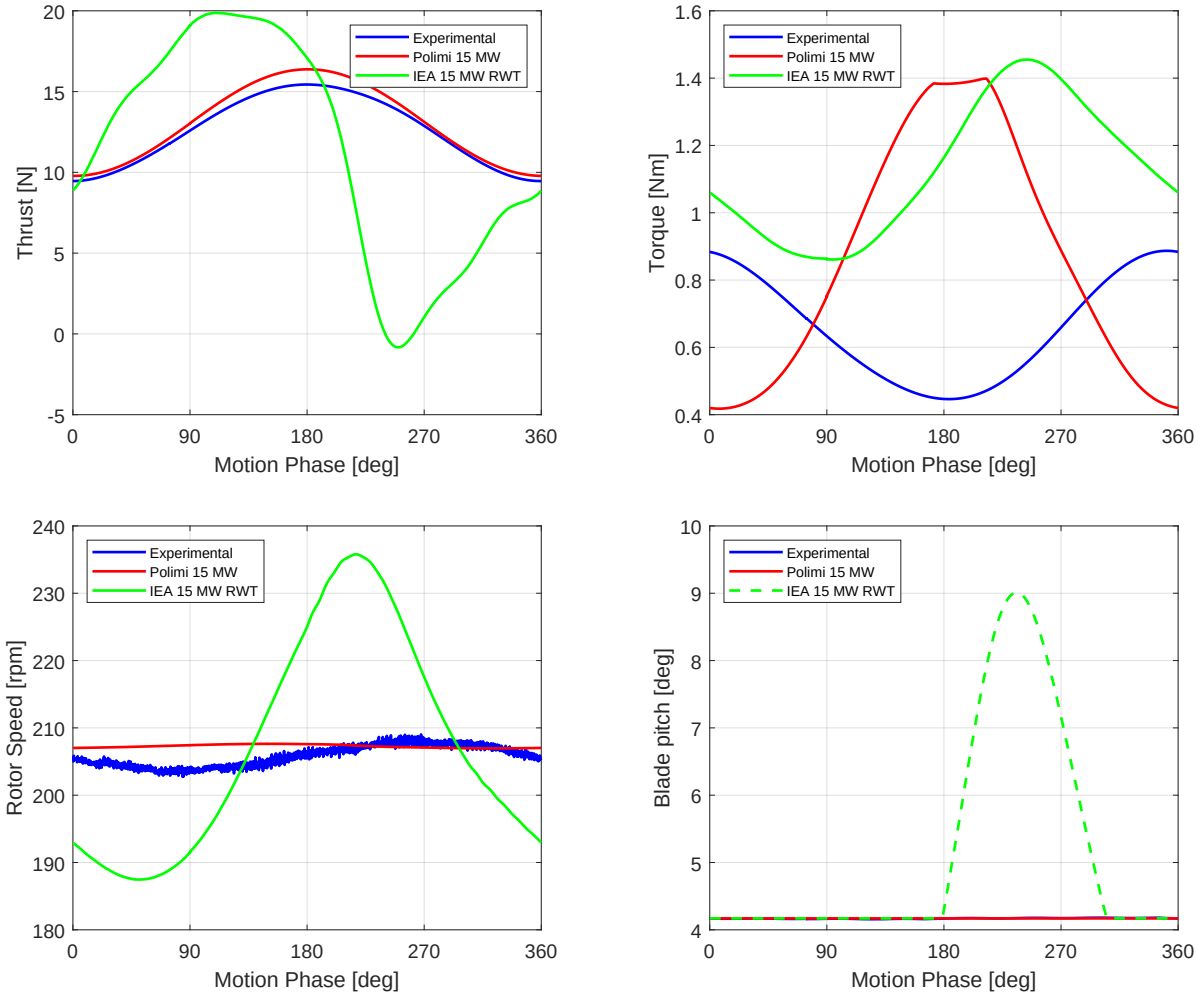

Figure 6.12: Comparison with the IEA 15 MW RWT for imposed motion test at f = 1.25 Hz, in below-rated region.

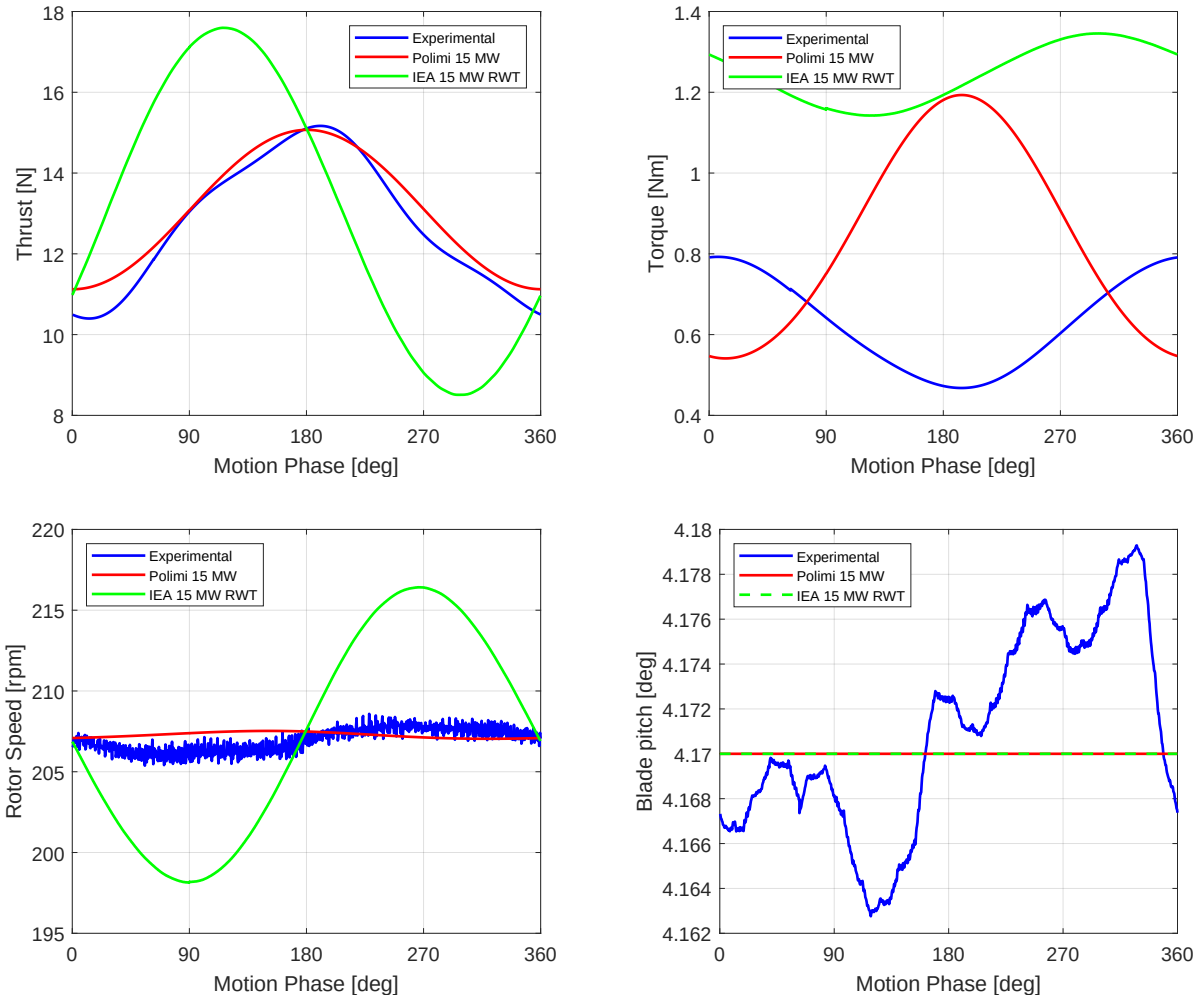

Figure 6.13: Comparison with the IEA 15 MW RWT for imposed motion test at f = 2.0 Hz, in below-rated region.

Passing to above-rated region, figure 6.14, shows the results for the test at f = 0.25 Hz.

In this case the thrust matching in terms of mean value is not ensured. The thrust mean value for the IEA 15 MW RWT is lower than the experimental results and even than the results for the numerical model of the Polimi 15 MW. This is due to the higher blade pitch angle. The higher pitch angle derives from the difference in steady state operating point already discussed in the static tests. Despite the differences in the mean pitch angle, the trend between the two numerical models is the same. For the rotor speed the trend between the two numerical models is similar, but the oscillations amplitudes for the IEA 15 MW RWT are notably higher due to the lower inertia of the rotor. These high oscillations in rotor speed causes the high oscillations in rotor thrust. Discussing the matching with the experimental results in terms of rotor speed is not meaningful,

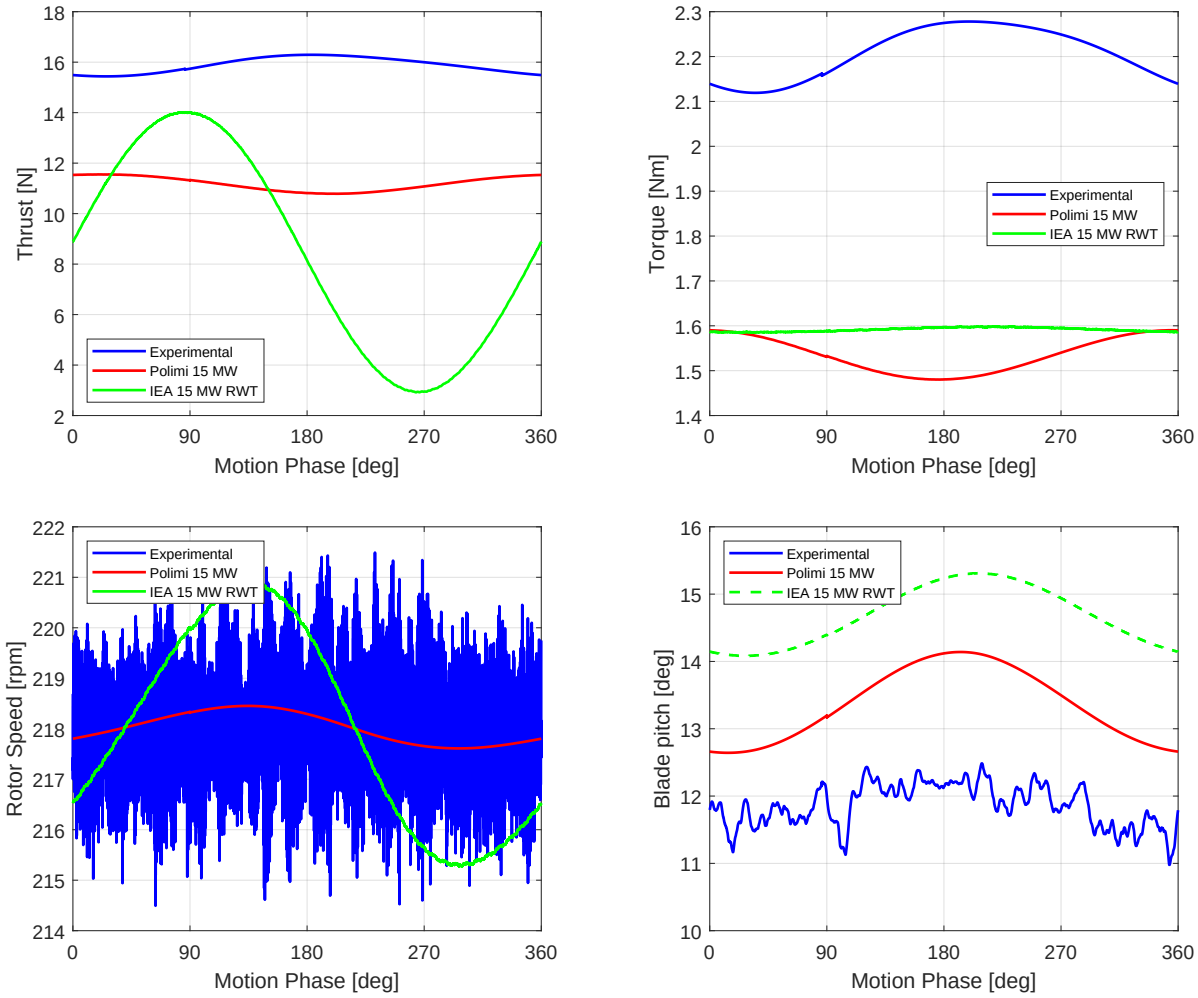

Figure 6.14: Comparison with the IEA 15 MW RWT for imposed motion test at f = 0.25 Hz, in above-rated region.

being the experimental data very noisy. For what regards rotor torque, the mean value for the IEA 15 MW RWT is slightly lower than the one of the Polimi 15 MW, due to the differences in the steady state value.

Figures 6.15 and 6.16 show the results for the tests at f = 1.25 Hz and f = 2.0 Hz respectively. Also for this two cases the findings are the same. What can be observed, is that the difference in amplitude of oscillation in thrust signal between the two numerical models is less pronounced. That is because the lesser oscillation in rotor speed signal for the Polimi 15 MW is compensated by the higher oscillation in blade pitch angle.

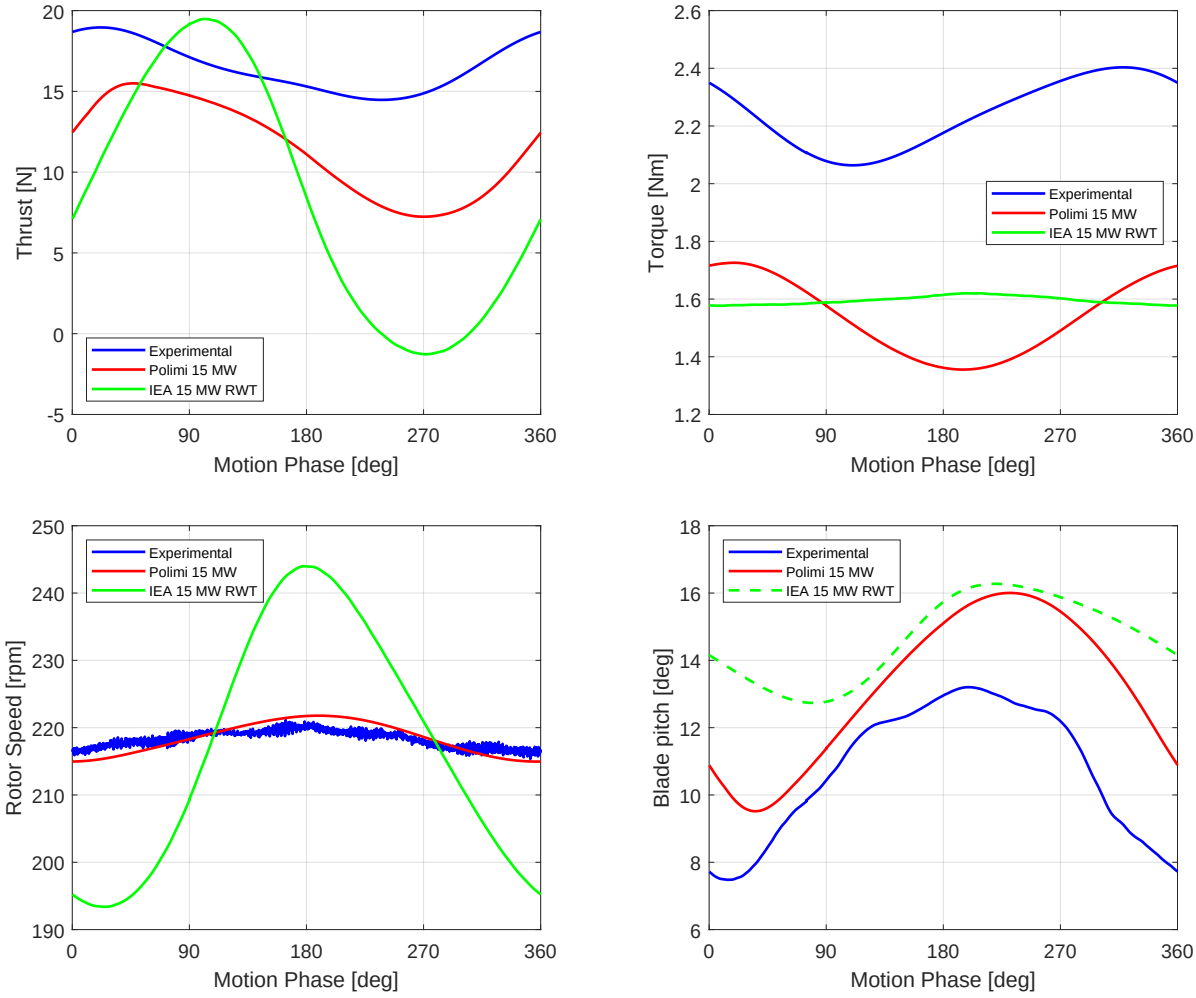

Figure 6.15: Comparison with the IEA 15 MW RWT for imposed motion test at f = 1.25 Hz, in above-rated region.

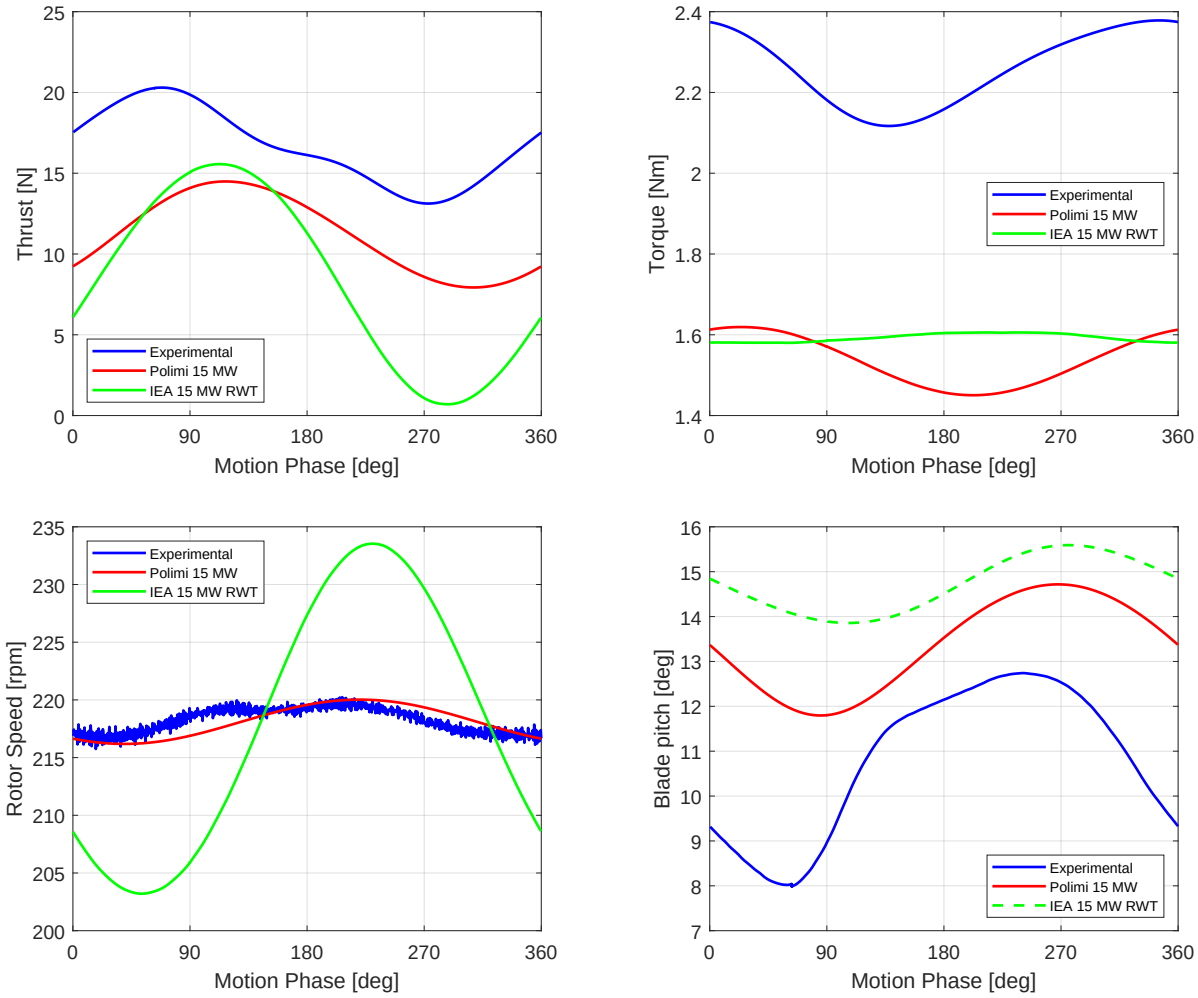

Figure 6.16: Comparison with the IEA 15 MW RWT for imposed motion test at f = 2.0 Hz, in above-rated region.

7 | Conclusions and future works

The present work is focused on the development of a numerical model for the Polimi 15 MW WTM. More attention has been paid on the wind turbine controller, in particular the ROSCO controller was tuned for the model. The controller was implemented in Simulink® allowing to implement the controller on the prototype.

The response of the numerical model under different wind speed conditions was verified through OpenFAST simulations, comparing the results with the ones of the IEA 15 MW RWT. An overall good matching between the two models was observed, especially for the steady state operating points for wind speeds higher than 7 m/s. Discrepancies at very low wind speeds are due to the low aerodynamic efficiency of the Polimi 15 MW blades at low Reynolds number. Differences in the dynamic performances of the controller are mainly due to the different rotor inertia.

The tuned controller was scaled to fit the model-scale prototype and wind tunnel test has been performed. Two kind of tests was taken under investigations, static tests and imposed motion tests. During static tests the goal was to verify that the model coupled with the controller correctly reproduces the steady state operation points obtained by the numerical model. The matching between experimental and numerical results is satisfying. Discrepancies are mainly due to the errors in parameter estimation, like the gearbox and generator efficiency, and to the Reynolds effect of the rotor. In the imposed motion tests a sinusoidal motion was imposed to the exapod and the response of the system was analyzed in terms of oscillations of rotor torque, thrust, rotational speed and blade pitch angle oscillations. Tests were repeated at different amplitudes and frequencies of oscillations. The comparison between experimental and numerical results shows contrasting results. For some cases the matching is good, but in others discrepancies are not negligible.

In conclusion, the results are promising, even though some aspects need further studies. The Reynolds effect can be verified for the rotor, performing the characterization at different wind speeds. This can help to better tune the controller for the low wind speeds and can also explain some of the differences between experimental and numerical results. Moreover, better parameter estimation is required from the hardware point of view. Also the coupling between the hexapod and the wind turbine model can be further investigated,

to verify if it introduces undesired vibrations in the system, that can affect the imposed motion tests.

In future works the dynamic performances of the controller can be investigated experimentally under different wind condition as step wind or turbulent flow. This tests can than be compared with the numerical results to further validate the numerical model. An Extended Kalman FIlter can be implemented to estimate the wind speed and its performance can be checked, improving the knowledge on this tool.

The behavior of the controller in off-shore conditions can be verified exploiting the Hardware-in-the-Loop implementation, where the hexapod reproduces the platform motion through a numerical model. This can further increase the knowledge on the control of floating systems.

Bibliography

[1] International Energy Agency. *Wind Electricity*, 2022. URL `https://www.iea.org/reports/wind-electricity`. Last checked on 04/03/2023.

[2] Yogesh Kumar, Jordan Ringenberg, Soma Shekara Depuru, Vijay K. Devabhaktuni, Jin Woo Lee, Efstratios Nikolaidis, Brett Andersen, and Abdollah Afjeh. *Wind energy: Trends and enabling technologies. Renewable and Sustainable Energy Reviews*, 53:209–224, 2016.

[3] S. Gueydon, I. Bayati, and E. J. de Ridder. *Discussion of solutions for basin model tests of FOWTs in combined waves and wind. Ocean Engineering*, 209(May):107288, 2020.

[4] Bianchi Fernando D., Hernan. De Battista, and Ricardo J. Mantz. *Wind Turbine Control Systems Principles,Modelling and Gain Scheduling Design.* Springer, London, 2011.

[5] Nikhar J. Abbas, Daniel S. Zalkind, Lucy Pao, and Alan Wright. *A reference open-source controller for fixed and floating offshore wind turbines. Wind Energy Science*, 7(1):53–73, 2022.

[6] T. J. Larsen and T. D. Hanson. *A method to avoid negative damped low frequent tower vibrations for a floating, pitch controlled wind turbine. Journal of Physics: Conference Series*, 75(1), 2007.

[7] Mohammad Youssef Mahfouz, Mohammad Salari, Sergio Hernández, Fernando Vigara, Climent Molins, Pau Trubat, Henrik Bredmose, and Antonio Pegalajar-Jurado. *Public design and FAST models of the two 15MW floater-turbine concepts.* 2020.

[8] G. J. Van Der Veen, I. J. Couchman, and R. O. Bowyer. *Control of floating wind turbines. Proceedings of the American Control Conference*, pages 3148–3153, 2012.

[9] Christopher Allen, Anthony Viselli, Habib Dagher, Andrew Goupee, Evan Gaertner, Nikhar Abbas, Matthew Hall, and Garrett Barter. *Definition of the UMaine VolturnUS-S Reference Platform Developed for the IEA Wind 15-Megawatt Offshore Reference Wind Turbine.* Technical report, National Renewable Energy Laboratory, 2020.

[10] Evan Gaertner et al. *IEA Wind - Offshore Reference Wind - 15MW.* Technical report, National Renewable Energy Laboratory, 2020.

[11] WindEurope. *Offshore wind in Europe - Key trends and statistics 2020. WindEurope*, 3(2):14–17, 2021. URL `https://windeurope.org/intelligence-platform/product/offshore-wind-in-europe-key-trends-and-statistics-2020/`.

[12] Siemens Gamesa. *SG 14-222 DD Offshore wind turbine*, 2022. URL `https://www.siemensgamesa.com/products-and-services/offshore/wind-turbine-sg-14-222-dd`. Last checked on 04/03/2023.

[13] Ilmas Bayati, Marco Belloli, Luca Bernini, and Alberto Zasso. *Aerodynamic design methodology for wind tunnel tests of wind turbine rotors. Journal of Wind Engineering and Industrial Aerodynamics*, 167:217–227, 2017.

[14] M. Borg, M. Mirzaei, and H. Bredmose. *LIFES50+ Deliverable D1.2: Wind Turbine Models for the Design.* 2015.

[15] Bonnie Jonkman and Jason Jonkman. *FAST v8.16.00*, 2016.

[16] National Renewable Energy Laboratory. *OpenFAST Documentation*, 2022. URL `https://openfast.readthedocs.io`.

[17] J M Jonkman, G J Hayman, B J Jonkman, and R R Damiani. *AeroDyn v15 User's Guide and Theory Manual*, 2015.

[18] Andy Platt, Bonnie Jonkman, and Jason Jonkman. *Inflow Wind User's Guide*, 2016.

[19] Morten H Hansen, Anca Hansen, Torben J Larsen, Stig Øye, Poul Sørensen, and Peter Fuglsang. *Control design for a pitch-regulated , variable-speed wind turbine*, 2005.

[20] Neil Kelley, Bonnie Jonkman. *TurbSim User's Guide: Version 1.50.* Technical report, National Renewable Energy Laboratory, 2009.

[21] Alessandro Fontanella. *Numerical model of a floating wind turbine controller and experimental implementation.* Master's thesis, Politecnco Di Milano, 2016.

[22] M. Belloli, I. Bayati, A. Facchinetti, A. Fontanella, H. Giberti, F. La Mura, F. Taruffi, and A. Zasso. *A hybrid methodology for wind tunnel testing of floating offshore wind turbines. Ocean Engineering*, 210(April 2019):107592, 2020.

[23] R. Amaral, K. Laugesen, M. Masciola, D. Von Terzi, P. Deglaire, and A. Vire. *A frequency-time domain method for annual energy production estimation in floating wind turbines. Journal of Physics: Conference Series*, 2265(4), 2022.

[24] E. Branlard, M. Shields, B. Anderson, R. Damiani, F. Wendt, J. Jonkman, W. Musial, and B. Foley. *Superelement reduction of substructures for sequential load calculations in OpenFAST. Journal of Physics: Conference Series*, 1452(1), 2020.

List of Symbols

Variable	Description	SI unit
$\boldsymbol{A_r}$	Rotor Swept Area	m^2
$\boldsymbol{a}$	Peak-Shaving Factor	-
$\boldsymbol{b}$	Blockage Ratio	-
$\boldsymbol{C_Q}$	Torque Coefficient	-
$\boldsymbol{C_p}$	Power Coefficient	-
$\boldsymbol{C_t}$	Thrust Coefficient	-
$\boldsymbol{F_r}$	Froude Number	-
$\boldsymbol{F_t}$	Aerodynamic Thrust Force	N
$\boldsymbol{J^*}$	Equivalent Inertia	kg m^2
$\boldsymbol{K_{\omega Q}}$	Speed to Torque Sensitivity	Nm s rad^-1
$\boldsymbol{K_{\beta Q}}$	Pitch to Torque Sensitivity	Nm deg^-1
$\boldsymbol{K_{UQ}}$	Wind-Speed to Torque Sensitivity	Nm s m^-1
$\boldsymbol{k_{vs}}$	Set-Point Smoother pitch factor	-
$\boldsymbol{k_{pc}}$	Set-Point Smoother torque factor	-
$\boldsymbol{k_p}$	Proportional Gain for Torque Controller	Nm s rad^-1
$\boldsymbol{k_i}$	Integral Gain for Torque Controller	Nm rad^-1
$\boldsymbol{k_{p,pc}}$	Proportional Gain for Pitch Controller	s
$\boldsymbol{k_{i,pc}}$	Integral Gain for Pitch Controller	-
$\boldsymbol{k_{\beta_{float}}}$	Floating Feedback Gain	
$\boldsymbol{M_a}$	Mach Number	-
$\boldsymbol{N_{gb}}$	Gearbox Ratio	-
$\boldsymbol{n_l}$	Lenght Scale Factor	-
$\boldsymbol{n_M}$	Mass Scale Factor	-
$\boldsymbol{n_t}$	Time Scale Factor	-
$\boldsymbol{n_v}$	Velocity Scale Factor	-

n_ω	Frequency Scale Factor	-
n_F	Force Scale Factor	-
P_N	Rated Power	W
R	Rotor Radius	m
T_r	Rotor Thrust	N
U	Wind Speed	m/s
V_N	Rated Wind Speed	m/s
$\dot{x}_{nac}$	Nacelle Fore-aft Velocity	m/s
β	Blade Pitch Angle	deg
β_{ff}	Floating Feedback Pitch Angle	deg
β_{ptfm}	Platform Pitch Rotation	rad/s
$\Delta\omega$	Set-Point Smoother speed offset	rad/s
η_{gb}	Gearbox Efficiency	-
λ	Tip-Speed-Ratio	-
λ_{opt}	Optimal TSR	-
ξ_{des}	Desired Closed-loop Damping	-
ξ_f	Filter Damping Ratio	-
ρ	Air Density	kg/m^3
τ_a	Rotor Aerodynamic Torque	Nm
τ_g	Generator Torque	Nm
ω_{des}	Desired Closed-loop Bandwidth	rad/s
ω_f	Filter Cut-off frequency	rad/s
ω_g	Generator Speed	rpm
$\omega_{ref,\tau}$	Torque Controller Reference Speed	rad/s
$\omega_{ref,\beta}$	Pitch Controller Reference Speed	rad/s
ω_{rot}	Rotor Speed	rpm

List of Abbreviations

DLL	Dynamic Link Library
DTU	Technical University of Denmark
EKF	Extended Kalman Filter
FOWT	Floating Off-shore Wind Turbine
FS-FP	Fixed-Speed Fixed-Pitch
FS-VP	Fixed-Speed variable-Pitch
GVPM	Galleria del Vento Politecnico di Milano
HIL	Hardware In the Loop
HPF	High-Pass-Filter
IEA	International Energy Agency
LPF	Low-Pass-Filter
NREL	National Renewable Energy Laboratory
PI	Proportional-Integral
ROSCO	Reference Open-Source COntroller
RWT	Reference Wind Turbine
Re	Reynolds
TSR	Tip-Speed-Ratio
VS-FP	Variable-Speed Fixed-Pitch
VS-VP	Variable-Speed variable-Pitch
WTM	Wind Turbine Model